THE UNIVERSITY OF SHEFFIELD

Department of Mechanical Engineering

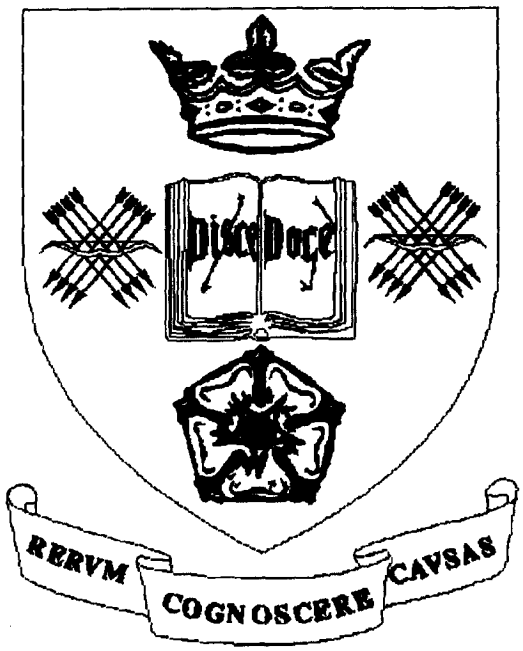

MODELLING OF TENNIS RACKET IMPACTS IN 3D USING ELITE PLAYERS

Simon Brian Choppin

Submitted for the Degree
of
Doctor of Philosophy

April 2008

THE UNIVERSITY OF SHEFFIELD

Department of Mechanical Engineering

Modelling of Tennis Racket Impacts in 3D Using Elite Players

Simon Brian Choppin

Submitted for the Degree of Doctor of Philosophy

April 2008

The modern era of tennis has seen large changes in racket design and playing style. As regulators of the game, the International Tennis Federation have assumed a role of constant investigation. Recently, impact models have been used to assess the characteristics of various rackets. Whilst existing models are powerful, they are limited in terms of impact position and racket and ball movement.

Realistic shot characteristics of 13 elite level players at the 2006 Wimbledon Qualifying Tournament were obtained. Two high speed cameras running at 1,000 frames per second were used to record ball and racket movements within a fully calibrated 2×2×2 m control volume to an accuracy of ±2.5 mm.

It was found that players tend to hit a point on the racket stringbed which generates little to no frame vibration. Forehand shots had an outbound ball spin of 800 – 2,200 rpm, ball velocities in the region of 25 – 40 ms^{-1}.

The results from the player shot analysis were used in the design of a repeatable impact methodology. Nine hundred laboratory based racket/ball impacts were analysed in 3D. A custom racket mount simulated grip torque. The experimental outputs were interpreted using a multi-variate fitting technique. The experimental results were used in model validation.

A predictive impact model was developed. When validated against the laboratory and player testing results, the model showed good correlation. The model was used to investigate the effects of shot weighting, movement and accuracy on post-impact ball behaviour. It was found that: Increasing swing action weighting increases the velocity of tip impacts. Increasing weight towards the edge of the racket reduces the penalty for hitting off the racket's longitudinal axis. A 'chopping' action generates ball spin.

The model developed in this study can be incorporated into existing shot prediction software used by the International Tennis Federation.

Keywords: Tennis, Impact, Player Shot, High Speed Video, Predictive Model

Acknowledgements

I would like to thank my supervisors Professor Steve Haake and Dr Simon Goodwill for providing endless and patient support throughout the duration of this study.

I would also like to thank, Jamie Capel-Davies, Stuart Miller and Janet Page and all other members of the Technical Centre at the International Tennis Federation for supporting this study.

My extended thanks goes to all members of the Sports Engineering Research Group past and present whom have helped me over the past three years. Their friendship and support has been invaluable.

Contents

Nomenclature

General ball/racket dynamics

ACOR	Apparent coefficient of restitution
COR	Coefficient of restitution
e	Coefficient of restitution (alternative)
e_A	Apparent coefficient of restitution (alternative)
I	Moment of inertia (unspecified axis)
I_1	Moment of inertia about the racket's central axis
I_2	Moment of inertia about the racket's transverse axis
I_3	Moment of inertia about the racket's perpendicular axis
I_B	Moment of inertia of ball
I_{COM}	Moment of inertia about centre of mass
I_R	Moment of inertia of racket
I_{RDC}	Moment of inertia given by racket diagnostics centre
M	Mass of racket
$m_{(B)}$	Mass of Ball
m_e	Effective mass of impact point
r	Radius of ball
η	Efficiency of impact
μ	Coefficient of friction
ρ	Mass per unit surface area of ball

Spring/damper mechanics

a_k	Constant used in determination of stringbed stiffness
$A_{C,K}$	Constants used in formulation of viscoelastic spring coefficients
b_k	Constant used in determination of stringbed stiffness
$c_{B\,etc.}$	Spring damper coefficient values
c_k	Constant used in determination of stringbed stiffness
d_{CONT}	Diameter of ball in contact with stringbed
F_B	Force acting on ball
F_S	Force acting on stringbed
$k_{H,B\,etc.}$	Spring constant coefficients
M_1	Mass of ball *not* at rest on stringbed
M_2	Mass of ball at rest on stringbed
r_t	Radius of ball at specific instant t
t	Denotes particular time instant
Δt	Denotes a particular time period
x	Deflection (of spring)
x_B	Displacement of ball (spring calculations)
$\dot{x}_B$	Velocity of ball (spring calculations)
$\ddot{x}_B$	Acceleration of ball (spring calculations)
x_S	Displacement of stringbed (spring calculations)
$\dot{x}_S$	Velocity of stringbed (spring calculations)
$\ddot{x}_S$	Acceleration of stringbed (spring calculations)

Multi-variate calculations

v_{ix}	Inbound velocity of ball in local x direction
v_{iy}	Inbound velocity of ball in local y direction
v_{iz}	Inbound velocity of ball in local z direction
v_{ox}	Rebound velocity of ball in local x direction
v_{oy}	Rebound velocity of ball in local y direction
v_{oz}	Rebound velocity of ball in local z direction
i_{px}	Distance from COM to impact location along local x direction
i_{py}	Distance from COM to impact location along local y direction
T	Restrictive torque about racket handle
SSE	Sum of squared errors

Racket modelling

a	Distance of grip point from COM/ distance of impact point along transverse axis
$\bar{a}$	Acceleration over a particular time-step
b	Distance of impact point from COM
c	Straight line distance from COM to impact point
F	Horizontal force (in case of Daish spin model)
F_{Spin}	Resultant force from ball spin
F_x	Force acting in local x direction
F_y	Force acting in local y direction
k	Radius of gyration of ball
R	Perpendicular force resulting from impact (Daish impact model specifically)
r_0	Uncompressed radius of ball
$\mathbf{R}$	Transformation matrix used to switch between local and global axes sets
S	Displacement of point over a particular time-step
ΔT	Duration of impact
T_x	Torque acting about local x axes
T_y	Torque acting about local y axes
T_z	Torque acting about local z axes
v	Inbound vertical velocity of ball (Daish impact model specifically)
v'	Rebound vertical velocity of ball (Daish impact model specifically)
v_{angx}	Velocity of impact point in local x direction due to angular velocity
v_{angy}	Velocity of impact point in local x direction due to angular velocity
v_{angz}	Velocity of impact point in local x direction due to angular velocity
V_{ang}	Global velocity vector of impact point due to angular movement only
v_b	Inbound velocity of ball
v'_b	Rebound velocity of ball
V_{COM}	Global velocity vector of racket centre of mass
v_{IP}	Inbound velocity of impact point
v'_{IP}	Rebound velocity of impact point
V_{IP}	Global velocity vector of impact point
v_r	Inbound velocity of racket
v'_r	Rebound velocity of racket
κ	Compression factor
θ	Angle between resultant ball force and straight line distance c
ω	Inbound spin of ball
ω'	Rebound spin of ball
ω_l	Angular velocity in swingwise direction

ω_2	Angular velocity in twistwise direction
ω_3	Angular velocity in spinwise direction
ω_x	Swingwise angular velocity of racket
ω_y	Twistwise angular velocity of racket
ω_z	Spinwise angular velocity of racket

This Thesis is Dedicated to Timmy O'Toole,
who fell down the well.

1 Introduction

The following chapters describe a three year study into the dynamics of a tennis impact. Specifically, this involves the racket movements exhibited by professional players at impact and methods of modelling such an interaction.

1.1 Study Motivation

The modern era of tennis arguably began with the introduction of the oversized racket in 1975. The larger head size and higher stiffness of the newer rackets resulted in a corresponding increase in serve velocities and game speed. Since this time the onus has been on the International Tennis Federation (ITF) to govern future progression in playing equipment. Such governance is felt to be necessary in order to preserve the essence of the game.

Some argue that the opportunity for governance has been missed. This attitude was perhaps epitomised by Jim Baugh, President of Wilson Sporting Goods when commenting in 1996. *"The actions the ITF is taking for the professional game is too late. The pro's that are playing today are playing with rackets from ten years ago. The goals of the Wilson's, Prince's and Dunlop's are to bring up new kids and have them start out with the latest technology frames. That would mean in five to ten years we are going to have young pro players with very large, stiff, head heavy rackets. Then that power level would reach the pro game in the years to come..... So my fear is that in five to ten years the professional game may be too quick."* Coe **2000**. This fear, echoed by many commentators over the years is that excessive speed will lead to a game dominated by the serve. Shorter rallies and less exciting games would inevitably lead to lower viewing figures.

In the men's grand slam tournaments, the average speed of serves has continued to rise since Baugh commented on the game. However the number of aces has continued to reduce after a peak in the year 2000, Miller **2007**. Instead of dwindling, spectator enthusiasm has thrived since the turn of the century. In 2007, 444,810 people attended the Wimbledon grand slam tournament with a one day record of 30,137 being set on the second Saturday. Whilst the modern game may not be as fast as feared, the ITF has nevertheless adopted a role of constant investigation into the physical principles underlying tennis and the equipment involved.

Much of the investigative work is centred on the impact between ball and racket. In order to conduct such experiments reliably, knowledge of the likely input parameters is necessary. This includes likely relative velocities at which impact takes place and probable impact positions and racket orientations. An impact model developed by Goodwill **2002** has been used by the ITF to predict resultant ball velocities for impacts along the longitudinal axis of the racket. Whilst this model contains an extensively validated ball/stringbed model, it is limited in terms of ball impact position on the racket, and inbound ball angle. Each impact is set perpendicular to the racket face and along the racket's longitudinal axis. Such a model is

very useful in making objective comparisons between particular balls and rackets. However, in practice, a player will very rarely perform an impact in which the racket is perpendicular to the ball. Even the best player will occasionally hit the ball off the longitudinal axis of the racket. Further work is therefore required in order to mathematically predict the post-impact ball velocities and spins from a realistic shot. Such a model would allow the ITF to assess accurately what effect particular equipment developments may have on the speed and nature of the game of tennis.

1.2 Aims and Objectives

The overall aim of this study was to develop an accurate predictive model which is not restricted in terms of ball/racket movement. This model should be validated using accurate experimental data based on realistic player shot values.

This aim shall be achieved through meeting a number of objectives divided into three main sub-sections.

1. *Literature review*
   - To compile a review of previous work relevant to this study.
2. *Player shot characteristics:* Obtaining the movement of the racket and ball close to impact requires a number of distinct steps.
   - To select and develop an appropriate analysis methodology.
   - To develop said method into a specific player shot analysis protocol and methodology.
   - To analyse any obtained data in order to extract accurate and useful ball and racket motion.
3. *Predictive model:* The overall objective of this study was to produce a model of the impact between a tennis ball and realistically supported tennis racket. It must be capable of simulating the complete dynamic response of the ball/racket for typical tennis shots. Achieving the following objectives are necessary:
   - To develop an impact methodology capable of fully recording a series of realistic impacts between a ball and racket.
   - To be able to fully recreate the motion of the ball and racket through analysis of recorded data.
   - To utilise a method capable of finding trends and relationships within obtained ball/racket motion data.
   - To develop a predictive model capable of recreating all aspects of a realistic shot.
   - To validate the predictive model using the experimentally based motion data.
   - To investigate the player shot analysis using the validated predictive model.

2 Literature Review

2.1 Introduction

Lord Rayleigh's account of the irregular flight of a tennis ball (Rayleigh **1877**) is the earliest example of a scientific investigation into the world of tennis. Published in 1877 the paper is almost as old as the game itself. Since then, understanding the physical principles governing tennis has become a greatly expanded field. Tennis science is now used to market tennis equipment, form the rules of the game and further scientific knowledge. Interest in tennis as a scientific pursuit has greatly increased since the introduction of the oversized racket first patented by Head **1975**. After 100 years of very little change, the modern game is now a compromise between player performance and spectator enjoyment. As such, much of the scientific investigation is divided between developing equipment and furthering understanding.

Much of the work into tennis has been duplicated, which has led to firmly established conclusions or contradicting findings.

This study is an investigation into the impact between a ball and racket in six degrees of freedom i.e. translation and rotation along and about three orthogonal axes. This chapter aims to review the current literature with regards to such an investigation. Beginning with a look at the fundamentals of tennis; the ball and racket, this chapter goes on to look at player motion, including previous examples of athlete testing and current methods of capturing player data. The final sections look at earlier attempts at impact modelling and the tools used to develop them.

2.2 The Ball

The rules of tennis (ITF **2007c**) state that any ball approved for competitive play must fall within strict bounds for mass, size and bounce height. In 2000 three different types of ball were introduced, each with a different pace rating. The medium (type 2) ball had exactly the same specification as all balls prior to 2000. The fast (type 1) ball was designed to be harder and bounce lower. The slow (type 3) ball was designed to be 6% larger in diameter and decelerate more as the ball travels through the air.

Capel-Davies **2007** states that since their introduction, usage of the type 1 and type 3 balls has been minimal. For this reason only type 2 balls will be considered in this study.

Any manufactured type 2 ball must fall within the following bounds:

- *Mass:* Between 56.0 and 59.4 grams
- *Size:* Between 65.41 and 68.58 mm in diameter
- *Bounce:* Bounce more than 134.62 cm but less than 147.32 cm when dropped from a height of 254.00 cm.

Two manufacturing methods are used in order to achieve the requisite bounce properties:

1) A pressurised ball contains a volume of pressurised air within two halves of a rubber core.

2) A pressureless ball uses a stiffer rubber core, or a core filled with foam.

Pressurised balls lose their bounce properties over time as the porous core drops in pressure, a disadvantage which pressureless balls avoid. When using tennis balls in laboratory testing it is essential that ball properties are as homogenous as possible. Thomson **2000** tested a series of tennis balls by compressing them between two flat plates, over a distance of 30 mm. It was found that tennis balls can be considered homogenous and that pressurised balls are stiffer than pressureless balls when compressed over this distance. Goodwill **2002** fired type 3, type 2 (pressurised and pressureless) and punctured tennis balls normally at a force platform. The force platform was used to measure contact time and force throughout impact. A set of light gates were used to measure inbound and outbound velocity. The pressureless ball had a rebound ball velocity around 7% lower than the pressurised balls at high velocities. The measured contact time and ball deformation was also higher, suggesting that pressureless balls are less stiff at typical game velocities.

Koziol and Reed **1978** measured the pressure loss in standard pressurised tennis balls in order to justify a patent for a pressurised ball type which minimises pressure loss. The pressure loss of a standard ball was measured as 23% over a period of 236 days. Although the pressure loss was significant, the time period was also prolonged. A player rarely uses a ball for longer than a single set in competitive play, therefore the pressure loss during this period will be negligible. The biggest determining factor in the degradation of ball bounce properties in standard play is the effect of repeated impact.

Miller and Messner **2003** fired tennis balls at a solid surface at 20 ms^{-1} and 40 ms^{-1}. The inbound and outbound velocity was measured using a set of light gates. The coefficient of restitution (outbound velocity divided by inbound velocity) was calculated for each impact. The ITF rules for bounce height represent a coefficient of restitution value of between 0.73 to 0.76 for inbound velocities of around 8 ms^{-1}. This value drops to 0.575 at inbound velocities of 20 ms^{-1} and 0.40 at 45 ms^{-1}. This reveals the variable dynamic properties of a tennis ball depending on the inbound ball velocity. In agreement with Thomson **2000** and Goodwill **2002** this testing also showed that pressureless balls tend to be less stiff than pressurised balls at higher velocities and deformations. Wear of the tennis ball was simulated by repeatedly firing a ball at a surface inclined at 15° at a speed of 20 ms^{-1}. The coefficient of restitution of balls was tested after being fired 50, 100, 150 and 300 times. At 20 ms^{-1} there was very little difference in the coefficient of restitution for balls fired 50, 100 and 150 times. Only for balls fired 300 times did a difference in coefficient of restitution become apparent. At 40 ms-1 a

difference in coefficient of restitution became apparent at only 100 impacts. In competitive play balls are changed every 9 games, with 6 balls in play at one time. It is player choice as to which of the six balls is in play at any one time. Miller argues that it is not unreasonable to assume that 1 or 2 balls could have undergone around 100 impacts, therefore exhibiting different characteristics at higher velocity.

Felt wear can also change the characteristics of the ball, specifically its flight through the air. Chadwick and Haake **2000** used a wind tunnel to measure the drag coefficient of unused tennis balls and balls which had had their felt shaved. It was found that the drag coefficient was around 6% lower with shaved felt. Goodwill and Haake **2004a** measured the drag and lift coefficient of tennis balls which were spinning at 2750 rpm. Balls were artificially worn using the same apparatus as Miller and Messner **2003**. In this case balls underwent 0, 60, 500, 1000 and 1500 impacts. This is considerably more than Miller argued a ball would undergo during competitive play. Heavily worn balls were found to have a drag coefficient around 5% lower than an unworn ball. The lift generated by a spinning ball was also found to be reduced. The overall effect resulted in the receiver having around 1.5% less reaction time which could significantly affect the outcome of a point. Although the number of impacts in this testing was significantly higher than a tennis ball would experience in real play, the racket and court surface may cause a similar amount of wear, resulting in the drag and lift reductions stated above.

2.3 The Racket

Haake **2007** outlines the progression of tennis racket technology and trends in size and shape. The earliest tennis rackets were made from solid wood which was steamed and pressed into shape. As these rackets were adapted from those used in *real* or *royal* tennis they had bent heads which were necessary to reach into the corners of the court. As lawn tennis grew in popularity, production moved away from small workshops and onto the production line. Rackets became symmetrical and were made from many thin veneers of laminated wood. This increased the strength/weight ratio and allowed manufacturers to mix wood types to incorporate different properties into the racket, ITF **2007b**. Over time the dimensions of the wooden racket became standardised to a length of around 685 mm, a mass typically around 350 g and a headsize of 80 in^2.

Alternative frame materials had been experimented with as early as the 1930's but couldn't improve on the existing design. It wasn't until the introduction of an oversize aluminium racket by Head **1975** that the frame could be made bigger without sacrificing stiffness. Such was the impact of this design that it prompted a rule change by the International Tennis Federation. Before 1981 any material could be used to construct the racket and it could be any size or shape. The current rules, as stated by ITF **2007c**:

The frame of the racket shall not exceed 29.0 inches (73.7 cm) in overall length, including the handle. The frame of the racket shall not exceed 12.5 inches (31.7 cm) in overall

width. The hitting surface shall not exceed 15.5 inches (39.4 cm) in overall length, and 11.5 inches (29.2 cm) in overall width.

Modern rackets are constructed from graphite based composite materials and come in a wide variety of masses and head sizes. Figure 2.1 shows an example of an early tennis racket, a typical wood racket and a modern graphite racket.

Figure 2.1. Three racket examples, an early racket with a bent head (left), a traditional laminated wooden racket (centre) and modern composite racket (right).

Specific terms are commonly used to describe certain points or areas of a racket's anatomy, Figure 2.2 shows the terms and their described regions as given by Brody et al. **2002**.

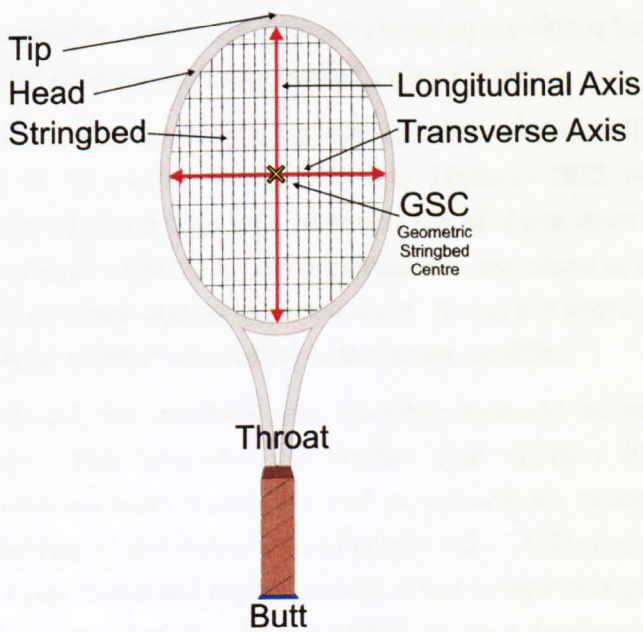

Figure 2.2. Nomenclature of racket terms.

The rule change in tennis coincided with an explosion in scientific tennis research. With new materials and racket sizes available, much work was put into investigating the effects of different racket mass, stiffness and head size.

2.3.1 Simulating Player Grip

In order to assess the performance of a tennis racket, controlled repeatable tests must be carried out. Whilst the most realistic impact conditions come from testing an actual player, it is very difficult to obtain repeatable impact positions and speeds. Also, accurate measurement of these parameters is very difficult and costly in terms of time and equipment. In order to investigate fully the effect of different input parameters complete control over every variable is desirable.

If an impact system is reduced to a ball and racket, it is essential that the interface between the racket and player is correctly simulated. Five types of handle support have been used to simulate a player's grip in the laboratory, and these are listed below.

1) Hand-Held: In this form it is difficult to regulate grip strength and reliably generate shot conditions.

2) Freely Supported: In this case the racket's motion is not constrained in any way.

3) Handle-Pivoted: A racket supported by a pivot near the handle. After impact the racket is free to rotate about this point.

4) Handle Clamped: The handle is clamped such that no translation or rotation around the handle can take place.

5) *Head Clamped:* The head of the racket is clamped such that no movement can take place, effectively isolating the stringbed.

It was vital to establish what effect different clamping conditions had on the post-impact ball velocity and which condition best represented a player's grip.

It was commonly taught that a firm grip and set wrist improves ball rebound velocity by reducing the recoil of the racket. Broer **1973** and Tilmanis **1975** being two examples. Plagenhoef **1970** claimed that a firm grip increased the effective mass of the racket hence increasing the effectiveness of the shot. These publications are aimed at the recreational level player and are based on observational evidence alone. It was not stated what type of shot is improved by a firm grip, whether it is central to the racket, or offset.

Hatze **1976** claimed that increased grip tightness increased the rebound ball velocity from racket/ball impact. This conclusion was reached from validated theoretical analysis. A simplified, one dimensional beam model was used to represent the racket frame. In doing so, ball impacts were limited to the racket's longitudinal axis. A Dunlop Maxply racket was modelled using the beam model and experimentally tested using strain gauges to measure the impulse of impact. It was stated that the model was in good agreement with experimental data. The results showed that the impulse increased by 10 to 15% by gripping the racket tightly as opposed to loosely. From this Hatze concluded that shot power could be increased by tightly gripping the racket, the rebound ball velocity was not measured to confirm this. The impulse values obtained in this experiment showed that it is impossible to prevent racket

recoil by tightly gripping the racket. The forces and torques generated during impact are 16 times what can realistically be exerted by the hand.

Watanabe et al. **1979** provided evidence that grip conditions have little affect on the ball rebound velocity, a finding which was built on by other authors and provided the rational basis for many freely suspended racket impact tests performed since. The coefficient of restitution (COR) of a ball was measured by tracking its velocity prior to and after impact using a high speed camera. The ball was fired at a tennis racket when hand-held, handle clamped and freely suspended. It was seen that the COR value was independent of grip condition, directly contradicting Broer **1973**, Tilmanis **1975**, Plagenhoef **1970** and Hatze **1976**. The reason that the gripping method has no effect is due to the time taken for the impulse to travel along the racket. The time for the impulse to travel from the ball impact position to the racket butt and then return to the point of impact is longer than the duration of impact itself. Therefore the grip conditions are unable to affect the post-impact ball velocity. It should be noted that the speed of impulse propagation is dependent on the fundamental frequency of the racket. The grip has no effect in wooden rackets of the type used by Watanabe, where the fundamental frequency is generally less than 100 Hz. Modern rackets are considerably stiffer, exceptionally stiff rackets (with fundamental frequencies around 200 Hz) have been observed to behave differently for impacts close to the racket throat. The time period of the fundamental mode is similar (or shorter) to the contact time, hence no vibrations are excited, as shown in Brody et al. **2002**. The conclusions described above are only valid for impacts along the racket's longitudinal axis. For impacts off this axis, a moment impulse is applied to the racket and the gripping condition may effect the ball rebound velocity.

Elliott **1982** experimentally tested the effect of racket grip using a pneumatic arm. Three levels of grip firmness were used in the experiment; light, medium and tight. The corresponding forces for each of the grip levels were measured using a racket equipped with force transducers. A college level tennis player was asked to grip the racket very lightly, moderately and tightly. These grip levels were replicated in the pneumatic arm which was then used to swing a racket at 7 ms^{-1}. A ball was projected at the racket in four locations; the geometric stringbed centre (GSC), ± 5 cm above and below the GSC and 5 cm offset. A 7% increase in ball rebound velocity was observed at tight grip levels, this was determined to be statistically insignificant. However, a 20% increase in ball rebound velocity was observed at tight grip levels for offset impacts. From this it was concluded that a tighter grip is beneficial in order to maximise ball rebound velocity as a player cannot always hit the ball along the racket's central axis. However, grip was simulated using four tension bolts placed at intervals along the rackets shaft. The position of these bolts did not correspond to the likely position of a player's grip. As a result the proportion of the racket under free vibration was considerably smaller in the experiments by Elliott than might be the case under realistic conditions. This may explain the results observed by Elliott and also cast doubt on the relevance of this experiment in accounting for a player's grip.

Baker and Putnam **1979** also compared handle clamped and freely standing conditions. Ball impacts on stationary freely supported and handle clamped rackets (strung at 178-267N) were recorded using high speed video. After testing different racket and stringing combinations, clamping conditions were found to have no effect on ball rebound velocity. It was noted that a difference was observed for impacts off the racket's longitudinal axis. It was concluded that the change in ball trajectory was due to high rotational displacements for the freely suspended condition. More extreme conditions were used to compare ball velocity than in the study by Elliott **1982**. Baker used freely supported and handle clamped, whilst Elliott used three degrees of grip tightness. In the experiment by Elliott, the grip was never low enough to count as freely supported or pivoted, yet never tight enough to be classed as clamped.

Hatze **1993** made a further attempt to simulate a player's grip when developing an experimental rig dubbed the 'manusimulator'. The manusimulator was a device simulating a player's arm in mass, joint location and damping properties and is described fully in Hatze **1992**. The rebound ball velocity of impacts with a handle clamped racket and racket secured in the manusimulator was measured. It was found that the manusimulator gave ball rebound velocities around 5-10% higher than the handle clamped condition. These results led Hatze to the conclusion that grip condition affects ball rebound velocity. The reasoning here is somewhat reversed. According to the results, a hand gripped racket gives a *higher* result than a handle clamped racket. This contradicts the findings of Hatze **1976** and Elliott **1982**. It is doubtful whether the grip simulated in this experiment truly represented the *firm* grip which was intended.

Cross **1999b** performed a theoretical analysis of the effect of grip conditions using a one dimensional flexible beam model. Handle clamped, handle pivoted and freely suspended grip conditions were assessed. All three methods of grip gave almost identical results over the majority of the stringbed. For impacts within around 100 mm of the throat, the handle clamped condition gave fractionally higher rebound ball velocity values. The freely supported and handle pivoted conditions gave very similar values for every point along the longitudinal axis of the racket.

Another method of analysing grip condition is to scrutinise the vibrational response of the racket.

The shapes of the first mode of vibration of a handle clamped and freely supported racket are equivalent to a cantilever and free beam respectively. These mode shapes are shown in figure 2.3.

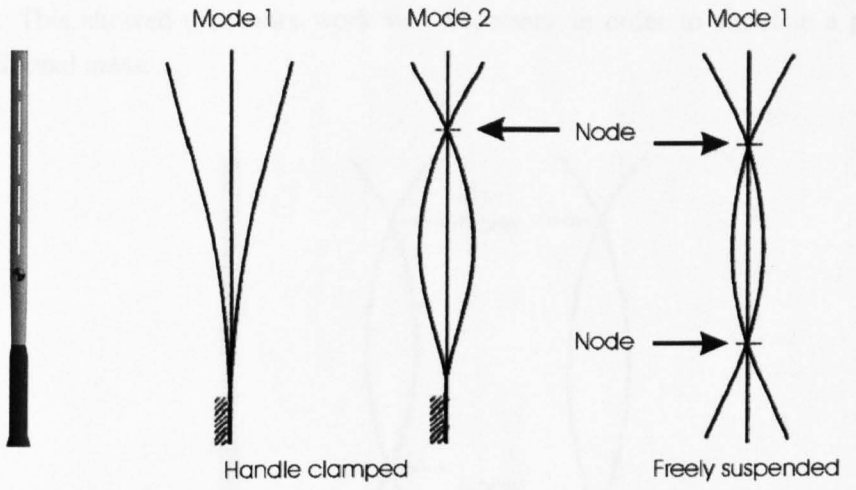

Figure 2.3. The first and second mode of a handle clamped racket and the first mode of a freely supported racket.

Brody **1981** commented on the difference in the first mode of vibration of handle clamped and freely supported rackets. The fundamental frequency of the handle clamped racket was reported as being typically 25-40 Hz, the second mode was between 127 and 168 Hz. The second mode value of 127 to 168 Hz is very similar to the fundamental frequency of a freely supported racket. It is also illustrated in figure 2.3 that the position of the node points for a handle clamped and freely supported racket is very similar. From this Brody dismissed the importance of mode shapes and vibration frequencies between the two grip conditions. In practice the ball will behave very similar for both handle clamped and freely suspended conditions.

Brody **1987a** extended the above analysis to look at the vibrational response of a hand held racket. A thin piezoelectric film was attached to a racket handle and struck at various points along its longitudinal axis. This was done in order to find the racket node point positions and induced vibration frequencies. This testing showed that the cantilever, handle clamped mode of vibration does not occur in a hand-held racket. The measured frequency of oscillation was much closer to that of a freely suspended racket.

Cross **1998** further compared the racket response under freely supported and hand-held conditions. Piezoelectric transducers were added to several points along a racket in order to ascertain vibration frequency, mode shape and node location. The fundamental frequency of a freely supported and hand-held racket was measured as 109 and 102 Hz respectively. When hand held the node point of the racket at the handle end of the racket moved 10 cm toward the handle, as illustrated in figure 2.4. The fundamental frequencies of a hand-held racket closely matched that of a freely supported racket rather than handle clamped. It was found that adding a 40 g mass to the racket handle of a freely supported racket lowered the fundamental frequency to 103 Hz, closely matching the hand-held value. However, an additional 80 g had to be added in order to achieve the same shift in node position as observed for the hand-held

condition. This showed that more work was necessary in order to simulate a player's grip using additional mass.

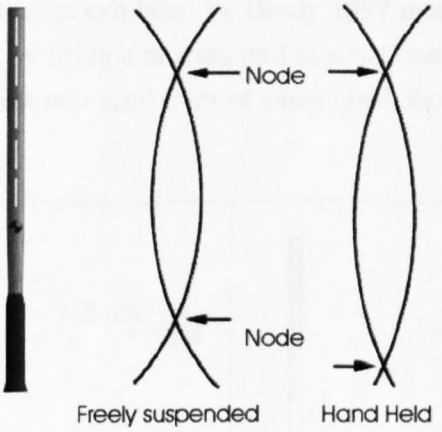

Figure 2.4. The difference in handle end node point for a freely supported and hand-held racket condition.

Brody **1979** provided an explanation of why grip conditions may be irrelevant. The contact time of the ball on the stringbed and half period of oscillation of several rackets were measured. Whilst the contact time was found to be around 4.5 – 6.8 ms the frequency of racket oscillation was such that the ball had left the stringbed before the racket had completed an oscillation. A number of rackets were used including two metal framed rackets with fundamental frequencies of around 160 Hz. This work was concerned with how racket stiffness may be increased in order to maximise ball velocity but this finding can be similarly applied to the effect of grip conditions. Brody states that a ball has left the stringbed before the racket 'snaps' back from impact. Any particular conditions acting at the racket handle do not have chance to influence the ball trajectory before it leaves the stringbed. Although the measured contact time was for a ball dropped from a height of only 1 m, Goodwill **2002** notes that ball impact time is relatively independent of impact velocity. This analysis suggests that the stiffer the racket and shorter the half period of oscillation the more relevant the grip condition becomes.

Cross **1998** investigated the idea of wave propagation in more detail by considering higher modes of vibration. A series of piezoelectric transducers were placed at 50 mm increments along the frame. The time measured for an impulse to travel from the stringbed centre to a point 120 mm from the butt was 1.5 ms. This time is much shorter than the duration of impact and is due to higher orders of vibration which are also excited at impact. Higher order vibrations have a much higher frequency and hence travel much faster along the racket frame. They are also excited at much lower amplitude and hence are not as significant as the fundamental frequency. Higher orders of vibration possess a much smaller fraction of the energy, and therefore do not significantly affect the ball rebound velocity.

2.3.2 Racket Impact Testing

A freely supported racket may be the most suitable condition to use when simulating a hand-held grip, but it is very difficult to recreate true racket motion experimentally. A simple change of the reference frame as exhibited by Brody **1997** means that any potential impact conditions can be recreated by firing a moving ball at a stationary racket this as illustrated in figure 2.5. A stationary racket was used in most cases cited above in order to investigate the effect of grip.

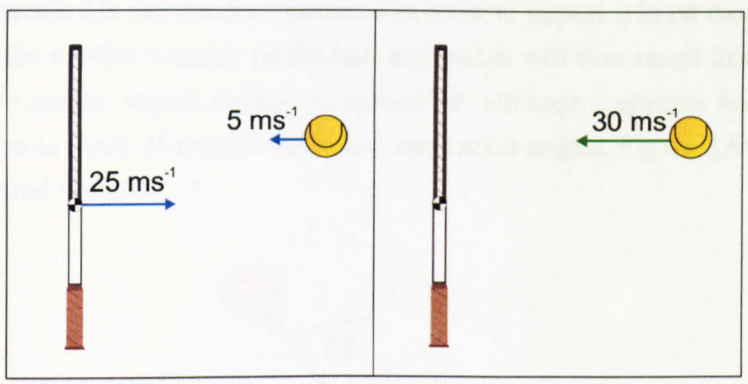

Figure 2.5. A change of reference can be used to calculate appropriate velocity values for a stationary racket impact.

Mitchell et al. **2000a** fired a ball at 35 ms^{-1} at a stationary, freely supported racket in order to simulate a player's serve. Goodwill **2002** recreated normal racket impacts by hanging a racket on a pin and firing a ball at different positions along the longitudinal axis using a compressed air cannon.

Ball Projection Devices

Goodwill used a compressed air cannon in order to achieve sufficiently high ball velocities that reflect realistic impact conditions. It was noted that previous tests such as Brody **1979** performed racket impact testing by simply dropping the ball onto the racket. This method limits maximum ball velocity to around 7 ms^{-1}. It is also difficult to control impact location and spin using this method. An air cannon can generate ball speeds in excess of 40 ms^{-1} with zero spin. An accurately machined barrel also grants greater control over the impact position although Goodwill quotes no figures for accuracy.

Alternatively, Elliott and Blanksby **1980** used a commercial ball firing mechanism to test the rebound velocity and vibration characteristics of normal and oversized rackets. Two rotating wheels projected a ball at a handle clamped racket at 21 ms^{-1}. Elliott quotes velocity variations of ± 2% and accuracy of ± 1.2 cm over the distance tested. An added advantage of a ball projection device is that the wheels can be rotated at different speeds in order to generate spin. Generally such devices lack a barrel, meaning that impact accuracy may be lower than an air cannon.

Recreating Realistic Shot Conditions

Generally, racket impact testing has been restricted to varying impact position along the longitudinal axis, normal to the racket face. This is the case in Brody **1979**, Elliott and Blanksby **1980** and Goodwill **2002**. These conditions are useful for investigating objective racket behaviour such as vibrational response or rebound ball velocity. However, other than the tennis serve, a normal impact cannot be said to best represent realistic shot conditions. Knudson **2006** gives an overview of biomechanical shot technique. A continuous upward stroke is recommended in the standard forehand in order to impart spin on the ball. As such, it is unlikely that the relative velocity of the ball and racket will ever result in a purely normal impact. Knudson quotes 'impact angles' of around 30° although a specific breakdown of this value is not given in terms of relative velocities and racket angles. Figure 2.6 shows how this angle is represented visually.

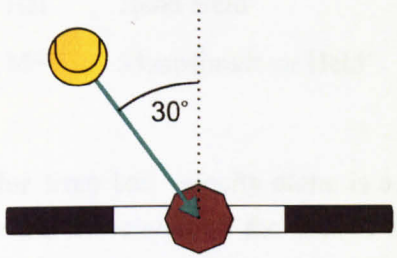

Figure 2.6. how an impact angle of 30° is represented visually

Realistic shot conditions can be created experimentally by changing the impact position on the racket and the relative orientation of the racket and inbound ball. Knudson **1993** investigated how string tension and impact location affect ball rebound accuracy. A racket was held stationary, clamped at the handle and balls were fired at it from a ball projection device. Balls were fired at the stringbed centre and 8 cm off the longitudinal axis at a mean angle of 25.4° from the normal. The angle of impact went some way to recreate more realistic shot conditions. The handle clamped racket may not truly represent grip conditions as described above, although it is unknown how grip is best simulated for offset impacts.

It is clear from this work that in order to accurately recreate shot conditions in a repeatable impact test, the shot conditions of a player must be accurately quantified. This is discussed in more detail in section 2.5.

2.3.3 Coefficient of Restitution of a Racket/Ball Impact

The coefficient of restitution (COR) is defined as the ratio of the restoration impulse magnitude to the deformation impulse magnitude between two bodies (Kotze et al. **2000**). With regards to a racket/ball impact, the COR can be simply defined as the ratio of their respective velocities before and after impact (Daish **1972**)

$$COR = \frac{v_r' - v_b'}{v_b - v_r} \qquad [2.1]$$

Confusion arises in this definition in that many different conditions can be used in which to measure the value. For example, when a racket is hand-held a player may accelerate the racket after impact bringing ambiguity into the result. The COR value itself does not reveal any further information regarding the mechanisms of impact. Despite this, investigations into what factors affect COR have proved to be valuable research from which many conclusions have been drawn.

In the following section the following suffixes are used corresponding to the manner in which the COR value was obtained:

FS	Freely Supported
GC	Grip Clamped
HC	Head Clamped
HH	Hand Held
MS	Manusimulator Held

Measuring the COR value from ball velocity alone is a commonly used experimental practice, because it discounts the movement of the racket. It was later referred to as the apparent coefficient of restitution (ACOR) in Hatze **1993**. The ACOR value is only valid in impacts where the racket is stationary prior to impact.

As evidence for a patent application, Head **1975** fired tennis balls at a stationary racket at up to 27 ms^{-1}. The racket was handle clamped and the balls were fired with zero spin from a compressed air cannon. The ball was fired at a number of locations on the stringbed of a traditional wooden framed racket and the aluminium framed racket specified in the patent.

High speed video was used to obtain the impact position and inbound and outbound ball velocities. In this testing only the ball velocity was used in order to calculate the coefficient of restitution which simplifies equation 2.1 to:

$$ACOR_{GC} = \frac{v_b'}{v_b} \qquad [2.2]$$

Head found that not only were the COR_{GC} values higher for the larger headed racket tested, but $ACOR_{GC}$ values are higher over a larger overall region. Figure 2.6 depicts the comparative $ACOR_{GC}$ values over the face of a traditional and oversized racket. Higher $ACOR_{GC}$ values are present the closer the impact to the throat of the racket. It can be seen from figure 2.8 that the zones are substantially larger for the larger headed racket. Referring back to the beginning of this section, this evidence gives an insight into why the ITF felt compelled to restrict the size of the racket head. To quote from the patent application.

'It is clear that the largest possible zone of high coefficient of restitution will be of great advantage to a tennis player. His return shots will then have more velocity with the same

power of swing, or alternatively he can slow down his swing for greater control and still obtain satisfactory velocity on his return shot'.

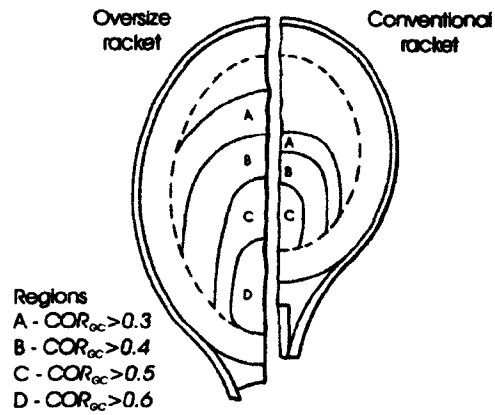

Figure 2.8. The zones of COR as given by Head **1975**.

Elliott and Blanksby **1980** reached similar conclusions to Head **1975** by assessing the ball rebound velocity for impacts at several locations along a racket's longitudinal axis and transverse axis. $ACOR_{HH}$ values varied from close to zero at the tip of the racket to a maximum approximately 2 cm before the throat. A significant drop in $ACOR_{HH}$ value was observed as the impact position moved along the transverse axis of the racket. In this experiment, the racket was hand-held which suggests that the racket twists in the hand during impact, supporting the claim made by Hatze **1976**. The ACOR values obtained in the experiment were significantly lower than those obtained by Head **1975**, especially along the racket's transverse axis. Head claimed that the wider racket proposed in his patent would increase the rebound velocity for off centre impacts. The increased polar moment of inertia of the wider racket was claimed to rotate less during impact, increasing ball rebound velocity and decreasing the angular deviation after impact. The lower values observed by Elliott and Blanksby **1980** support this claim, although it was stated specifically that measuring the moment of inertia values was beyond the scope of the paper.

In stationary racket conditions, the method used to clamp the racket can significantly affect the measured outcome. Brody **1979** quoted COR_{HC} values of around 0.85 when testing several head clamped rackets. The COR_{HC} value was assessed by dropping a ball from 3.7 m onto the stringbed of a head clamped racket. In a head clamped racket, no energy is transferred into the racket frame so the ball rebounds with a higher ball velocity. Head clamped testing is especially useful in assessing the effect of different string parameters. Goodwill **2002** made use of head-clamped testing in order to isolate the stringbed when developing a viscoelastic ball/stringbed model. However, COR_{HC} values obtained during head clamped testing do not represent a good measure of the racket's effectiveness. Although head clamping significantly affects ball rebound velocity, Watanabe et al. **1979** showed that handle

clamping a racket has little effect on the ball rebound velocity. This has been discussed in more detail earlier in this section.

Hatze **1992** accounted for the difference between head clamped and handle clamped/freely supported COR testing. The ACOR and COR values were clearly distinguished. Using a high speed camera, COR_{MS} values were obtained for ball impacts against a racket held in the manusimulator device discussed earlier in this section. As might be expected, when accounting for racket movement COR_{MS} values of between 0.758 and 0.885 were observed. These values tally very closely with the COR_{HC} values obtained by Brody **1979**. Other energy losses resulting from impact, such as frame vibration, which can't be measured using a high speed camera and aren't present in a head clamped impact, explain why the value is lower in some cases.

From this it seems that COR_{HC} testing can be used to obtain approximate COR_{FS} values. This method does not account for energy lost through frame vibration. This is a fair approximation as most energy loss is due to ball deformation. Brody **1997** utilised this approximation in order to predict COR_{FS} values. A simple rigid body model of a racket and the head clamped COR_{HC} value was used to predict post-impact ball velocities. Whilst good correlation was seen in the middle of the stringbed, the predictions became less accurate at the tip and throat of the racket. This shows that the COR_{HC} value is only so effective at being used to predict energy losses. For impacts towards the tip and throat of the racket, frame vibrations become larger in amplitude and represent a greater proportion of the lost energy.

Brody et al. **2002** describes the utilisation of a concept called the *effective mass*. The effective mass can be described as the striking mass of a specific impact point. The effective mass of a point is dependent on the moment of inertia of the racket (I) and distance from the COM to the impact point (b) and can be described as:

$$m_e = \frac{IM}{I + Mb^2} \qquad [2.3]$$

The concept of effective mass allows the impact to be reduced to a calculation between two point masses. This relies on a simple rigid body assumption and is subject to inaccuracies resulting from neglecting frame vibration. Despite this, Brody et al. **2002** describe a simple method to predict the ACOR value of a racket from the effective mass and COR_{FS} value (which can be obtained using head clamped impact testing described above).

$$e_A = \frac{e \cdot m_e - m}{m_e + m} \qquad [2.4]$$

where e_A is the ACOR, e the COR and M_e the effective mass value of the impact point.

Equation 2.4 was used to explore simple perpendicular impact mechanics. Two interesting results are obtained when m_e is equal to M and when m_e is equal to m. In the first case, the effective mass is equal to the mass of the racket (an impact on the COM) and the ACOR is the maximum for the racket/ball system. In the second case the ACOR is equal to 0

(an impact towards the tip of the racket) such that a ball inbound at a stationary racket will have no rebound velocity after impact. These two cases correspond to two *sweet spots* which are discussed later in this section.

2.3.4 The Sweet Spots of a Racket

Published research and marketing literature commonly refer to the concept of a *sweet spot*. The definition of this term is muddied by that fact that very diverse claims are often made about what the sweet spot does and where it is situated. From a marketing viewpoint it is better to refer to a region rather than a specific point. The larger the region the better the racket may appear to prospective purchasers. The term sweet spot or region came into common use with the introduction of the racket designed by Head **1975** discussed above. Head claimed that the sweet region on his larger racket was four times larger than that of a more traditional wooden racket. In this case the region was defined by having an ACOR above a certain value.

Brody **1981** recognised the sweet spot as a distinct point on the racket face which varies in location depending on the required outcome of impact. Sweet spots could be identified as a point which when hit resulted in minimum discomfort to the hand, or maximum ball rebound velocity. Three sweet spot locations were indentified which were later expanded to four by Cross **1997**. Brody and Roetert **2004** clarified this situation by later identifying four distinct points on the racket face, but noting that only three points are *sweet* during any particular shot. Two of the four points share the definition of a *sweet spot* dependent on the type of shot being played.

Brody **1979** originally defined the sweet spot as the *centre of percussion* (COP), a point on the racket face which when hit results in an instantaneous point of rotation about the wrist. As a result, the hand experiences no jarring effect at impact. Figure 2.9 illustrates how the summation of translation and rotation about the COM results in instantaneous rotation about the wrist or handle end.

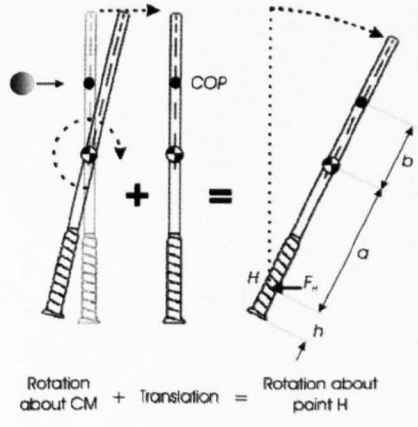

Figure 2.9. An impact at the COP results in instantaneous rotation about the wrist.

Brody **1979** showed that the distance of the COP from the COM (b) can be calculated as:

$$b = \frac{I}{a \cdot M} \qquad [2.5]$$

It can be seen from equation 2.5 that not only does the location of the COP depend on the mass and moment of inertia of the racket being used, but also on where it is gripped, which alters the value a.

The COP gives an easily calculated point which can be used to increase comfort during a tennis impact. Hatze **1998**, argued that such an analysis is overly simplistic. Due to forces and torques exhibited by the hand such a sweet spot does not exist in realistic play conditions. Hatze **1994** had earlier shown that a player is much more likely to hit the *node point* during play. The impact points of nine players were recorded using high speed video and a probability density function calculated according to the results. A region centred on the node point of the racket face received 80% of all recorded impacts. It could be argued that the node point is the most likely point of impact due to it being located at the stringbed centre in the majority of cases.

Brody **1981** described the node point according to the first mode of vibration of a vibrating beam. The relative position of these node points can be seen in figure 2.4, from which it can be seen that only one is situated on the racket stringbed. An impact on the node point will not excite the particular mode of vibration to which it corresponds. The amplitude of the first mode of vibration in a tennis racket is considerably larger than any higher mode. This led Brody to conclude that a player will not experience any vibration at the hand when hitting the ball on the node point.

Brody **1995** confirmed the relevance of the node point as a sweet spot by measuring handle vibration using a piezoelectric transducer. The racket was hit at several points along the longitudinal axis. Figure 2.10 shows clearly the existence of the node point near the centre of the stringbed.

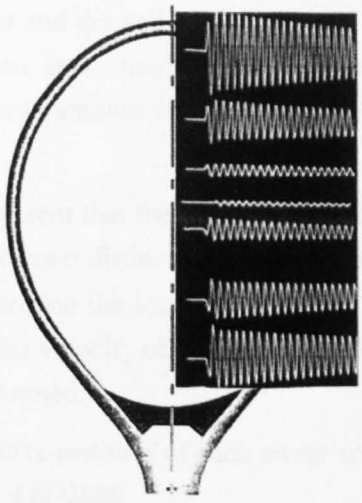

Figure 2.10. The handle vibrations as measured by a piezoelectric transducer for ball impacts at several points along the racket's longitudinal axis.

Cross **1998** experimentally investigated the node point of a racket and noted that its position is affected when the racket is hand-held. It was noted that the force acting on the hand was a minimum for an impact at the stringbed centre close to the node point. This was due to a lack of vibration. The force acting on the forearm during impact was also measured. In this case an impact at the COP showed the least recorded force.

The third sweet spot is perhaps much more relevant in competitive play and was originally defined by Head **1975**. That is, the point on the stringbed which results in the highest post-impact ball velocity. Head argued that the sweet spot is therefore in a region on the stringbed with a high ACOR value. It has been stated previously that the ACOR value is only relevant in the case of a moving ball on a stationary racket. These conditions are very rarely experienced during competitive play. Cross **1997** noted that whilst a point exists on the racket for which rebound velocity is a maximum, there also exists a point for which rebound ball velocity is zero. This point was called the *dead spot* of the racket. In opposition to what one might expect from such nomenclature, Brody and Roetert **2004** stated that the dead spot can also be a sweet spot of the racket. When the racket is stationary, an impact at the dead spot results in all momentum being transferred into the racket. The ball stops and the racket recoils quickly. However, in a case when the ball is stationary and the racket is moving, the reverse is true, the racket stops and the ball accelerates in the direction of impact. Brody et al. **2002** describes a simple method of calculating the post-impact velocity according to the pre-impact ball velocity and mass, and the effective mass and velocity of the impact point.

$$v_b' = \frac{e \cdot m_e (v_{IP} - v_b) + m_e \cdot v_{IP} + m \cdot v_b}{m + m_e} \qquad \textbf{[2.6]}$$

It follows from this that when the ball is moving slowly it is more effective to hit the ball towards the tip of the racket where the velocity of the impact point is likely to be higher. When the ball is moving quickly it is more effective to hit towards the throat of the racket

where the ACOR value is higher and the ball retains more of its initial velocity after impact. Cross **1997** stated that the dead spot should be utilised in the serve, when the ball is effectively stationary and the large amount of wrist action gives considerably higher racket velocities towards the tip.

From this analysis it is apparent that the point on the racket face resulting in maximum post-impact velocity is not one of two distinct points but a continuously variable point along the racket face. In order to determine the location of such a point it would be necessary to measure the full linear and angular velocity of the racket and ball. This may explain why such an analysis has not yet been performed.

For completeness, the relative position of each sweet spot or region is shown below in figure 2.11 as taken from Kotze et al. **2000**.

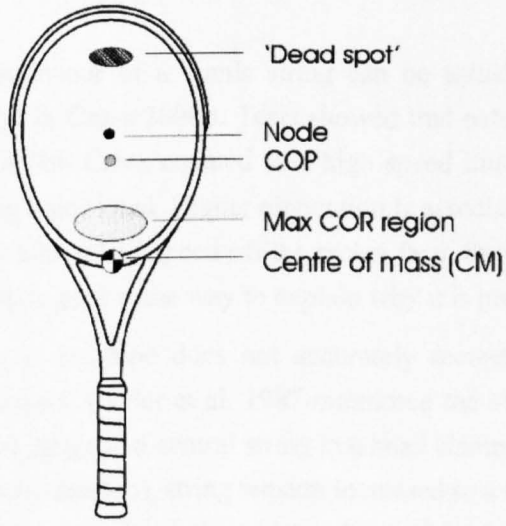

Figure 2.11. The relative positions of the four sweet spots as discussed in the literature.

2.4 The Racket Stringbed

The stringbed has a significant role to play in any racket/ball impact. As the medium of contact between the ball and racket, the type of string used, the tension they are set at and their configuration can greatly affect the ball's flight after impact.

2.4.1 String Configuration

A number of different string configurations have been attempted since the invention of tennis. The majority are variations on the same theme, a uniform interlaced pattern of strings, as directed by the current rules of tennis (ITF **2007c**).

Fischer **1977** introduced a method of racket stringing which used two separate planes of strings and a series of rollers and interconnecting *spaghetti* strings. The introduction of this racket led to players being able to impart considerably more spin than was previously possible. Such a dramatic change to the nature of play led to a swift rule change by the ITF.

The new rules specifically ruled out such string arrangements, strings had to be in a single plane and no extraneous pieces such as rollers were allowed. Goodwill and Haake **2002b** investigated this stringbed arrangement using high speed video and found that significantly higher lateral string displacement took place during oblique impacts. As the strings returned to their normal position, the ball was 'catapulted', imparting almost twice as much spin as a conventionally strung racket. The interlaced pattern of a normal stringbed prevents such large lateral string displacements from taking place.

2.4.2 String Type

String type can be divided into two main categories; *natural* and *synthetic*. Natural strings or natural gut strings are manufactured from the stomach lining of a cow. Whilst not as durable as synthetic strings, and more expensive, they are preferred by the majority of tennis players. Synthetic strings are usually manufactured from nylon, polyester or Kevlar, each with different properties.

The stress/strain behaviour of a tennis string can be tested simply using an Instron tensile testing machine, as in Cross **2000b**. Tests showed that natural gut is more elastic. In loads of 200 to 350 N (which Cross equated to a high speed impact) natural gut elongated more than any other string type tested. Higher elongation is associated with a smaller impulse at the hand and a slightly higher ball speed off the racket face. Such aspects of the behaviour of natural gut as a string type goes some way to explain why it is preferred by many players.

Testing in an Instron machine does not accurately recreate the high-load dynamic conditions of an actual impact. Calder et al. **1987** monitored the strain behaviour of a single string by attaching a strain gauge to a central string in a head clamped racket. A ball was fired at the racket (strung at 50 lbs tension), string tension increased to a maximum of 70 lbs during the 2.5 ms impact. Using the stress/strain behaviour obtained from the experimental impact, a single string was tested in a purpose built rig. This experiment aimed to find differences between synthetic strings and natural gut. It was found that whilst the stiffness of a synthetic string is strongly dependent on the preload tension, natural gut is relatively independent. Therefore, at higher tensions, natural gut is less stiff when stretched.

Cross et al. **2000** tested the dynamic properties of 90 different tennis strings. Stress/strain behaviour was monitored by attaching a single string in a tensioning rig with an attached load cell. A 0.45 kg hammer was swung at the string on a pivot. The incident velocity of the hammer was quoted as 2.63 ms^{-1}. A laser and optical grid measured the rebound hammer velocity which was observed to be -2.5 ms^{-1} after an impact of 30 ms. The string was preloaded at 60 lbs tension. Cross found that the stiffness of natural gut did not increase during impact, unlike synthetic strings, supporting the findings of Calder et al. **1987**. Cross also tested the creep of strings over time, by loading a single string statically for a period of time and measuring the tension loss. It was found that some strings lose tension rapidly, such that the string bed tension can significantly decrease after a matter of hours. It

was found that after around 100 s, a plot of string tension and log(time) showed a linear relationship. Calder et al. **1987** monitored the response of a single string in a stringbed. Cross et al. **2000** tested a single string independent of the interaction present in an interwoven stringbed. Whilst the work by Calder may better reflect the actual behaviour of a strung racket, Cross was able to look at individual parameters by isolating a single string. There may be very many variables present in a complex interwoven stringbed which were eliminated in the testing by Cross.

Goodwill et al. **2006** tested two types of synthetic string explicitly to ascertain their spin generation properties. Thirty identical rackets were strung at 60 lbs tension with various nylon and polyester strings. In order to better differentiate between these two string types, the string stiffness was given and used to compare experimental results. The nylon strings had stiffnesses between 150 and 220 lb/in whilst the polyester strings lay between 230 and 300 lb/in. Balls were fired at each racket at an angle of 40° and 60° from the perpendicular with 100 or 400 rad/s of backspin. It was found that at 40° the polyester strings generated more post-impact spin whilst at 60° less spin was generated. These results were attributed to the stringbed stiffness and lateral deformation. At 40° the lower stringbed deformation (exhibited by the stiffer polyester strings) generated more spin through rolling as higher relative ball/stringbed velocities were generated. However, at 60° the polyester stringbed was more analogous to a rigid surface and caused the ball to slip throughout impact, generating less spin. The impact angles used in this experiment were not directly compared to actual values from player testing. It is therefore unknown whether impact angles as high as 60° are seen in real play.

2.4.3 String Tension

String tension affects a number of factors involved with the ball racket impact. Modern coaching knowledge advises that strings be set loosely for more power and more tightly for increased control. Cross **2003** noted that when a steel ball bounces off a racket stringbed, the string tension has no effect on the height or speed of bounce. In the case of a rigid ball, the strings absorb almost all of the energy from impact regardless of the string tension. Leigh and Lui **1992** dropped a pool ball onto a head clamped racket and found that it bounced to 95% of its original height. From this it is clear that a stringbed is very efficient, losing very little energy in deformation. In an impact between a stringbed and ball, ball deformation accounts for the majority of energy loss (as stipulated by the rules of tennis ITF **2007c**). If a racket is strung with less tension then the stringbed is able to deform more, as a result the ball deforms less. Less energy is lost in the overall impact and the ball leaves the stringbed with more velocity.

Goodwill and Haake **2004c** investigated the claimed relationship between string tension and control. A ball was fired at a freely suspended racket inclined at 36° at velocities between 15 and 40 ms^{-1}. Stringbed tensions of 40 lbs and 70 lbs were tested. Each impact was recorded

using two high speed cameras set perpendicularly to each other. Previous tests in these conditions had shown that string tension had no effect on the rebound velocity or spin on the ball. However, the contact time of the ball on the stringbed and lateral string deflection were both reduced at higher string tensions. At a higher tension, higher normal forces are present within the stringbed meaning that greater frictional forces are acting on each string. It therefore requires more force to make the strings move relatively to each other. The outbound spin was very similar for each string tension at any given velocity, therefore *higher* spins are generated for a given lateral stringbed deflection at higher stringbed tensions. This was equated to the reputed increased control claimed by players and coaches. Goodwill used the example of a heavy top spin shot. Such a shot requires precise timing and extreme accuracy. A racket strung at a higher tension may well give the player a greater feeling of control.

From this testing it seems apparent that lower tensions result in a higher outbound velocity (at least for relatively perpendicular impacts) whilst higher string tension gives a greater degree of control. Although it should be noted that control is a relatively ambiguous term with regards to scientific investigation.

2.5 Player Testing and Motion Capture

In order to validate any predictive model, knowledge of the model's likely input and output parameters is required. With regards to a tennis impact model, an awareness of the typical shot characteristics exhibited by players of a high standard is necessary. Literature reviewed to date has often used ball velocities, impact angles and positions without citing recorded values from actual players.

Previous studies have attempted to recreate realistic impact conditions. A general lack of data means that the values used may not represent a typical player's shot. In many cases the values used in the experiments may have been chosen arbitrarily. As playing styles change and analytical methodologies improve, the need for an accurate and in-depth player testing methodology increases. This need for accurate player data already exists in scientific analysis, coaching and refereeing. This has led the development of many different methods of obtaining such information, as described below.

Light gates or radar guns can be used to measure velocities. Sensor systems use radio or infra-red emitters to track points in 3D space. Videogrammetric methods use video footage to visually track points in a 2D or 3D environment and also provide a qualitative visual recording of the subject. Previous work into shot analysis has been performed in a variety of different ways and in a number of different environments. Kotze et al. **2000** gives a comprehensive review of previous research into tennis shot analysis, citing papers investigating biomechanical movements and shot performance both outdoors and in a laboratory environment.

The methods used and the type of data obtained varies according to the nature of the testing. The areas of testing to date can be approximately divided into two categories:

1) Player perception

2) Motion analysis

2.5.1 Player Perception

Player perception deals with the subjective measures of player performance. It often includes recording ordinal data from players based on preference. This is usually divided into categories such as *feel*, *comfort* and *control*. In many cases these difficult to define concepts are substantiated with more objective scientific measures.

Unstructured interviews often form a large part of the information gathering process. Scanlan and Ravizza **1989a** used in-depth interviews to record the retrospective experiences of 26 former elite figure skaters. The 1000 + pages of transcribed conversation were analysed for sources of pleasure in Scanlan and Ravizza **1989b** and sources of stress in Scanlan et al. **1991**. This method is exhaustive and time consuming, but ensures that the bias and inexperience of the researchers does not affect the results.

'Structured relationship modelling' was developed by Roberts et al. **2001a**, who recognised the large psychological aspect of sports performance. How a player perceives their equipment and its abilities can greatly affect the athlete. Structured relationship modelling allows the inter-relation of the various parameters identified during interviewing to be uncovered. Roberts et al. **2001a** interviewed 15 elite golfers regarding their perception of the *feel* of a variety of different clubs and balls. In a follow up study Roberts et al. **2001b** compared the subjective opinions obtained in the previous study with objective data regarding contact time during a strike. Golf balls coated in a 70 μm layer of aluminium foil were used to measure contact time. Little correlation was found between the actual and perceived values. This revealed that although a player may categorise their experiences with regards to objective quantities such as mass, speed and contact time, physical correlations are rarely observed.

Interviews and structured relationship modelling have been used in the field of tennis. Davies et al. **2003** assessed the perceptions of 16 tennis players when using six different tennis ball types. Interviews with the players were transcribed and any common themes investigated, such as the perceived weight and *feel* of the ball. The small sample size of players and lack of mechanical assessment means that perceptions were not linked to any real physical parameters. Barrass et al. **2005** attempted to quantify the *feel* of tennis racket handles according to their surface, size and shape. Unstructured interviews were used to obtain a series of qualitative parameters although these were not prioritised or compared to any physical quantities.

Although interviews are useful for assessing the relationship a player has with their equipment, it is not an essential tool when attempting to identify and investigate physical relationships. The knowledge of a player's perceptions and preferences is valuable when

attempting to maximise their performance or produce a more marketable product. When testing a player in order to obtain typical shot characteristics it is not be necessary to interview players regarding their experience. A player's shot is a combination of a multitude of factors, of which the psychological aspect cannot be underestimated. Any intrusion into a player's surroundings will have an un-quantified affect on their performance, whether this is in the form of sensors directly attached to the body, or an unfamiliar training regime. Minor environment changes have been shown to change the perception of high level tennis players, such as the study by Davies et al. **2003** evaluating the player perception of a variety of tennis balls. It therefore seems necessary to present a minimal intrusion into the player's environment when obtaining shot characteristics in order to minimise any associated negative effects.

2.5.2 Motion Analysis

In contrast to perception analysis, motion analysis deals with objective measures. Other objective measurements of sports players do exist, Crespo et al. **2003** mentions three:

- *Dynamometry:* Recording of force
- *Electromyography:* Recording of muscle activity
- *Cinematography:* Visual recording of motion

This current study is focused on racket and ball dynamics, and therefore the motion of the player will not be measured. For this reason the focus will be towards racket and ball motion, and electromyography and dynamometry will be largely disregarded in this case. Although Crespo et al. **2003** mention cinematography as the visual capturing of motion, non-visual methods of motion capture do exist. With regards to sports player testing it is more relevant to distinguish between intrusive and non-intrusive techniques.

Intrusive techniques

Any method of obtaining player data which necessitates a change in the player's environment is classed as intrusive. In almost every case this involves attaching some kind of marker to the player or their equipment. The markers themselves are often classified as active or non-active. An active marker transmits a signal as part of a unique identifier and way of pin-pointing its location. A non-active marker relies on tracking equipment picking up reflections from the marker's surface.

Many commercial motion analysis systems exist. Bartlett **1997** and Jenkins **2005** describe modern commercially available systems. These range from those using cameras such as: ELITE, Kinemetrics, MacReflex, Motion Analysis, Peak and Vicon. Those using a scanning mirror such as CODA-3, and those using LED's such as Selspot, IROS or watsmart. Generally, these systems are expensive and complex to set-up. The accuracy and automation being reliant on the use of several cameras.

Not all motion analysis systems are visual, JZZ Technologies **2007** use a series of accelerometer based sensors to track accelerations, velocities and displacement of various points around the body. Figure 2.12 shows that without wireless technology, this method prohibits tracking large movements of the player and may prove a considerable distraction to any athlete.

Figure 2.12. The accelerometer based system by JZZ technologies. A physical connection of the athlete to the recording system prohibits any large movements by the athlete.

Wireless technology has been utilised by Xsens **2007** in the 'moven'. A full body suit utilising a series of wireless accelerometers and gyroscopes which allows full motion analysis within a radius of 150 m. Figure 2.13 shows one of the accelerometers used in the suit. This technology offers considerably more freedom than the wired sensors shown in figure 2.12. Despite this, the bulk of several sensors, transmitting equipment and batteries still presents a considerable distraction to any player and is unlikely to be used in realistic play conditions.

Figure 2.13. One of the accelerator/gyroscope units used in the moven full body motion capture system developed by Xsens **2007**.

Modern computer animation commonly makes use of visual, marker driven motion capture in both the film and video game industries. Menache **2000** gives an outline of the history of motion capture and the techniques adopted by these industries. Quite often, full

body suits covered in an array of markers are used in order to capture very complex body movements which are then translated into computer animation.

When using markers to capture the motion of sports players it is important that the player is still able to perform as one would expect in a competitive environment. When capturing human movements in sport, the relative joint orientations are more important than facial features and bodily detail. For these reasons, far fewer markers are used in sport motion analysis.

The tennis serve has been subject to considerable motion analysis. Elliott **1983** tracked the position and movement of tennis players' joint centres during a racket serve. High speed cameras were used to record the movement of the player and racket in 2-dimensions. This information was used to obtain the racket and ball velocity, the height of impact and ball spin. Elliott et al. **1986** later completed a similar study but using the 3D Direct Linear Transform (DLT) method and two high speed cameras. Both of these studies analysed the entire swing at relatively low frame rates (200 – 300 frames per second) and concentrated on biomechanical aspects. The speed at which this testing was performed means that relatively little information was given regarding the impact. This is reflected in other early 3D studies by Van Gheluwe and Hebbelinck **1985** and Bahamonde **1989**. Both studies obtained comprehensive body and racket movements. However, the frame rate used was not high enough to obtain detailed information regarding the impact. Mitchell et al. **2000b** concentrated on the movement of rackets of different moments of inertia during a tennis serve. Active markers using infra-red LEDS were attached in four positions around the racket frame. The impact points, angular velocities and centres of rotation were tracked in every case. Six separate players were tested. A frame rate of 400 frames per second was used throughout the testing giving a resolution of 1 frame every 2.5 ms, the method was accurate to ±0.6 mm. A tennis impact lasts around 5 ms, ideally, a higher frame rate should be used to obtain detailed racket movements at the instant of impact. The active marker system gave a high level of accuracy but detrimentally affected the testing in other ways. The markers and transmitting equipment add mass to the racket frame and present a distraction to the player. Whilst this may not have been deemed detrimental in this testing, any change to the perception of a player will affect the results when trying to obtain representative racket/ball impact characteristics. Also, interpolation was required as the markers were read sequentially rather than simultaneously.

Compared to the serve, standard tennis groundstrokes have been subject to relatively little motion analysis. A tennis serve is very controlled. The player is stationary and has complete control over the racket and ball. It is therefore easier to set up equipment to fully capture the motion. Standard tennis strokes by comparison are much more fluid, the player moves around the court in a variety of orientations. This makes accurate capture of the motion much harder to achieve. This uncertainty can be reduced by using a ball projection device. The ball is fired into a specified region of the court, making it easier for the player to return

and easier to film the movement. This method has been used in analysing the forehand (Elliott and Marsh **1989**) and backhand strokes (Elliott et al. **1989**, Reid and Elliott **2002**).

Non-intrusive methods of motion capture

Intrusive markers or sensors cannot be used in competitive play. Non-intrusive techniques record and analyse player data without altering the player's environment or equipment. As of writing, non-intrusive techniques cannot obtain the detailed information which intrusive techniques allow, but are able to be used during competitive play.

The application of non-intrusive systems in sport depends on the sport in question. The governing bodies of football have so far resisted calls to introduce video-based refereeing. Despite this, video based player tracking systems such as Prozone **2007** are used for coaching. Xu et al. **2004** described the mathematical operations involved in the Prozone system. Around 8 stationary cameras are used to track the position of every player and referee during a match. The system is able to recognise individual players according to pre-defined parameters such as likely position and uniform colour. Figure 2.14 shows the system isolating two players from a trained background image. The system is able to distinguish the players even when close together.

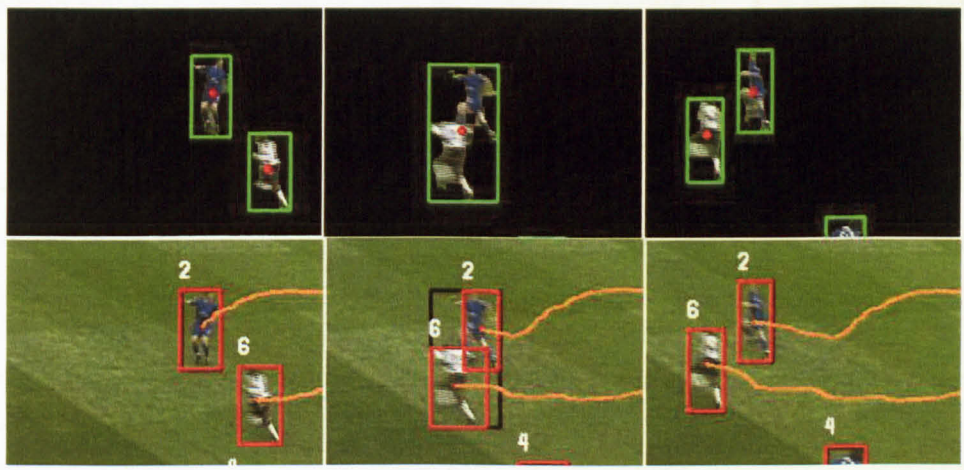

Figure 2.14. A visual method of tracking players by removing a saved background image.

This system reduces the player's position to a single point (located at the centroid of the detected image) and is unable to reveal more complex aspects of the player movement. This is a useful tool for tactical analysis but not for an investigation into more complex insights such as the mechanics of the player's shot.

Tennis has used non-intrusive motion analysis to aid in refereeing since 1980. The Cyclops line calling system, discussed in an article by Pallis **2004**, uses a series of infra-red lasers to determine whether a serve contacts the court's service line. This was replaced by a camera based system in 2006. Hawkeye **2007** was patented by Sherry and Hawkins **2001** and is a multi-camera ball detection system. It allows the player to query a referee's line-call and

is not limited to the service line. This system also gives a visual representation of the ball's flight. It also accounts for ball deformation, rolling and slip during impact. Features of this system have been utilised in other sports such as snooker and cricket. They allow the spectator to visualise shot possibilities and in cricket, validate a leg before wicket judgement. At the time of writing, this system has not been incorporated into refereeing in either of these sports.

Pallis **2000** performed non-intrusive player testing at the US-Open tournament. Ball spin and velocity values were calculated from images taken at 250 frames per second. Ball spin was measured by counting the frames for a full resolution using the position of the ball's logo. The highest recorded ball spin was 3571 rpm from a forehand, the highest spin from a serve was 4998 rpm. It was noted that higher spin was usually applied on the second serve which in most cases is slower than the first. Ball velocity was tracked by measuring the change in the ball position over time. The highest ball velocity from a serve was measured at 127 mph, and 82 mph from a ground stroke.

This testing signified the first comprehensive player testing during realistic play conditions. It was noted that coaches, players and commentators often estimated levels of spin to be around 500 rpm. The values of ball velocity were also used to validate the radar method of obtaining ball velocity. It was found to be accurate to within 3%. A major disadvantage of this testing is the omission of markers. It was possible to extract the movement of the ball, but complex racket tracking was impossible. A rudimentary attempt at tracking the racket tip was made by visually following its position on a computer. Without a distinctly marked point, the accuracy of this method is low.

Pingali et al. **1998** and Yan et al. **2005** describe methods for tracking tennis player and ball positions from broadcast television images. Both use zoning techniques and colour recognition to differentiate the player and ball from the background image. Figure 2.15 shows two images from Yan et al. **2005** where the players and ball have been tracked in two separate instances.

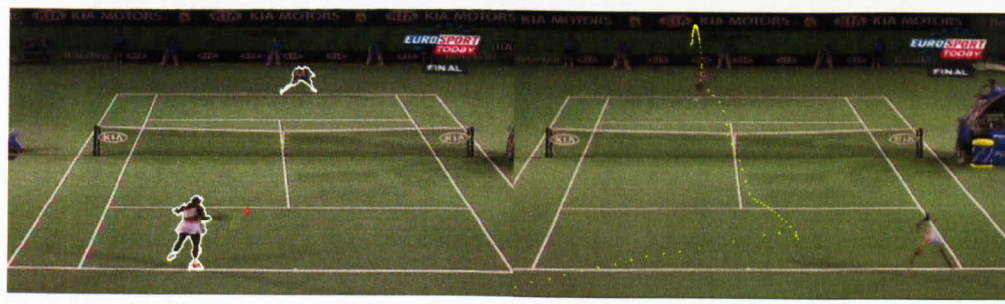

Figure 2.15. The ball and players tracked positions taken from broadcast quality images Yan et al. **2005**.

These techniques are powerful and especially useful for tracking typical player movements around a court in order to assess player performance. The algorithms used to track the player and ball often use colour information to distinguish features. This is not possible in

many digital high speed camera systems which record in greyscale for maximum light sensitivity. These techniques also have rudimentary spatial analysis but accurate 3D tracking of the racket and ball is not possible.

Non-intrusive techniques track the motion of a player or ball without interfering with the players themselves. In the case of Hawk-eye the accuracy has been deemed high enough by the ITF (Capel-Davies and Miller **2007**) to officiate the game.

Without the addition of markers as reference points, this technique is currently limited in terms of the analytical possibilities. It is not possible to obtain detailed 3D movements. A compromise between intrusiveness and depth of analysis must be reached in order to obtain meaningful shot characteristics in realistic play conditions. It is clear that high speed video must be used to obtain racket and ball movements. Sensor systems are not yet discrete enough and deprive the user of the qualitative analysis which high speed video enables.

2.5.3 High Speed Video

Both intrusive and non-intrusive techniques make use of high speed video in order to obtain player information. Most modern techniques translate the data points from the image plane, into a calibrated 3D environment, this will be discussed in more detail in the next section.

High speed video (or high speed photography) enables the user to observe and measure aspects of movement which aren't visible to the naked eye. Eadweard Muybridge is seen by many as the founder of high speed photography. He invented a method using a series of 24 cameras in order to capture high speed motion. Figure 2.16 shows the motion of a horse captured using his method.

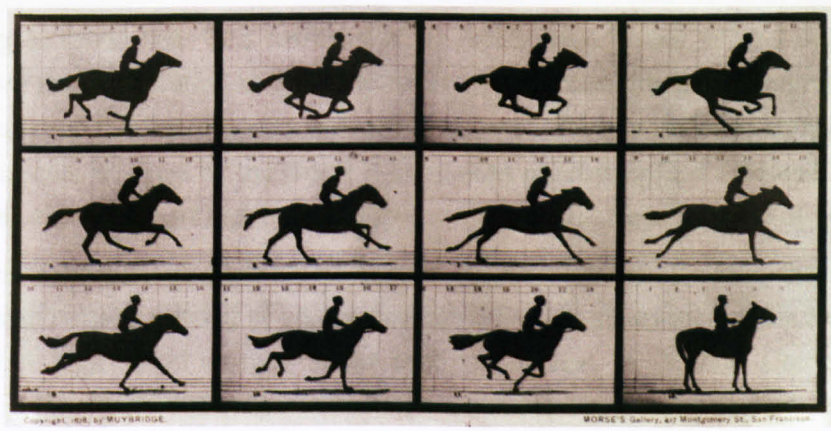

Figure 2.16. 12 Frames of a high speed recording of a horse's motion, as captured by Eadweard Muybridge.

The Society of Motion Picture and Television Engineers SMPTE **2007** in 1948 defined high speed photography as being any set of images recorded at over 128 frames per second.

A commonly used method of high speed photography is stroboscopy. A single frame of photographic film is sequentially exposed using a stroboscopic light. Figure 2.17 shows a tennis ball bounce captured using the strobe method.

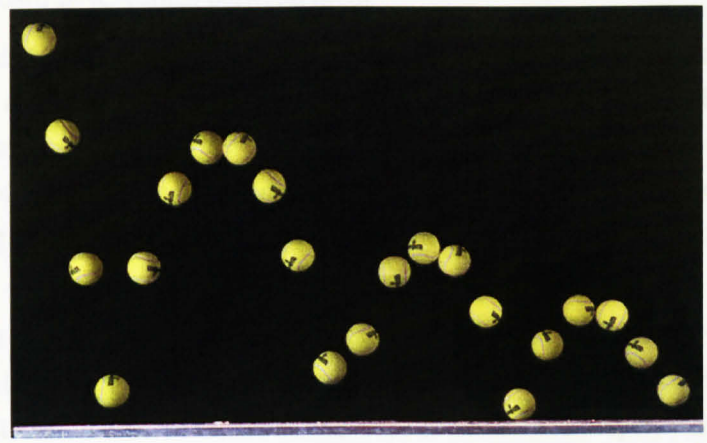

Figure 2.17. Three tennis ball bounces recorded using a strobe light and single frame.

Haake **1989** and Carré et al. **1998** used stroboscopic photography to record and investigate the impacts of golf balls and cricket balls respectively. The stroboscopic method is useful for recording relatively large displacements. At higher speeds stroboscopy produces blurred, overexposed images as the reference object remains in the same part of the image for each exposure. For this reason small displacements or stationary deformations cannot be analysed using this method. The high frequency flashes produced by the stroboscopic light rule it out as a method of recording player movements in realistic conditions. Despite this, Blanksby et al. **1979** used a stroboscope to measure player serve speeds by separating the player from the camera with a curtain.

At higher frame rates it is more useful to record each instant using a separate image frame. Before the proliferation of digital technology, sequential images were projected onto a series of frames of film. A rotating prism or mirror was utilised in order to increase the upper limit of frame-rate imposed by the physical limitations of moving film. Hadland **1974** gives a review on the state of the art high speed camera systems available at the time of writing.

Modern sensor based high speed camera systems are smaller than their film based counterparts and offer a number of other advantages. Early systems such as the Kodak Motion Corder output high speed images in an analogue format. A Motion Corder was used extensively in Goodwill **2002** to ascertain rebound ball velocities and stringbed deformations.

More recent systems connect directly with a computer via an Ethernet or IEEE 1394 interface to give a series of digital images. Complementary Metal Oxide Semiconductor (CMOS) sensors are most commonly used due to their low power consumption, allowing the sensor and memory to be manufactured in a single unit without overheating. CMOS sensors can also be *windowed*, allowing only a portion of the sensor to be used at a time enabling higher frame rates at lower resolutions. Lutwiller **2001** highlights specific differences between

the CMOS sensor and the Charge Coupled Device (CCD), commonly used in digital stills cameras. The electronic shutters used in these sensors make it very simple to synchronise a number of digital high speed cameras. Several cameras can have their shutters synchronised by attaching standard BNC cables between them.

With regards to high speed recording of tennis, the frame-rate used has varied according to the aim of the analysis and technology available at the time. Plagenhoef **1970** recorded the motion of a racket at 64 frames per second (fps) which was sufficient to obtain qualitative data but could not ascertain the speed of the racket. Cross **2002b** required a digital high speed camera operating at only 100 fps to measure the bounce characteristics of a superball and tennis ball.

Elliott used two cameras running at 200 and 300 fps to analyse the serve, forehand, and backhand of tennis players in three separate papers, Elliott et al. **1986**, Elliott and Marsh **1989** and Elliott et al. **1989**. The slower camera was used to record the player, whilst the faster was focused on the ball. At the frame rate used, it was only possible to track joint positions and simple racket movements over a relatively long time period compared to the duration of an impact.

Pallis **2000** performed a study during a grand slam competition. Images were recorded at 250 fps from which the ball velocities and spins were extracted. Due to the frame rate and nature of the testing, more detailed information on the player's racket movement was impossible to calculate.

Higher frame rates have been used to generate 3D data points from multiple cameras, Van Gheluwe and Hebbelinck **1985** used four cameras running at 400 fps to assess the kinematics of the tennis serve. Adrian and Enberg **1971** used a single film based Hycam camera running at 730 to 775 fps to assess the timings of overhead shots in tennis, badminton and volleyball. Only a single camera was used due to the difficulties in synchronising mechanical shutter based film cameras. Lewis and Peck **1958** described a method of synchronising high speed 16 mm film cameras using a strobe, which would be unusable for player testing.

Conversely, Dignall et al. **2000** used a digital Kodak EktaPro 4540 camera operating at 9000 fps to record oblique tennis ball impacts on court surfaces. Groppel et al. **1987** recorded ball/racket impacts at 3500 fps using a 16 mm Hycam system.

High speed video is an extremely effective method of recording physical events. In the field of tennis, it has been used extensively in player and impact testing. The advent of digital technology and the refinement of the CMOS sensor have meant that events can be recorded digitally, at high resolutions and frame rates. Recorded video images can be used for qualitative analysis and to obtain physical results. Videogrammetry allows accurate measurement of physical systems in 2 or 3 dimensions using recorded video images.

2.6 Videogrammetry

Videogrammetry is a derivation of photogrammetry, which is a method of obtaining measurements from a single or series of photographs. It is classed as a *remote-sensing* technology in that it obtains measurements through a non-direct methodology.

2.6.1 Single camera Videogrammetry

Simple 2D photogrammetry has been used extensively in tennis analysis. A calibration grid of known size is used to ascertain a ratio between the dimensions in the recorded image and dimensions in reality. Figure 2.18 shows an image taken from Taniguchi and Miyazaki **2005**. A single high speed camera was used to measure the deviations of a baseball pitched by a player and pitching machine. To measure the horizontal and vertical deviations a simple calibration grid was placed in front of the camera. The calibration grid is shown in figure 2.18 and has been enhanced to account for the poor image quality.

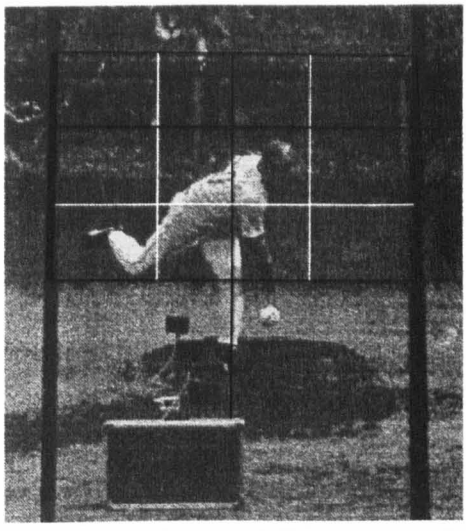

Figure 2.18. A snapshot of a baseball player pitching a ball with a calibration grid which was used to measure the ball's deviations.

The testing by Taniguchi and Miyazaki **2005** highlights the inherent weakenss of 2D videogrammetry in that large movements occur directly out of plane with the recorded image. The greatest weakness of 2D videogrammetry is that it is difficult and inaccurate at measuring out-of plane movements, i.e. those towards or away from the camera. To account for this Taniguchi and Miyazaki **2005** set up a series of light gates to measure the ball's velocity out of plane and ascertain when it had reached a particular position.

Carré **2000** measured the dynamics of the cricket ball bounce using digital stroboscopy. In this case ball movement out of plane was kept to a minimum by aligning the ball's trajectory with the digital camera. The translation and rotation of the ball was tracked using digital tracking software as seen in figure 2.19. Using spherical geometry the 3D spin was calculated from a single image.

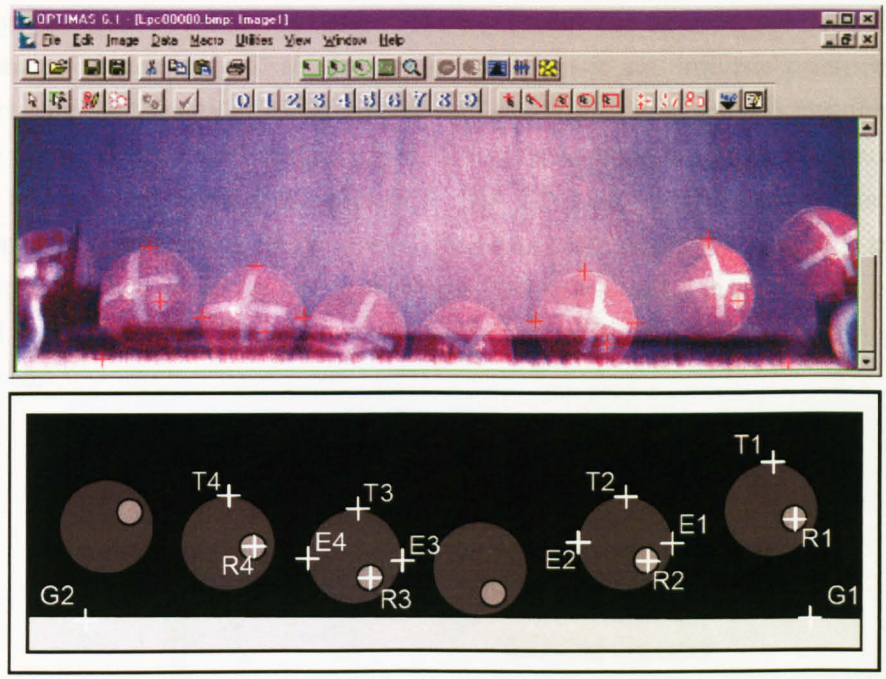

Figure 2.19. Strobed images of a cricket ball bounce on a cricket pitch including the tracked points used to calculate velocity and spin.

Due to the limitations of single camera recording, investigation into tennis impacts has invariably been restricted to variation along the longitudinal axis. Elliott **1982** used a single camera to measure the inbound and outbound velocity of a tennis ball impacting a tennis racket under a variety of clamping conditions. Impacts were limited to the racket's central axis. Goodwill **2002** utilised a single Kodak Motioncorder to measure the inbound and outbound ball velocities, stringbed deformations and impact points. Impacts were limited to the central axis. In order to accurately track the outbound ball trajectories resulting from impacts off the longitudinal axis a 3D videogrammetric method would have been necessary.

2.6.2 Multiple Camera Stereoscopy

Whilst depth can be perceived in a single image it cannot be measured. A second image taken from a different angle is necessary in order to be able to resolve depth accurately. A variety of methods exist which allow one to recreate 3D points from two or more 2D images. Extending analysis into a third dimension decreases error by eliminating issues with camera alignment and parallax. A 3D analysis method also increases the amount of information which can be obtained from testing.

The ability to accurately track the position of a ball and racket in 3D space is a necessity in order to satisfy the objectives of this overall study. Analysis in 3D is a vital tool for validating complex impact models and gaining a better understanding of how the many factors in a tennis impact can affect performance. Whilst 3D analysis has been used relatively frequently in biomechanical stroke analysis (Elliott et al. **1986** and Van Gheluwe and Hebbelinck **1985**) it has been used very rarely for impact testing in a laboratory.

A system must be calibrated before 3D co-ordinates can be extracted from 2D images. The calibration method is used to obtain a set of extrinsic and intrinsic parameters. These parameters describe the way in which a 3D co-ordinate from object space is translated into the 2D image plane, as illustrated in figure 2.20. The 3D co-ordinates are described according to an origin and axes-set defined at calibration. The 2D image co-ordinates are measured in pixels from one corner of the image. Once the camera parameters are obtained, any 2D co-ordinate in the image plane can be re-projected into object space subject to an error E, as illustrated in figure 2.21. The error varies according to the quality of calibration and the method used.

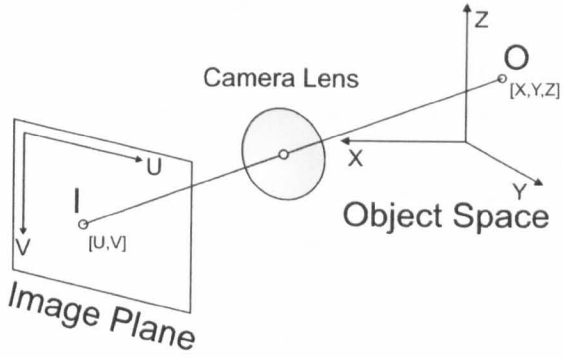

Figure 2.20. A diagrammatic explanation of the two reference frames used in 3D videogrammetry.

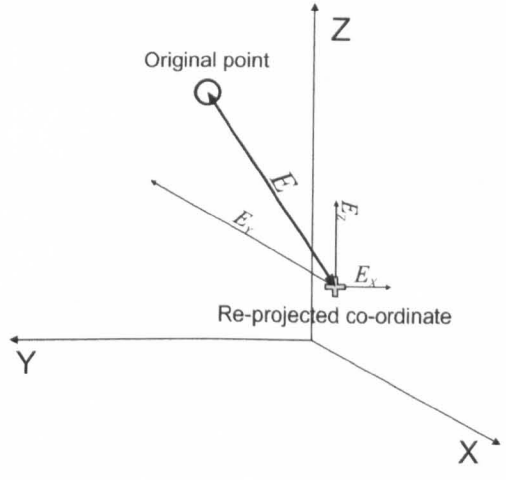

Figure 2.21. A diagrammatic illustration of 3D reproduction error

The calibration procedure generally involves recording a series of control points which are used to calculate the required parameters. The control points used to calibrate the system can be provided by an accurately manufactured 3D calibration object (Abdel-Aziz and Karara **1971**), a 2D planar grid (Zhang **1999**), or 1D laser pointer (Svoboda et al. **2005**).

The parameters are often calculated using the linear least squares approach outlined in Abdi **2003**, or in more complex non-linear cases using the Levenburg-Marquardt algorithm.

The Levenburg-Marquadt algorithm is outlined in two papers; Levenburg **1944** and Marquardt **1963**. Describing the exact operation of these techniques is unnecessary here. Both minimise an error function such that the error E described in figure 2.21 is as optimised.

The most commonly used method with regards to 3D tennis analysis is the Direct Linear Transform (DLT). First described by Abdel-Aziz and Karara **1971**, a set of 11 camera parameters are used to describe the system, a further five parameters can be used to model lens distortion if necessary. Calibration is performed using an object consisting of a physical mesh of control points. Hatze **1988** modified the DLT method to eliminate the issue of dependence between two of the eleven original camera parameters. This method included a non-linear constraint, thereby forcing orthogonailty upon the coordinate system.

Zhang **1999** outlined a method which reduced the required calibration object to a 2D plane of known dimensions. The system is calibrated by moving the plane into a variety of positions, a number of control points are usually provided by a checkerboard pattern . All these control points exist on a single plane. A series of different checkerboard orientations provide enough data to iterate an accurate set of parameters from initial assumptions.

The required calibration object was further reduced to a single point by Svoboda et al. **2005**. The paper describes a calibration method requiring only a single point (such as a laser pointer) to be moved randomly through the required volume. This method reduces the complexity of the calibration equipment to an absolute minimum, virtually eliminating manufacturing errors. In order to calculate each of the required parameters, a minimum of three cameras are required. The DLT and checkerboard methods require only two cameras. An extra camera increases the complexity in recording and adds time when analysing the recorded data points.

In an internal report, Neil Whyld assessed the DLT, modified DLT and checkerboard calibration methods in terms of suitability for two camera 3D reconstruction. The full report is included in Appendix A.

In order to calibrate the system for the two DLT based methods, a large physical mesh of control points was constructed from BoschRexroth **2007**, an image of this can be seen in Appendix A. The Checkerboard calibration method used a printed checkerboard design attached to a flat section of MDF hardboard. A typical checkerboard design is shown in figure 2.22.

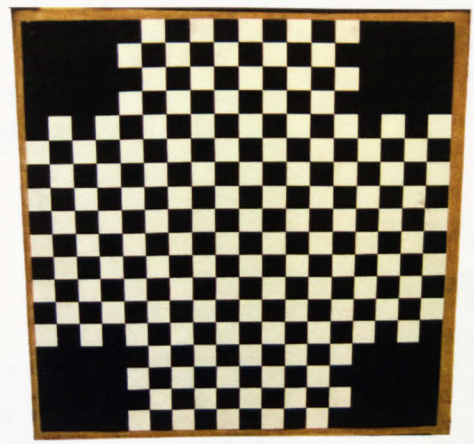

Figure 2.22. A typical checkerboard used in checkerboard calibration

To assess each method, two Kodak Motioncorder high speed video cameras were set-up at approximate right angles and focused onto a control volume, this volume was calibrated for each system. Using images of the DLT calibration object, a set of independent control points were re-projected back into 3D object space. With the 3D origin set as a corner of the calibration object (as illustrated in figure 2.23) the original positions of the control points were measured and compared with the re-projected positions to generate an error *E*. The average and maximum error for every calibration method is shown in figure 2.24.

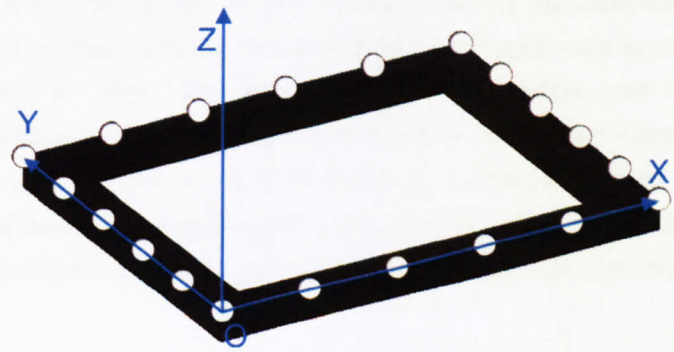

Figure 2.23. How the axes-set is aligned to the calibration object within the control volume, allowing re-projection error to be calculated easily.

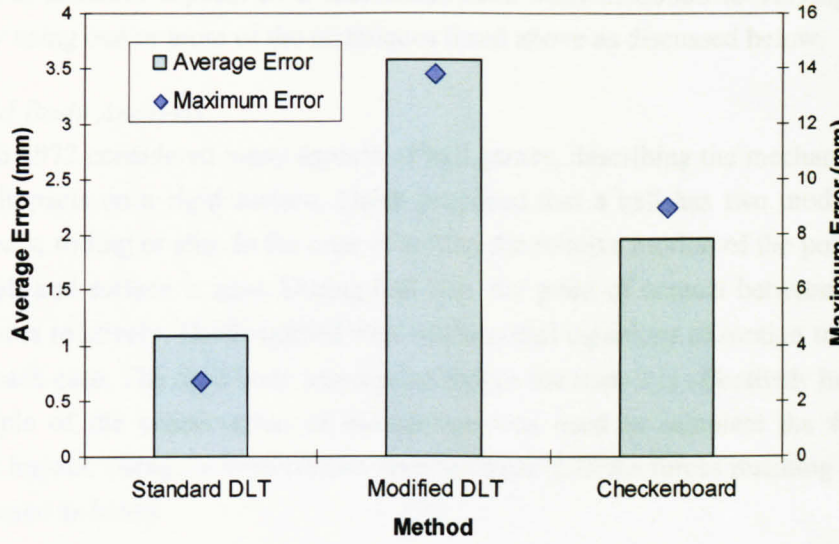

Figure 2.24. A comparison of average and maximum error for each assessed calibration method

Figure 2.24 seems to suggest that the DLT method is the most accurate, the results hide considerable error introduced by the calibration object. The modified DLT method, which forces orthogonality upon the system, reveals how inaccurate the DLT method is in reality. The majority of this error is due to the innate difficulty in manufacturing an accurate calibration object. The checkerboard method not only produced more accurate results, but the checkerboard itself is very easy to manufacture accurately and cheaply. Different checkerboards can be manufactured to calibrate volumes of different sizes whilst maintaining accuracy. This is very difficult to do with the DLT calibration object. The checkerboards robustness, ease of manufacture and superior accuracy led Neil Whyld to conclude that it is the most suitable calibration method given the methodological constraints of player and off-set impact testing.

2.7 Impact Modelling

The behaviour of the tennis ball and racket has been modelled in many ways but can be categorised into four main areas:

1) *Rigid body analysis:* Bodies assumed to be infinitely stiff, motion is based on Newtonian mechanics.
2) *Flexible body analysis:* Bodies assumed to be flexible with behaviour according to classical solid mechanics
3) *Visco-elastic analysis*: Energy losses are accounted for using modelled dampers.
4) *Finite element analysis*: The bodies are modelled by a number of small cells. This reduces complex bodily interactions to a series of partial differential equations which can be solved computationally.

Several different aspects of a ball/racket have been modelled to varying degrees of complexity using one or more of the techniques listed above as discussed below.

2.7.1 Rigid Body Analysis

Daish **1972** considered many aspects of ball games, describing the mechanisms of rigid body ball impacts on a rigid surface. Daish proposed that a ball has two modes of contact during impact; rolling or slip. In the case of rolling the relative motion of the point of contact between ball and surface is zero. During ball slip, the point of contact between the ball and surface moves relatively. Daish applied four fundamental equations of motion to describe the motion in each case. The rigid body assumption means the impact is effectively instantaneous. The principle of the conservation of momentum was used to calculate the forces acting throughout impact. Using the conventions seen in figure 2.25 the forces resulting from impact were expressed as below.

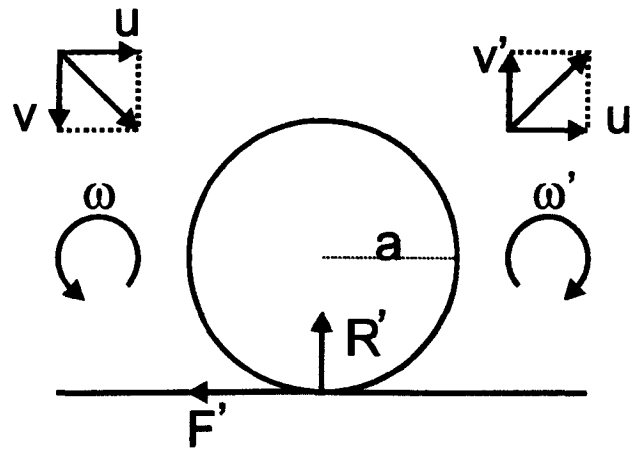

Figure 2.25. The notation used by Daish in formulating Newtonian equations of impact.

In the horizontal direction the force is:

$$-F' = M(u' - u) \qquad [2.7]$$

and vertically

$$R' = M(v' + v) \qquad [2.8]$$

In this case F' and R' represent the impulse of the forces acting over the duration of impact.

Equation 2.7 states that the sum frictional force opposing ball motion is equal to the horizontal change in momentum. Equation 2.8 states the same in the vertical direction.

The change in angular momentum is according to torque acting about the ball centre and the moment of inertia of the ball. The torque is equivalent to $F' \cdot a$. If k is the ball's radius of gyration the moment of inertia I is equal to Mk^2, this gives:

$$F'a = Mk^2(\omega + \omega') \qquad [2.9]$$

Using the concept of the coefficient of restitution described in the racket section above, the post-impact vertical velocity can be described as:

$$v' = ev \quad [2.10]$$

Slip

During slip, sliding friction acts throughout impact such that:

$$F' = \mu R' \quad [2.11]$$

If we equate a tennis ball to a thin walled sphere, the moment of inertia is:

$$I_B = \frac{2}{3} m_B a^2 \quad [2.12]$$

Using the above equations the post-impact velocities and spin can be calculated.

$$u' = u - \mu v(1+e) \quad [2.13]$$

$$v' = -ev \quad [2.14]$$

$$\omega' = \frac{3\mu v}{2a}(1+e) + \omega \quad [2.15]$$

Rolling

During rolling the resultant force between the ball and surface drops to zero. The spin of the ball is a function of the resultant speed between the ball and surface, in the case of a stationary surface this becomes:

$$\omega' = \frac{u'}{a} \quad [2.16]$$

These two observations can be used to formulate the post-impact velocities and spins during rolling which can be described as:

$$u' = \frac{3u + 2a\omega}{5} \quad [2.17]$$

$$v' = -ev \quad [2.18]$$

$$\omega' = \frac{3u + 2a\omega}{5a} \quad [2.19]$$

Rolling occurs when the frictional force is sufficient to cease relative movement. The minimum coefficient of friction necessary for this is defined as:

$$\mu \geq \frac{2(u - a\omega)}{5v(1+e)} \quad [2.20]$$

Ashcroft and Stronge **2002** experimentally investigated the coefficient of friction between a ball and racket stringbed using quasi-static loading. A ball was loaded normally (up to 400N) onto a stringbed and a tangential load was applied until sliding occurred. Coefficient of friction values between 0.453 and 0.535 were measured. Cross et al. **2000** measured the

coefficient of friction between tennis strings and a cylinder covered in tennis ball felt. The recorded values were between 0.11 and 0.36, much lower than those measured by Ashcroft and Stronge **2002**. In this case much lower loading values were used and it was assumed that ball felt was entirely responsible for the acting friction. As such, these values are less reliable than the higher values stated earlier, Cross stated that this was incomplete work in this respect. Cross **2000c** later updated these values to between 0.27 and 0.42. In this case an actual tennis ball was applied to a stringbed but with a maximum load 100 N lower than the method used by Ashcroft and Stronge **2002**. Considering the impulse occurring during impact is generally higher than any value used above, a higher value of the coefficient of friction is more applicable.

Whilst the rigid body approach is useful in understanding the basic mechanisms of spin, in reality a tennis ball deforms considerably upon impact. In a pseudo-flexible model, Brody **2000** reasoned that a ball deformed during impact according to simple un-damped harmonic motion. As such, the COM of the ball followed a modified sine wave over the duration of impact.

The radius of the ball r at an instant t during impact was said to be equal to:

$$r = r_B\left(1 - k \cdot \sin\left(\frac{\pi t}{T}\right)\right) \qquad [2.21]$$

where r_B is the uncompressed radius of the ball, T is the duration of impact and k is a compression factor.

Brody assumed in this case that the ball slips throughout impact and that the moment of inertia is equal to that of a hollow sphere, i.e. the same as in equation 2.12. By considering the angular impulse acting on the ball Brody concluded that the post impact spin could be expressed as:

$$\omega' = \omega + \frac{3}{2r_B}\left(1 - \frac{k\pi}{4}\right)(u' - u) \qquad [2.22]$$

according to the same notation as in figure 2.25.

Equation 2.22 suggests that the post-impact spin of a ball can be determined from the compression during impact and the change in horizontal velocity. This is useful as an approximation but disregards any damping properties the tennis ball may have and assumes that the ball slips throughout impact. This simple analysis could be repeated with modified assumptions to improve its compliance with reality.

The simple binary rolling *or* slip behaviour postulated by Daish **1972** was investigated experimentally in Cross **2002a**. A soft rubber ball and tennis ball were marked with a series of dots around the circumference and rolled along a glass plate to observe the behaviour with the eye. Whilst the soft rubber ball exhibited pure rolling, the tennis ball both gripped *and* slipped on the surface. The balls were rolled by hand at low velocity and normal forces on a surface

which would not be encountered in normal play conditions. These findings may be more relevant if observed in an oblique impact at typical impact velocities on a racket stringbed. The bounce and roll behaviour was investigated further by dropping ball onto a stationary floating platform. The velocity, bounce angles and spin were assessed using video recorded at 100 fps. The force and acceleration were monitored using a piezoelectric transducer. It was observed in a number of cases that the direction of the force acting between the surface and ball reversed towards the end of impact. Cross attributed this reversal in force direction as a result of ball vibration. This force reversal caused a decrease in ball spin and increase in horizontal velocity toward the end of impact. The spin ratio of each ball was measured after impact. The spin ratio is defined as:

$$\frac{r\omega'}{V_x'} \qquad \textbf{[2.23]}$$

where ω' is the post impact ball spin and V_x' is the post impact horizontal ball velocity.

A reversal of horizontal force was accompanied by a spin ratio of greater than unity suggesting that the ball spin was greater than that due to rolling alone. This effect is known as overspin. Cross modelled overspin by off-setting the normal force due to impact. Horizontal ball deformation during impact causes the reactive normal force to act behind the ball COM, increasing the torque acting on the ball and increasing spin.

The experiment was performed at very low impact velocities (2.25 to 3.5 ms^{-1}) on a high friction surface (sandpaper). At higher velocities on a different surface it is possible that different behaviour may be observed which has not been accounted for in this paper.

Cross **2005** modelled the impact between a ball and racket based on the slip/grip behaviour observed in Cross **2002a** by using horizontal and vertical coefficients of restitution to account for energy losses due to string and ball deformation. This work represented the first attempt to model oblique racket/ball interactions. The coefficients of restitution represent a crude method of accounting for complex mechanisms of impact such as string tension and impact location. These cannot be accurately altered without experimental measurement. Cross avoided this by impacting the ball centrally on the racket face.

Rigid body assumptions have been adopted frequently in modelling the impact between a ball and racket. The general approach is to resolve the system according to the principle of conservation of momentum. This was used separately by Lui **1983**, Brody **1997** and Cross **1999b**, Cross **2000a**.

Generally, the linear and angular momentum is resolved before and after impact.
Using the notation in figure 2.26:
Linearly,

$$m_B V_B + m_R V_R = m_B V_B' + m_R V_R' \qquad \textbf{[2.24]}$$

Rotationally,

$$m_B V_B z + I_R \omega_T = m_B V'_B z + I_R \omega'_T \qquad \textbf{[2.25]}$$

Using the standard definition for the coefficient of restitution,

$$COR = -\frac{V'_B - V'_{IP}}{V_B - V_{IP}} \qquad \textbf{[2.26]}$$

where V_{IP} and V'_{IP} are the velocity of the impact point before and after impact.
The above equations can be solved for V'_B such that,

$$V'_B = \frac{V_B\left(m_B z^2 + I_R\left(\frac{M_B}{M_R} - COR\right)\right) + V_{IP} I_R (1 + COR)}{m_B z^2 + I_R\left(1 + \frac{m_B}{m_R}\right)} \qquad \textbf{[2.27]}$$

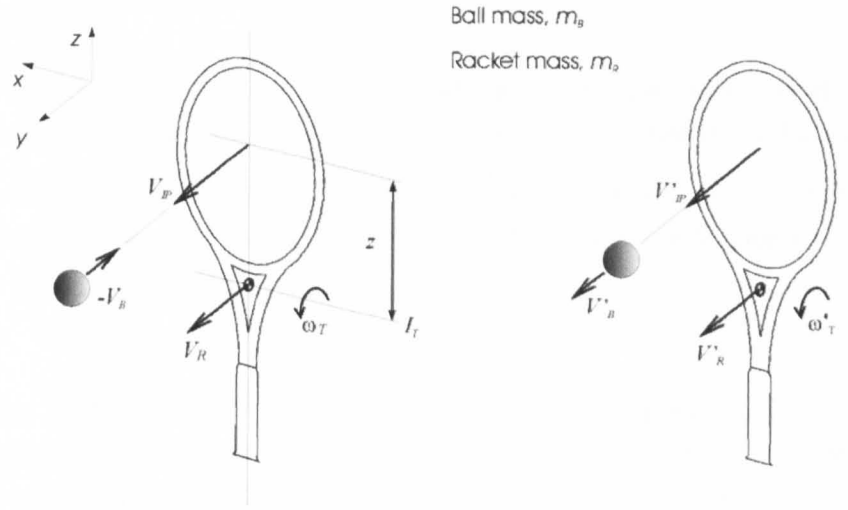

Figure 2.26. The linear and angular velocity notation used in a typical rigid body model and used in the equation shown above.

This simple approach allows one to calculate the post impact ball velocities according to previously measured COR values. This approach has a number of weaknesses. It has only 2 degrees of freedom, the linear and angular velocity are expressed in a single dimension. Whilst the impact position can be altered vertically the ball and racket are not able to move in that direction.

Both Brody and Cross recognised that towards the tip and throat of the racket this approach becomes increasingly less accurate. Frame vibrations (and hence deformations) are considerable in these regions, detracting from the rigid body assumption. A comprehensive overview of racket frame vibration is given in Brody et al. **2002**. Validation of the rigid body approach has shown that the best agreement with experimental results is seen for impacts at the geometric stringbed centre. This point is often close to the node point of racket vibration i.e. the point at which no vibrations are excited upon impact, shown in Brody **1995**. Hatze **1994** used an impact point probability distribution to show that high level players are most

likely to hit the node point of the racket. This observation gives the rigid body frame assumption some credibility in certain analytical situations. At other impact points on the racket face the rigid body model overestimates the ball velocity, losses due to frame vibrations which are not accounted for.

A rigid body approach could be extended to include more degrees of freedom, but this leads to unsolvable differential equations. A rigid racket frame combined with a flexible ball and stringbed impact model would allow a finite difference method to be used, avoiding this problem.

2.7.2 Flexible Body Analysis

Accounting for body deformation allows several new aspects to be incorporated into a predictive model.

The Ball

In the case of a sealed hollow ball (which represents most cases in sport) this allows the effects of material hysteresis, increased pressure and surface vibrations to be accounted for.

In the simplest models, Hertzian impact theory was used to account for elastic bounces. Hertzian impact theory states that the force F resulting from a deflection x is due to a spring constant k such that:

$$F = kx^{3/2} \qquad [2.28]$$

Maw **1975** used this simple basis to consider contact regions and forces during oblique elastic impacts. Ball rotation and velocity were considered according to seperate regions of slip and stick as in Daish **1972**, as such the body was assumed to be rigid in the tangential direction. Cross **1999a** performed a similar analysis using Hertzian impact theory with a specific application to sports balls. Energy losses were accounted for with hysteretic material losses and surface vibrations. This approach does not directly consider the geometry of the deformed ball, as such pressure changes and momentum flux cannot be accurately considered.

Bridge **1998a** and Johnson et al. **1972** considered the bounce of air-filled balls using a truncated sphere to predict momentum flux during impact. As the ball deforms the impact force is equivalent to the momentum impulse necessary to bring a region of the ball to rest. This assumption was used to calculate the contact area and contact time of a bouncing ball. The approach assumed that the ball remained spherical at all points other than the circle of contact. Due to weaknesses in these assumptions, the model is modified in Bridge **1998b** to account for surface waves, energy losses and internal pressure increases. This approach calculated the forces and deformations of small elements on the ball surface. A predictive model was programmed using BASIC and much more satisfactory predictions were obtained.

Haake et al. **2005** modelled a ball impact against a rigid surface by including separate normal and tangential elements. The normal impact was modelled as a non-linear Kelvin

Voigt spring damper system, the likes of which are discussed in the next section. In addition to the force due to the spring damper system (which acted centrally through the ball COM) a momentum flux component at the front and rear of the ball also generated a normal reaction force. Ball spin caused a difference in these momentum flux forces such that the resultant reaction force acted off-set, echoing the model proposed by Cross **2002a**. The ball was said to deform as a truncated sphere shown diagrammatically in figure 2.27. The figure in this case is intended purely as visual illustration.

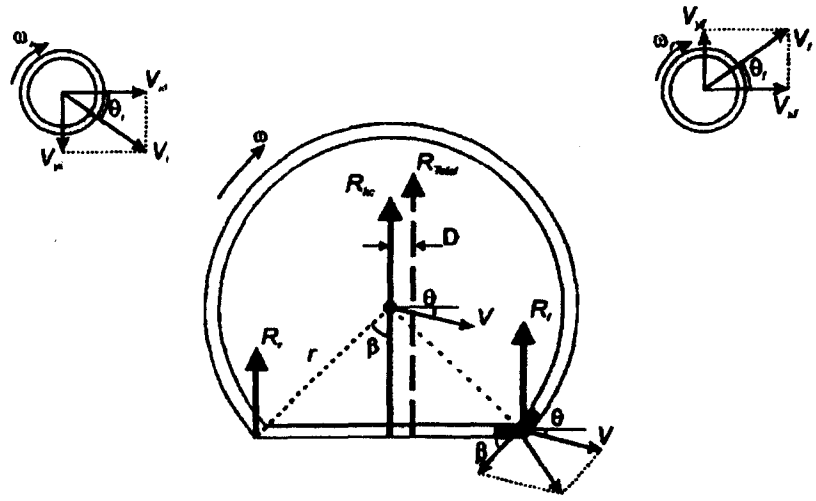

Figure 2.27. The geometry and forces involved in an oblique impact as proposed by Haake et al. **2005**.

The geometry of the deformed ball was used to calculate the distance from the COM at which the momentum flux forces and tangential frictional forces act. The moment of inertia of the ball was variable in this model, decreasing by around 5% for vertical deformations of 10 mm. In this model overspin can occur during the restitution phase of impact due to the increasing radius of the ball. This causes the torque and frictional force acting on the ball to reverse direction.

In order to validate the model, tennis balls were projected without spin onto an acrylic surface at angles between 10 and 40 degrees at speeds between 20 and 50 ms^{-1}. Each impact was recorded at 7100 fps and the images were analysed for angle, deformation and outbound spin. The model showed reasonable correlation with the observed results although it was noted that the model systematically under-predicts horizontal displacements by around 5 mm. In contrast to Cross **2002a** this model consistently predicts the resultant normal force to act in *front* of the COM. Despite this, the actual off-set distance was predicted as being around half a millimetre compared to nearly 3 mm by Cross. In this model, the ball is assumed to be slipping throughout impact which simplifies the model considerably and reflects the much higher velocities used in testing. Many aspects of this model could be used in a ball/racket model. It is also one of the few models validated for velocities and angles likely to be experienced during realistic play conditions.

The Racket

A rigid body assumption of a racket frame contains an inherent contradiction as stated by Cross **1999b**. This freely supported condition assumes that the time taken for the force pulse to propagate along the racket length is longer than the ball contact time. On the other hand, the rigid body assumption dictates that the propagation of any impulse is instantaneous.

Flexible body analysis assumes that the racket frame has a finite stiffness. By equating the racket frame to simple geometrical shapes, estimations of vibration magnitude can be made. Brody **1987a** showed that the vibration modes and node point locations of a freely suspended racket are very similar to those of a freely suspended one dimensional beam. This finding was supported separately by Kawazoe **1997** and Cross **1998**.

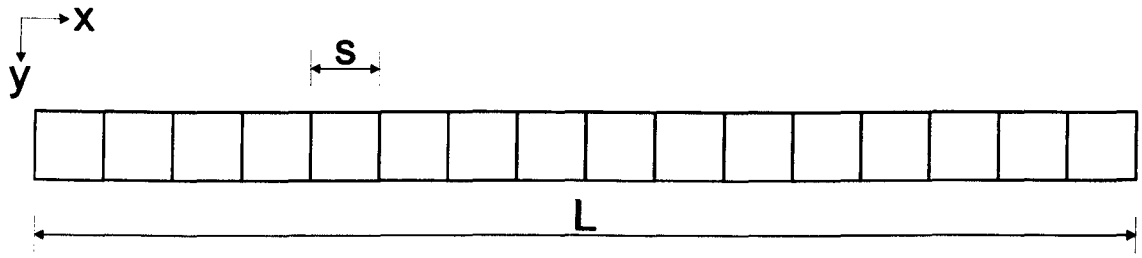

Figure 2.28. A typical one-dimensional beam used to model frame deformations

Given the similarities between a racket frame and uniform beam, Cross **1999b** theoretically modelled the impact between a ball and uniform aluminium beam. A segmented beam model as in figure 2.28 was used with a number of boundary conditions for freely suspended, rigidly clamped and pin-jointed ends. The model was validated by comparing the results against experimental impacts between a superball and aluminium rods of various dimensions. A high level of accuracy was observed. This paper also describes how this method may be used to model the impact between a ball and racket by assuming the racket behaves as a uniform beam. In this case the ball was modelled as a simple spring which is suitable for a superball which has a COR of 0.85 on a rigid surface. When modelling a tennis ball impact, the significant energy losses resulting from impact will have to be accounted for. Whilst Cross theorised that such a method could be used to model a racket frame, no experimental comparisons were made.

Cross **2000d** updated the uniform beam model to specifically represent a ball/racket impact. In this case energy losses in the tennis ball were modelled, the strings were modelled as lossless springs and a uniform beam represented the racket frame. The force acted on a single point and all impacts were perpendicular to the racket frame. Frame rotations resulting from impacts off the longitudinal axes were modelled by considering the rotational moment of inertia. This model was used to consider the energy losses through vibration and how post impact ball velocity is affected by altering frame stiffness and string tension. The model showed a significant advantage of stiffer rackets for impacts near the tip which is attributed to the generally higher serve speed in the modern game. Whilst it was mentioned that the model

results were *broadly* consistent with published data, no specific validation against a realistic impact situation was performed.

Cross **2001a** further modifies the beam model by using a non-uniform mass distribution. The racket was modelled as a two segment beam representing the racket handle and head. The analysis was performed to assess the effect of adding 30 g of mass to various points along the racket, for which a non-uniform mass distribution is required. The model was modified until the balance point and moment of inertia were equivalent in each case to the modified racket. The model was validated against experimental impacts at a velocity of 1.6 ms^{-1}. These speeds are not representative of realistic impact velocities. Ball and string deformations will be much lower than experienced during normal play.

Goodwill and Haake **2002a** described a 1D beam model designed to closely match the inertial properties of a racket. Initially a 2D approximation was made in which the racket head was assumed to be rectangular and the throat to consist of two straight sections. In the 2D approximation the mass per unit length of the frame and handle were constant. A unique solution was calculated ensuring the mass and balance point of the 2D beam model matched that of the racket. This 2D model was then reduced to a 1D approximation with the same mass approximation. This is illustrated in figure 2.29.

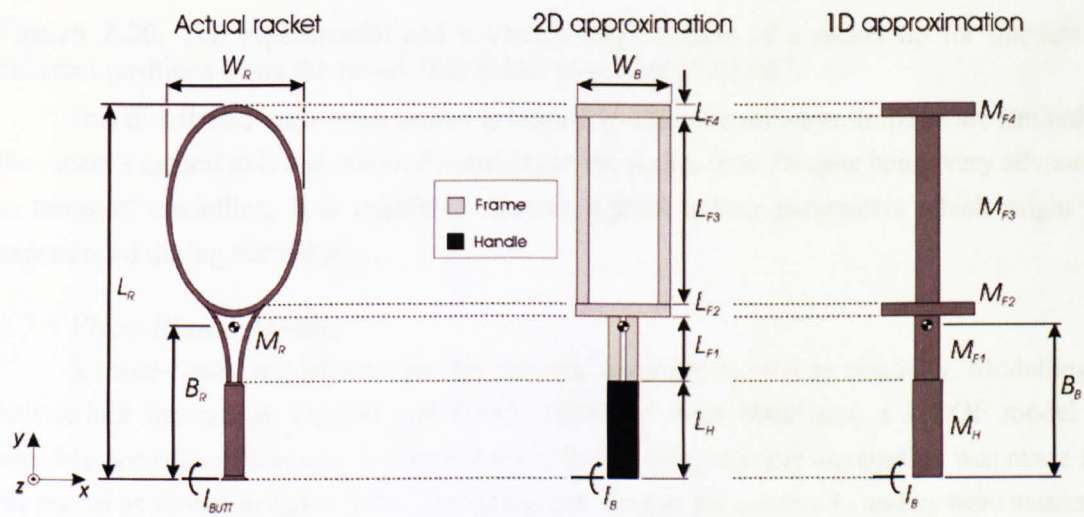

Figure 2.29. The 2D and 1D racket approximations compared with the actual racket dimensions as used in Goodwill and Haake **2002a**

This more complex beam approximation allowed a more complex mass distribution to be modelled. It was assumed that the flexural rigidity *EI* was constant for each segment of the beam. A mathematical assessment of the motion of a freely vibrating beam showed that the value of *EI* can be calculated from the frequency of vibration. This beam model was developed into a full freely suspended model using Visual Basic v6. The accuracy of the model was assessed by comparing the motion of the racket tip with that of a freely suspended racket for impacts at four different positions along the racket face. The motion and vibration

response of the racket were tracked using high speed video and a piezoelectric transducer attached to the racket handle. The results from this validation are shown in figure 2.30. Very good correlation was observed.

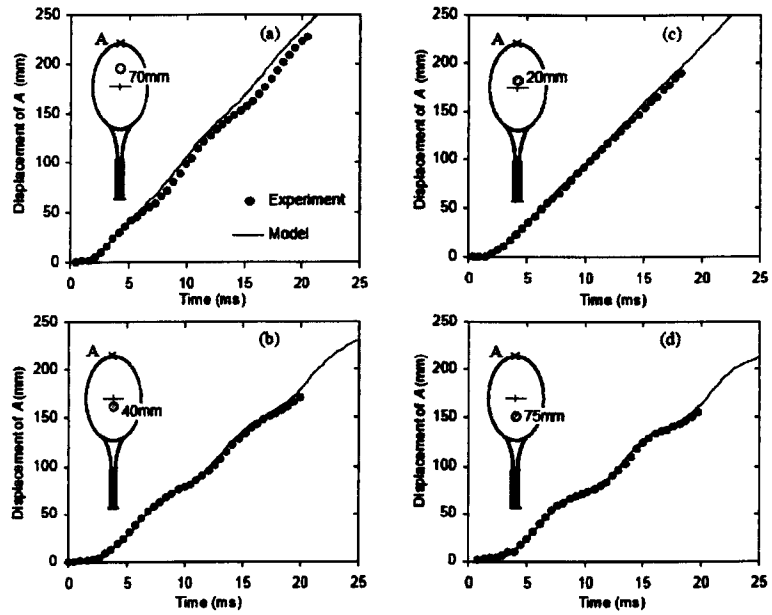

Figure 2.30. The experimental and modelled displacement of a racket tip for impacts at different positions along the racket face at ball velocities of 20 ms^{-1}.

This distributed mass beam model is limited in a number of ways. Impacts are limited to the racket's central axis and inbound normally to the racket face. Despite being very advanced in terms of modelling, it is unable to recreate typical impact parameters which might be experienced during normal play.

2.7.3 Visco-Elastic Models

A visco-elastic model accounts for material damping as well as elasticity. Modelling a ball/surface interaction, Dignall and Haake **2000** and Pratt **2000** used a 1 DOF model to simulate normal ball impacts. A simple Kelvin Voigt spring damper assumption was made for the model as shown in figure 2.31. The spring and damper parameters k_B and c_B were assumed to remain constant throughout impact, although the values could alter with ball velocity.

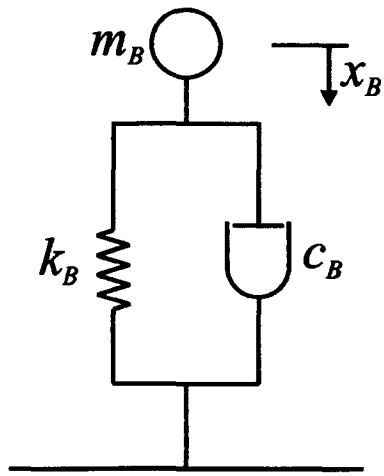

Figure 2.31. A simple 1 DOF Kelvin Voigt spring damper model.

The force of impact was calculated according to the following equation:

$$F = k_B x_B + c_B \dot{x}_B \qquad [2.29]$$

where the spring force is due to displacement, the damping force is due to velocity.

Dignall and Haake **2000** calculated the values of k_B and c_B from the measured values of the ball contact time and coefficient of restitution. This was done using a force platform and light beam timers. A linear relationship was stated between the values of k_B and c_B and the ball inbound velocity. Only a small number of data points (restricted due to the number of light beam timers) were used to establish this relationship. The relatively low ball speeds (20 ms^{-1}) and impacts against a rigid surface may not truly represent the characteristics of a high speed impact against a racket stringbed.

The end of the impact was designated to be the instant at which the ball displacement dropped to zero. Pratt **2000** illustrated another weakness of this model by observing the associated force-time curve over the duration of impact. Figure 2.32 shows such a curve. The force acting for the last 0.5 ms of the impact drops below zero. Such a tensile force is not physically possible and is due to the magnitude of the damping force being greater than the force resulting from material stiffness.

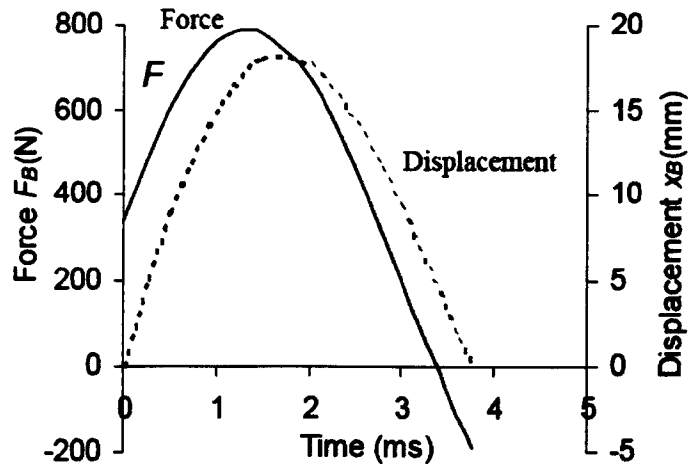

Figure 2.32. The force-time and displacement-time curves for the 1 DOF Kelvin Voigt spring damper model used by Dignall and Haake **2000** and Pratt **2000.**

Although both models showed good correlation with experimental data, a more complex model may be necessary to account for higher velocities and to create a physically realistic system.

Leigh and Lui **1992** created a visco-elastic model in order to predict the ball rebound velocity for an impact on a handle clamped racket. The behaviour of the ball, strings and racket were considered in turn. The ball was modelled as a spring and damper in parallel as shown in figure 2.31. In this case the stiffness parameter of the spring was assumed to be non-linear as a function of ball COM displacement. Leigh notes that the values used in the model were obtained using quasi-static ball compression testing. During such testing the inertial impulse present in high speed impacts will not be accounted for.

In agreement with earlier findings regarding the damping property of strings, Leigh and Lui **1992** found no appreciable damping effect resulting from string deformation. When modelled in isolation, the ball/stringbed interaction showed good correlation with experimental results for ball velocities below 7 ms^{-1}. It was noted that decreasing the tension in the stringbed increased the ball rebound velocity. This effect had been recognised by players and coaches and is due to the high relative damping present in the ball. The final section of the paper discusses the modelling of a ball impact against a handle clamped racket. A damping term was included for the racket such that the final spring damper system was as shown in figure 2.33; a visco-elastic ball and racket coupled by a purely elastic stringbed.

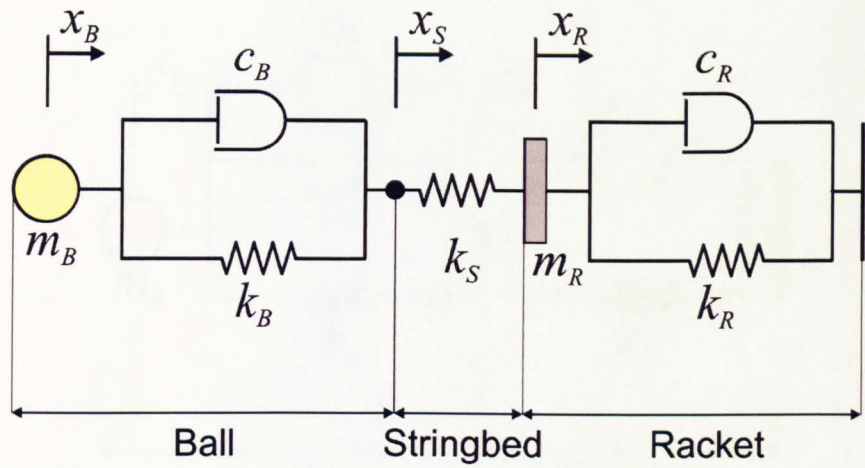

Figure 2.33. A schematic of the ball/stringbed/racket system modelled in Leigh and Lui **1992**.

Unfortunately, the final ball/racket model was not experimentally verified so no accurate judgement can be made regarding its effectiveness. Modification of the model parameters revealed that ball rebound velocity can be increased by increasing the damping present in the racket frame. However, a handle clamped racket behaves very differently from the more established freely suspended model thought to represent hand held impacts. It was not established as to whether high frame damping produces this effect in reality.

Goodwill and Haake **2001** used a spring/damper model of the same form as Leigh and Lui **1992** with a freely suspended rigid body model representing the racket. The stringbed deformation, COR values and ball and racket rebound velocity were validated experimentally. In contrast to earlier testing, ball velocities up to 32 ms^{-1} were used. The stringbed deformation was measured using high speed video.

A more complex spring/damper model was presented in Goodwill **2002** as part of the flexible beam model described in Goodwill and Haake **2002a**. The model uses a single spring in parallel with two dampers for the ball, and a single spring and damper in parallel for the stringbed. A schematic of this is shown in figure 2.34.

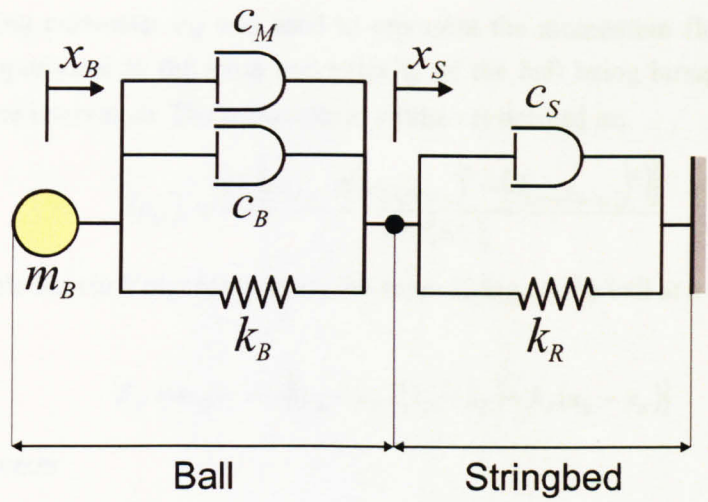

Figure 2.34. The spring/damper model used to model the ball and stringbed in Goodwill **2002**.

Goodwill used variable damping and spring parameters in each case.

Ball Parameters

The ball stiffness was said to be a function of the displacement of the ball COM. The relationship was derived by observing ball impact forces and deformations when fired against a rigid surface. It was noted that in impacts against a racket stringbed the ball deforms differently. Specifically, when impacted against a rigid surface, the centre of the contact region collapses inward after around 0.2 ms, giving a period of very high ball stiffness. When impacted against a stringbed, deformation of the stringbed means that this does not occur. The displacement of the ball COM is a function of ball and stringbed deformation, such that the stiffness parameter was defined as:

$$k_B = k_{B(0)} + A_K (x_B - x_S)^{\alpha} \qquad \textbf{[2.30]}$$

where $k_{B(0)}$ is the initial stiffness of the ball at a time $t = 0$, A_K and α are constants.

The damping parameter c_B represents material hysteresis. The magnitude of the material damping was said to be proportional to the volume of material being deformed, such that:

$$c_B = \frac{m_B}{M_1} A_C \cdot (d_{CONT})^2 \qquad \textbf{[2.31]}$$

where m_B is the ball mass, A_C is a parameter specific to the type of tennis ball used, d_{CONT} is the diameter of the region in contact with the stringbed. M_1 was defined as the difference between m_B and the mass at rest on the stringbed M_2, which was defined as:

$$M_2 = \rho_{area} \cdot \pi \left(\frac{d_{CONT}}{2} \right)^2 \qquad \textbf{[2.32]}$$

where ρ_{area} is the mass per unit surface area of the ball.

The damping parameter c_M was used to represent the momentum flux during impact. This was set proportional to the mass and velocity of the ball being brought to rest on the stringbed in a time interval Δt. The parameter at a time t is defined as:

$$(c_M)_t = \frac{m_B\left[\rho_{area} \cdot \pi\left(\left(d_{CONT(t)}\right)^2 - \left(d_{CONT(t-\Delta t)}\right)^2\right)\right]}{4\Delta t(M_1)_t} \quad [2.33]$$

Using simple Kelvin Voigt mechanics, the force acting on the ball at a time instant t was defined as:

$$F_B = m_B\ddot{x}_B = -\left[(c_B + c_M)(\dot{x}_B - \dot{x}_S) + k_B(x_B - x_S)\right] \quad [2.34]$$

Stringbed Parameters

To calculate the stiffness of the stringbed, several aluminium discs of different diameters were used to deform a head clamped racket stringbed. By monitoring the displacement and applied force, it was found that the stiffness has a polynomial relationship with deformation according to:

$$k_S = a \cdot x_S^{\,2} + b \cdot x_S + c \quad [2.35]$$

The coefficients a, b and c vary according to the stringbed stiffness.

Goodwill found that the damping present in the stringbed is small. A constant value of 2 Ns/m was used in this case.

After an initial attempt, it was found that modelling the stringbed as massless allowed the model to react as quickly as required. As such, the force on the stringbed was equal to that experienced by the ball at each instant and can be described in terms of the stringbed parameters as follows:

$$F_S = -\left[c_S(x_S - x_B) + k_S(x_S - x_B)\right] \quad [2.36]$$

Initially designed as a point force impact model, it was later modified to include a distributed loading condition to work in conjunction with the flexible beam model described in the previous section. This model was exhaustively validated experimentally. Two different ball types and two different string tensions at impact velocities up to 35 ms^{-1} were tested for rebound velocity, contact time and displacement. Generally a very good correlation was observed although it was noted that the experimentally obtained parameters are subject to error which caused systematic differences in predicted and observed values.

2.7.4 Finite Element Analysis

Computationally based techniques such as finite element analysis allow very complex geometries and systems to be modelled accurately. The relative ease with which a model can be created means that experimental validation is vital in order to ensure that the material properties are set accurately.

The Ball

Goodwill et al. **2005** created a finite-element model of a tennis ball to investigate the mechanism of oblique impacts. The model consisted of two layers, a hollow rubber core and felt cover. Each of these parts contained 23,328 separate elements as shown in figure 2.35.

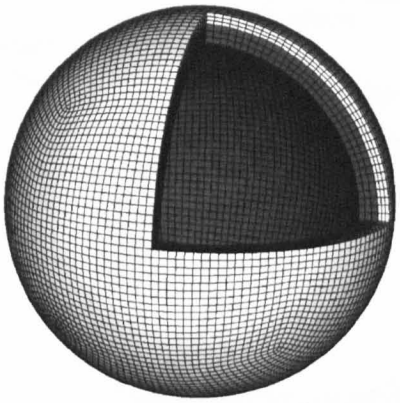

Figure 2.35. The 3D finite-element model of a tennis ball used in Goodwill et al. **2005**.

The non-homogenous felt cover was modelled as low density foam in order to account for the large displacements which occur. The rubber core was modelled as a pressurised airbag subject to an isentropic $PV^{1.4} = k$ relationship. The modelled tennis court surface contained 900 elements and was assumed to be rigid.

The material properties of the rubber core needed to be obtained experimentally in order to obtain the quasi-static stress/strain relationship. Tennis ball cores were obtained from a manufacturer and tested mechanically. The core was 30 mm in diameter with a wall thickness of 3.3 mm. A small sample of the core rubber was tested in a Hounsfield tensometer in order to measure the tensile and compressive stress/strain relationship. The compressive stress/strain relationship of a sample of tennis felt was also obtained in this way. The internal pressure of a tennis ball was measured with a pressure gauge by puncturing the rubber core with bespoke needle apparatus.

The values obtained in this testing were used in the finite element model which was then validated explicitly. A rubber core and tennis ball were fired perpendicularly at a rigid surface at inbound speeds between 13.5 and 27.5 ms^{-1}. Light gates were used to measure the inbound and outbound velocities. The results were compared with the finite-element model which showed good agreement with the rubber core but a poor correlation at higher inbound velocities for the complete tennis ball. This lack of correlation was attributed to the energy losses in the ball felt not being properly accounted for. Experimental force values, obtained from a force platform compared well with the model showing clearly the high force resulting from buckling of the ball which occurs in the first 0.2 ms of impact.

The ball model was also tested in oblique impacts to investigate the horizontal deformation and supposed increase in vertical COR compared to perpendicular impacts.

Haake et al. **2005** commented that the horizontal deformation of a ball during impact was very small and that an offset normal force acts around 0.5mm in *front* of the COR. Figure 2.36 shows the deformation of a ball during a normal and oblique impact as modelled by the finite element model.

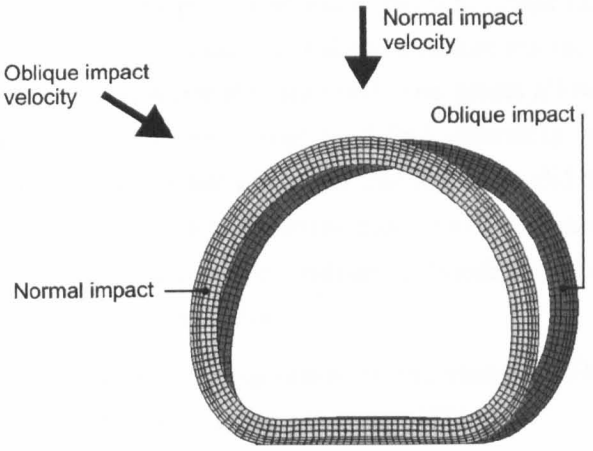

Figure 2.36. Cross-sections of the finite element model during a normal and oblique impact.

As can be seen from figure 2.36, the horizontal deformation is considerable for an oblique impact. The finite element model predicted that the normal reaction force is offset by as much as 1.6 mm *behind* the COM for impacts at 15 ms^{-1} and 30° from the normal. This offset reaction force increases the torque acting on the ball by around 5%. This deformation also led to a maximum decrease in moment of inertia of 6% during the midpoint of impact. The spin ratios as defined in equation 2.23 given by the model were compared with experimentally measured results. Both the model and experiment showed overspin but the model tended to slightly over-predict the values in most cases.

This finite-element model was experimentally validated and used realistic material values obtained from core samples. A key feature of an accurate finite element model is that it allows observation of physical behaviour from computational results. The horizontal displacement given by this model suggests that an offset force does act behind the COM although at a shorter distance than predicted by Cross **2002a**. The compliant felt layer allowed considerable rotational movement of the ball without direct interaction with the surface. The ball core could overspin without a reversal of the contact force. Previous attempts at modelling ball spin have effectively assumed a rigid shell such that the interaction between ball and surface is instantaneous. Taking into account, or at least being aware of this discrepancy between rigid modelling and reality is vital when considering ball spin.

Allen et al. **2007** performed a similar study on a finite element tennis ball which was validated experimentally at speeds between 5 and 30 ms^{-1}. Similarly, the model over-predicted rebound velocity for a complete ball. This was accounted for by suggesting that energy losses were underestimated. Allen notes that finite element models are useful in visualising mechanical deformations which are overly complex to mathematically predict.

The finite element tennis ball in this study represents the first stage in creating a full finite element racket impact model.

The Racket

Widing and Moeinzadeh **1989** published one of the first robust finite element models of a complete racket. Previous attempts made unrealistic concessions such as linearly behaving strings, or a single member to represent the stringbed. The model allows different racket and string geometries. Although each string was modelled discretely no relative movement between the strings was permitted. It was presumed that this was valid due to the high level of preload present in the strings. Such an assumption may be valid for normal impacts although high speed video analysis has shown lateral stringbed deformations of around 12 mm for oblique impacts (Goodwill and Haake **2004b**).

The racket frame was modelled using isoparametric elements. The number of elements was reduced to a minimum due to the computing limits of the time.

It was intended that the finite element model would reveal the stresses and deformations resulting from a normal impact. The model was clamped at the handle; the ball impact was represented as parabolic force acting on the stringbed mesh. The model was able to reveal mechanical deformations such as those resulting from stringbed tension and impact forces. No experimental validation was performed to compare the results obtained or set material properties.

Widing and Moeinzadeh **1990** advanced the model to include variable string tensioning. It was found that an increase in string tension stiffens the racket, increasing its resistance to bending, contradicting findings by Cross **2001c**. Several possible model advancements were discussed in this paper including relative string movement and dynamic modelling. The difficulty in performing such an analysis with the hardware available at the time was recognised.

This early attempt at a finite element model shows the advantages of using such an approach, mainly the visualisation aspect. Problems result from insufficient validation and computational limits. The small number of elements used means that this model may be of less use than a thoroughly validated flexible beam model.

Jenkins and Calder **1990** produced a finite-element racket model which was validated experimentally. Only one half of a symmetrical racket was modelled and no stringbed was included. It was stated that very little difference in strung or unstrung vibrational frequency was observed despite Cross **2001c** noting that racket frame vibration can decrease by 10% when strung. The static deflection under load and first fundamental node of a tennis racket were measured during clamped conditions. An accelerometer was used to measure frame vibrations. It was not mentioned explicitly whether the frame was strung or not during these

tests. Dynamic loading was performed using a strung, handle clamped racket. Balls were fired at the racket from an electronic pitching machine.

This study represents a compromised work resulting possibly from a lack of computing resources. Only half an unstrung racket was modelled. The validation was performed under clamped racket conditions which do not accurately represent a hand held racket. Although finite element modelling is a powerful technique, it is essential that the correct material properties are used and that any results are experimentally validated.

Kanda **2004** created a ball/racket finite element model in order to investigate racket power. A ball was modelled with a hollow single walled sphere containing 184 separate elements. The racket frame was modelled using 97 beam elements in order to economise the analysis. The stringbed was modelled with string elements which were fixed at each intersection. The mesh of the stringbed was made more complex around the impact region. In this case, the racket model was based on a Mizuno MS-21PW racket. The total mass COM and moments of inertia of the model are stated as being *nearly the same* as the actual specimen.

The model was tested dynamically for vibrational response and rebound ball velocity. In agreement with Cross **2001c** it was found that increased string tension decreases the frequency of vibration, although no figures are given for an unstrung frame.

A ball was fired at a freely suspended racket in a number of impact positions at 27.8 ms^{-1} and compared with the model response. Despite the differences in mass and MOI a relatively good correlation is observed, although only six separate impact points are given.

This paper gives a degree of experimental validation at realistic impact velocities. The model was not extensively validated for a number of conditions such as speed and offset impact position. The structure of the model was rather simplistic in its construction. Static load testing was not performed in order to obtain accurate material properties and the cross-section of the racket was taken from a standard beam element. Such aspects can have a considerable affect on the behaviour of the model. All non-linear aspects of the model such as ball and string damping were linearised with assumed material constants.

Each of these compromises will lead to inaccuracies in the model which may not have been revealed with the relatively simplistic validation given in this case.

Finite element modelling clearly has a role in modern analysis. However, without proper validation inherent errors and weaknesses in such models will not always be apparent. It would be wrong to draw rash conclusions from such models when the proper physical behaviour of the model may not have been considered. In many cases the models seen above are less useful than a well constructed and validated flexible beam model. When implemented well, as in the case of Goodwill et al. **2005** and Allen et al. **2007** finite element modelling can reveal behaviour and responses which cannot be obtained from more simplistic modelling

methodologies. Currently, racket finite element models are severely limited when modelling the interaction of the racket stringbed.

2.8 Model Validation

The above review of modelling impact behaviour reveals the necessity of sufficient validation. Without this step the results cannot be reliably compared with actual behaviour. In the majority of cases, the number of variables is small and easily validated. For example, Goodwill **2002** extensively validates a racket impact model with strictly controlled input parameters. Figure 2.37 shows an example set of model and experimental results. In this case the impact velocity is compared with the ball rebound velocity for two separate stringbed tensions. In this case the number of variables is sufficiently low such that the results can be displayed on two axes.

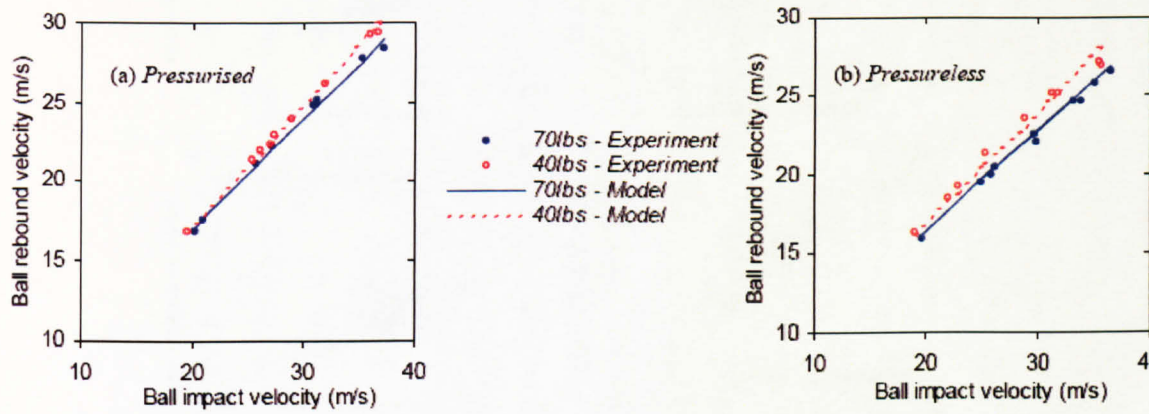

Figure 2.37. Ball impact and rebound velocities when comparing experimental and predicted results. In this case the variables are low enough that the results can be shown on two axes with two graphs.

Complex predictive model invariably contain many separate input variables. Whilst it is relatively simple to tightly control such variables in a computer model, it is particularly difficult to strictly control variables in a repeatable experiment. Unavoidable experimental variance can be accounted for when the number of variables is low. If a variable is accurately monitored it can be plotted onto a graph and observed visually. However, as the number of variables increases this visual observation no longer becomes possible. In many cases it is necessary to ascertain the effect a large number of variables have on a single output without observing any visual relationship. Such issues are common in areas of complex analytical modelling and risk classification. Sharma **1996** gives a number of examples and solutions to so called high dimensional multi-variate problems.

James **2004** validated a multi-variate predictive model visually by artificially restricting the input parameters. James used a series of different models in an attempt to predict the outbound speed, angle and spin of cricket balls incident to turf pitches. In order to validate the predictive models a series of impacts were made using a bowling machine and recorded using

high speed video. The experimental input parameters could be measured accurately using the high speed video, but could not be accurately controlled using the ball launching apparatus. To overcome this problem the individual input parameters of each impact were used in the predictive model and compared directly with the experimental results. In this case, the closer each point lies to the line $y = x$ the better the prediction. Figure 2.38 shows a series of predictions of rebound angle values for four different predictive models taken from James **2004**.

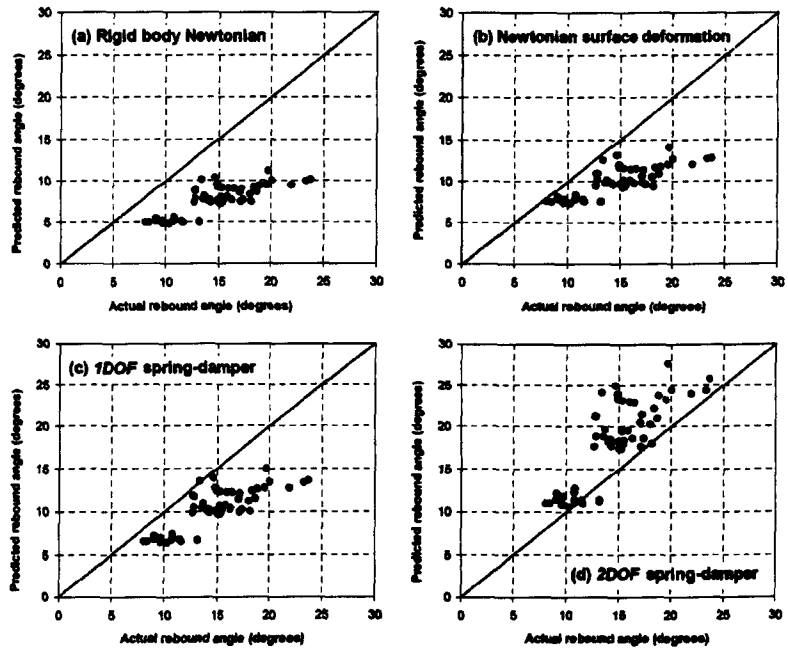

Figure 2.38. Predicted rebound angle values compared to experimental values as shown in James **2004**.

The main disadvantage of such an approach is that it only allows assessment of the model as a whole. It is very difficult to monitor the effect of changes in individual parameters on the outcome of the predictive model.

Modern computational techniques are able to find trends in sets of data with very high dimensionality. Kirk et al. **2006** used the neural network technique in order to find a relationship between 8 input parameters and the traction of a football boot stud on artificial turf. The major advantage of such an approach is that once established, the relationship can be used to observe the effect of a change in a single parameter. This is an advantage when attempting to experimentally validate a complex model in which strict control of each parameter is not possible.

The neural networks technique, whilst powerful is also complex. Many simpler techniques exist, many of which are simply expansions of 2D regression methods into higher dimensions. Multi-variate non-linear regression is a widely used example of this and is described in detail by Ratkowsky **1983** and Seber and Wild **2003**.

2.9 Chapter Findings

Each section can be summarised as follows:

- *The Ball*: From this research it is apparent that any racket/ball impact testing results will be affected by the type of ball used and its age. A pressureless ball is dynamically less stiff than a pressurised ball and exhibits lower rebound velocities at high impact speeds. As pressurised balls are used in almost every major tournament it would seem sensible to use such balls in realistic impact testing. Once a ball is exposed to the atmosphere its stiffness will continually reduce until the pressure in the core is equalised with the atmosphere. In competitive tournaments balls are not used for long enough periods for this to affect play. Despite this any balls which are used in testing should be continually renewed if a long enough time period has passed, regardless of the number of impacts. Repeated impacts cause a change in the ball's physical properties for two reasons.

  1) The coefficient of restitution drops at high impact speeds for as little as 100 impacts.

  2) The drag and lift coefficients both drop when the felt of the ball is worn.

  It is especially important therefore that pressurised balls are used and continuously renewed for high speed impact testing if results are to be consistently reliable and reflect realistic play conditions.

- *The Stringbed:* The literature regarding the racket stringbed shows that lower stringbed tension generally results in a higher post-impact ball velocity, although Goodwill and Haake **2004c** observed this not to be the case for oblique impacts. Whilst higher string tension does not generate any more spin, it does reduce the lateral distance travelled by the ball throughout impact. Whilst a factor such as control is hard to quantify it is possible that this reduced lateral distance could increase a player's ability to accurately control the ball as desired.

  Static and dynamic testing of string type has shown that many players' preference for natural gut is not misplaced. Whilst it is not as durable as synthetic strings, its stiffness is relatively independent of deformation. Regarding synthetic strings, polyester may be an advantage or disadvantage as far as spin generation is concerned, depending on the angle at which the ball is hit. At higher angles polyester generated less spin compared to nylon strings, whilst the converse was true at lower impact angles. This knowledge of string type, tension and expected behaviour is essential when attempting to design any realistic impact methodology.

- *The Racket:* Modern rackets consist almost entirely of carbon based composites and are considerably lighter and stiffer than more traditional wooden rackets. The larger head of a modern racket has a large region on the stringbed resulting in high

rebound ball velocity. A freely supported racket is closest to a hand held racket in terms of vibrational response. In terms of rebound velocity, the clamping condition at the handle is irrelevant. It has been noted however that grip may affect the ball rebound velocity for impacts off the central axis. Three distinct sweet spots have been identified. The *node point* which corresponds to zero vibration; the *COP* which corresponds to zero jarring at the wrist; and the *power point* which corresponds to maximum ball speed off the face of the racket. The position of the power point varies according to the movement of the racket.

- *Simulating Player Grip:* Much work has been repeated in similar circumstances and draws similar conclusions. Where the work agrees, the following conclusions can be drawn.
    - For impacts along the racket's longitudinal axis, grip conditions have no effect on the rebound ball velocity providing that the impact is sufficiently far away from the racket butt.
    - The distance from the butt required for no effect to be seen depends on the stiffness of the racket in question. Older wooden rackets, which have been used in a significant proportion of this work, show very little effect at all points along the longitudinal axis. A wooden racket has a smaller head and lower fundamental frequency. More modern, stiffer rackets may show some effect for impacts toward the throat of the racket due to the faster propagation of the impulse resulting from impact, and the fact that the throat is closer to the racket butt.
    - For impacts along the longitudinal axis a freely supported racket most closely represents the hand-held condition. The ball rebound velocity is effectively the same and the fundamental frequencies are closely matched.
    - Although very little work has been done to investigate the effect of grip on impacts of the longitudinal axis, the published data suggests that grip does play a role. For a freely supported racket, rotation during impact affects the post-impact trajectory of the ball.
- *Coefficient of Restitution:* The COR and ACOR represent a simple method of predicting ball rebound velocity and hence racket power and effectiveness. Generally, COR values are at a maximum for impacts at the throat of the racket and decrease towards the tip. Watanabe et al. **1979** showed experimentally that the ball rebound velocity does not vary with handle clamping condition. Hatze **1992** and Hatze **1993** differentiated between including and omitting racket velocity by referring to an apparent coefficient of restitution. True COR values were given by measuring racket rebound velocity. Values of between 0.758 and 0.885 tallied

closely with head clamped ACOR values measured by Brody **1979**. Brody et al. **2002** used the head clamped ACOR value to develop simple impact mechanics and the concept of effective mass in order to mathematically reduce an impact to a collision between two point masses. Such an analysis can be used to represent many impact scenarios, including two commonly cited sweet spots of a racket face.

- *Racket Sweet Spots:* The sweet spots of a racket face have been determined by what researchers in the field of racket dynamics consider to be the most favourable conditions when striking a ball. Their locations have been determined according to rigid and flexible body theory. The location of a sweet spot and the likely location of impact during play have been explored in very few cases. It is clear that more investigation is necessary in order to determine where on the racket face a player aims to strike the ball. It is also unknown whether a player can judge when a ball has more velocity after impact, or whether comfort at the hand is a more controlling factor in impact location. Hatze **1994** certainly suggests the latter. In his experiment, only 17% of recorded impacts fell within the power region as originally defined by Head **1975**.
- *Racket Impact:* In order to best represent the freely supported condition, the majority of impact testing to date has used a moving ball hitting a stationary racket. The objective of testing has varied. Generally; high speed video or light gates have been used to obtain velocities, an air cannon or ball projection device has been used to fire the ball, and simple piezoelectric transducers have been used to measure vibration. Impact testing to date has generally been limited to the central axis due to limitations in equipment and methodological techniques.
- *Player Testing:* Two methods of data capture are regularly used in objective player analysis. Invasive data capture techniques enable highly detailed and accurate information to be obtained through the use of active or reflective markers but are not suitable for filming in competitive conditions. Non-invasive testing can be used during competition conditions but currently cannot obtain information beyond simple position and velocity data. High speed video and small reflective markers offer a compromise between intrusiveness and data quality.
- *Videogrammetry:* A useful technique, used frequently to record and analyse movement. Stereoscopy allows analysis to be executed in 3D with a minimum of two cameras. In this case, calibration can be performed with a 3D, 2D or even 1D object. An internal report concluded that a 2D checkerboard object was the most effective and accurate method when limited to a 2-camera system.
- *Impact Modelling:* A wide variety of techniques have been used in order to model a racket/ball impact.

- *Rigid body modelling:* The simplest technique but does not account for deformation. In terms of ball modelling, energy losses are restricted to simple coefficients of restitution as in Daish **1972**. Ball spin is also limited when not accounting for radial deformations. The main disadvantage when modelling racket behaviour is the inability to account for vibrations. Brody **1997** showed this to be irrelevant for impacts at or near the racket node point.
- *Flexible body analysis:* Beam models of varying complexity have been created in order to account for frame vibration and associated energy losses. Goodwill and Haake **2002a** used a multi-section model allowing complex weight distributions to be accounted for. In the simplest case, Brody **1987a** showed experimentally that a racket has very similar node points to a freely supported uniform beam. When a ball is modelled as a deformable body, a time step method can be used to show force generation throughout impact and ascertain contact time. The contact time of a tennis impact is an important value, affecting many other areas of modelling. It was noted by Haake et al. **2005** and Cross **2002a** that obliquely incident balls often have more spin than can be accounted for by simple rigid body mechanics. To account for this overspin an offset normal force due to impact was proposed.
- *Visco-elastic analysis:* Goodwill **2002** used a complex spring damper model to better account for ball force and energy losses. The model used two dampers and a spring in parallel to represent the ball, whilst a single spring/damper represented the stringbed. This model stands as the most complex of its type.
- *Finite element analysis:* Perhaps the most advanced modern technique available but has only been used to limited success for ball/racket impacts to date. Goodwill et al. **2005** and Allen et al. **2007** produced thoroughly validated finite element models to model a ball impact. Goodwill noted that horizontal displacement during an oblique impact is large enough to produce an offset force *behind* the ball COM contradicting Haake et al. **2005**. However the force was not as far offset as proposed by Cross **2002a**. A variety of racket finite element models have been attempted with limited success. The age of these models means that the computing resources available at the time were not sufficient to give any particular advantage over well validated flexible beam models. Without experimental validation it is impossible to assess the success of these simplified attempts, especially when moving impacts onto the offset.

All these model types require vigorous and exhaustive validation which has only been performed in a number of cases. Without sufficient validation the results cannot be reliably compared to realistic results.

- *Data Validation:* Experimental validation can be a relatively straightforward process when the number of experimental variables is low. Direct visual comparison reveals trends and can be used to calculate the discrepancy between prediction and experiment. More complex models often involve many independent variables which cannot be compared visually. Simple methods of overcoming this problem involve comparing the model outcome directly with experimental results for a specific set of input parameters. Such an approach allows visual comparison but does not allow the effect of a change in a single variable to be monitored. Multi-variate analysis allows variables to be artificially varied and individually monitored. Many multi-variate techniques of varying complexities and applications exist. Simple techniques are still capable of modelling complex systems.

The literature reviewed in this chapter provides a good basis on which to build an investigation into racket/ball impacts. It is clear that a need exists to unobtrusively evaluate the racket movement exhibited by an elite player during impact. To date, predictive models have been limited in terms of the possible input parameters, it is now feasible to expand a model's capabilities to include six degrees of freedom.

3 3D Methods

3.1 Introduction

The literature review showed that within the context of this overall study, 3D videogrammetry would be the most suitable method of obtaining the experimental data required to develop a predictive model. Of the many videogrammetry calibration techniques available, a checkerboard based method devised by Zhang **1999** was deemed to be the most suitable for reasons of accuracy, ease of use and flexibility. In order for this technique to be effective, a number of methodological concerns must be evaluated so that its accuracy and efficiency is maximised during use.

3.2 Aim

This chapter will investigate the checkerboard calibration method; the calibration and 3D point reprojection. Any errors involved with these steps will be investigated and quantified where possible in order to ascertain how this method can be best utilised to produce the most accurate results. This involves firstly identifying the source of errors in calibration and reprojection and secondly performing an experiment to try and quantify realistic errors one might experience in its use.

3.3 Calibration Procedure, an Error Analysis

The process of calibrating a control volume, capturing data points and translating them into a series of 3D positions involves a series of steps and methodological considerations, all of which are subject to a variety of errors. By analysing the steps involved in calibration and reprojection, any unnecessary errors can be avoided, and unavoidable error can be minimised.

(a) Camera set-up.

Prior to any calibration it is imperative that the cameras are set-up correctly so that usable images are available to calibrate. Camera position, lens aperture, focus, shutter speed and lighting all have an affect on the final image. It is also essential that the shutters are synchronised, so that each pair of calibration images correspond to the same instant of time.

- *Camera Position:* Two cameras are needed to calibrate the system in 3D, as such the checkerboard must be visible to both cameras at all times. In order to transform a point into 3D it must be visible in both cameras, because the cameras cannot be moved after calibration it is vital that not only is the checkerboard clearly visible in both cameras, but that the subject of analysis will also be visible in both cameras over the period of analysis.
- *Aperture setting:* This controls the amount of light entering the camera and its depth of field. It is generally preferable to have the aperture as small as possible, the

increased depth of field will mean images stay in focus over a greater range of checkerboard movement.

- *Focus:* Usually focus should be set at the centre of the control volume or as close as possible. The focus cannot be changed after calibration, it is important then to consider not only the calibration but the overall subject of analysis. If the camera is poorly focused the ability to detect checkerboard intersections will be greatly diminished, introducing unnecessary error.
- *Shutter Speed:* If the speed of movement is very low, shutter speed can be set low to allow more light on to the subject. As long as no blurring is produced as a result of low shutter speed there is no discernible effect on calibration error.
- *Lighting:* This is one of the most important considerations. If too little light illuminates the checkerboard, intersections will be unidentifiable, rendering the system useless. If too much lighting is used the checkerboard can 'bloom' as shown in figure 3.1, effectively erasing the checkerboard intersections and introducing massive error.

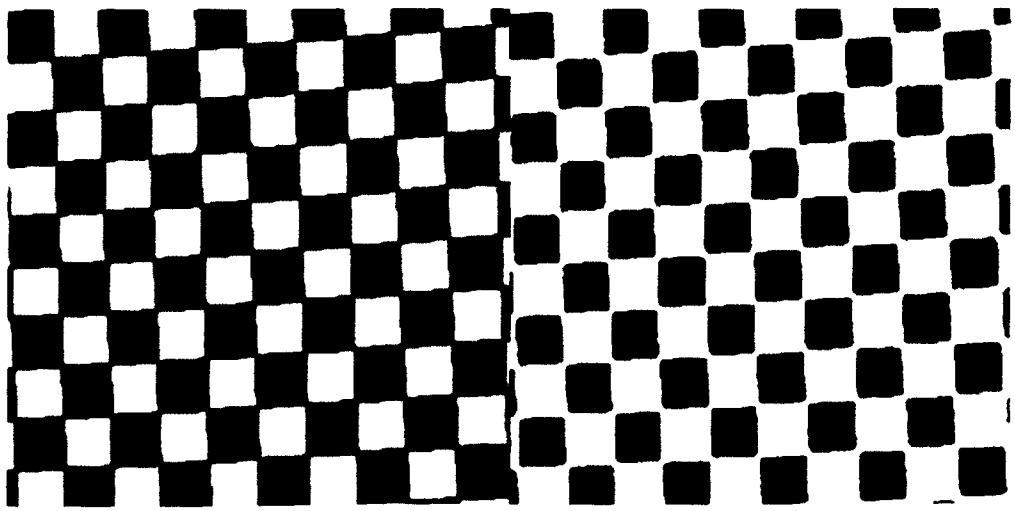

Fig 3.1. The image on the left shows an optimally exposed image, the image on the right shows an overexposed image where the checkerboard intersections have 'bloomed'.

(b) Recording Calibration Images

With the cameras set-up optimally, a volume is calibrated by moving a checkerboard into a number of positions within it, ideally 'filling' the space where the analysis is likely to take place. This section looks at the way to minimise error when recording the series of calibration images.

- *Checkerboard Manufacture:* Accurate calibration of 3D space relies on the accuracy of the checkerboard, regularity and precise knowledge of the square size ensures minimisation of errors. Checkerboard calibration uses the physical size of each

square to scale the calibrated volume, if the square size is measured incorrectly it will result in a systematic error present in every result.

- *Checkerboard Orientation:* Zhang **1999** analysed how the angle between the checkerboard and image plane affects the reproduction accuracy. Calibrations where the checkerboard is parallel to the image plane result in a high failure rate (the system is unable to be calibrated) whilst angles higher than 60° makes intersection detection difficult due to image foreshortening. An angle of around 45° to the image plane was deemed as the most accurate, but a variety of angles and orientations are necessary to ensure the system is well-conditioned and does not fail. Orientation angles of 20-50 degrees are most appropriate.

- *Number of calibration images:* Although it is possible to calibrate a system using only two different calibration images, as the number of images increases the error quickly reduces. Zhang **1999** showed that the error reaches a stable minimum for 15 images or greater.

- *Distance from camera:* The resolution of any image is limited to the capabilities of the photographic equipment used. It is preferable that the checkerboard occupies as much of the image as possible during calibration, it will be composed of more pixels and as such be easier to resolve the intersections, generating more accurate control points. Figure 3.2 illustrates this effect, the error resulting from pixelation of the checkerboard is discussed in the next section.

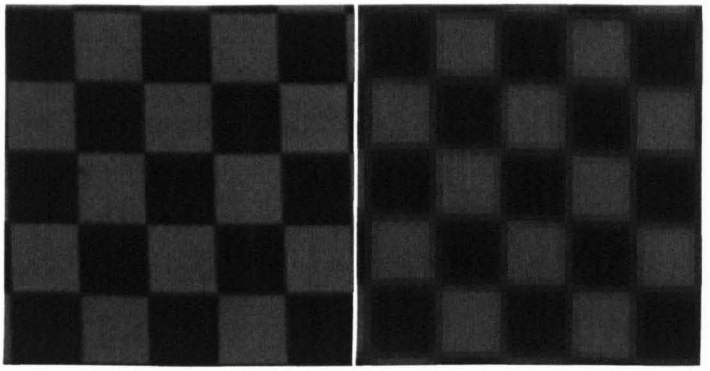

Fig.3.2. The same checkerboard at a similar angle composed of different numbers of pixels. The left image is in the higher resolution, it is clearly easier to distinguish features on this image.

- *Axes set-up:* The checkerboard calibration system aligns the 3D co-ordinate system to the left camera. However, it is often necessary to be able to describe the co-ordinates according to a different axes-set, e.g. aligned to the principle motion of a tennis ball.

  To create a new axes-set, 3 reflective spheres are placed accurately along a frame so that the three points form two axes at 90° to each other. The third axes is generated

from the cross-product of the original two, errors are minimised if these axes are orthogonal (within realistic margins). Figure 3.3 illustrates how axes are defined in (a) laboratory testing and (b) on a tennis court. In the first case the apparatus is designed such that the axes lie aligned to the trajectory of the ball, in the second the axes set is aligned along the baseline of the tennis court. This is described in more detail in chapters 6 and 4 respectively.

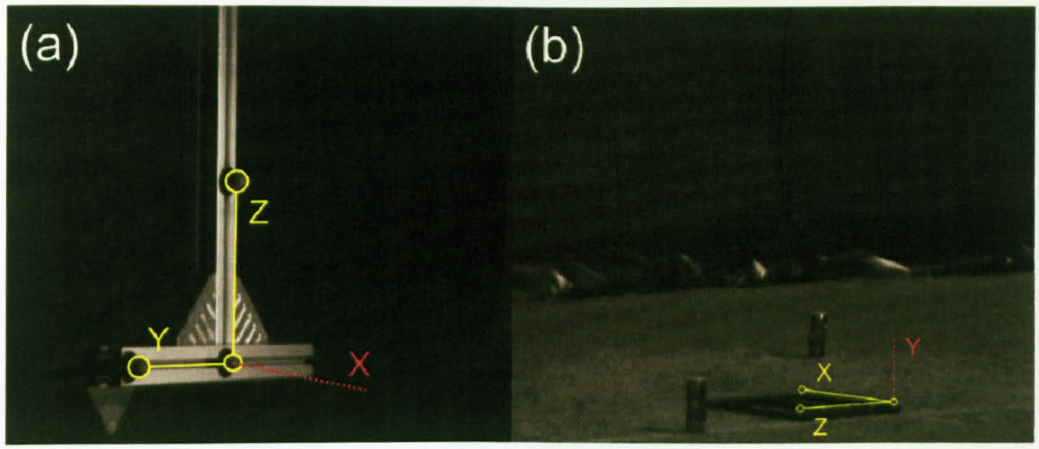

Figure 3.3. The axes-sets used in the laboratory (a) and on a tennis court (b), the dashed line shows which axes is generated from a cross-product.

(c) Generating camera parameters

Once a set of calibration images has been recorded, the camera parameters can be calculated from the extracted checkerboard intersections. Strobl et al. **2007** have produced a freely available Matlab toolbox for this purpose, it includes a graphical user interface for camera calibration, and a series of Matlab files which can be used to re-project 3D points. This software is used for camera calibration in this study.

- *Extracting checkerboard data points:* Each calibration image is loaded into the calibration software for analysis and corresponds to a different checkerboard position. A typical mosaic of checkerboard images is shown in figure 3.4. For each checkerboard position the data-points used in calibration are extracted from the intersections between the white and black squares on the checkerboard, as shown in figure 3.5.

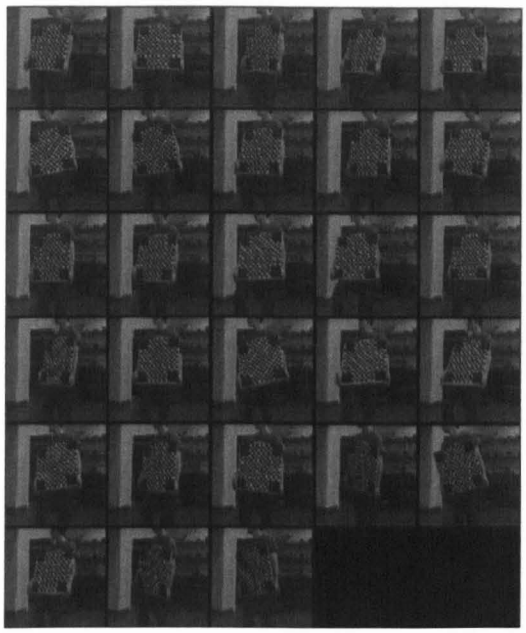

Figure 3.4. A mosaic of calibration images showing different checkerboard positions.

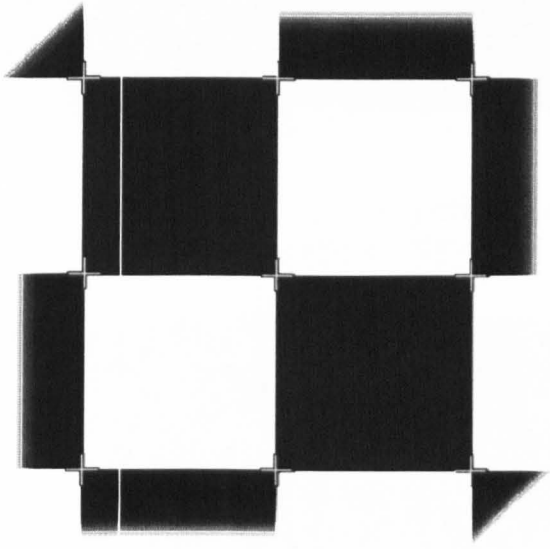

Figure 3.5. The data points used in camera calibration, once extracted they are given as a series of [U V] co-ordinates in the image plane.

Manual extraction of the intersection points would be subject to varying amounts of error depending on the skill of the user and the quality and resolution of the checkerboard images. Instead, the user clicks on the four outermost corners of the checkerboard, the software detects the number of squares contained within this area and allocates a series of regions known to contain an intersection. The calibration software automatically detects intersections within these regions by interpolating along white/black interfaces. The size of these allocated regions can be altered depending on the size of the checkerboard image in pixels. Figures 3.6 and 3.7 show

a checkerboard after automatic point detection. The software is able to resolve intersection positions to within 100,000th of a pixel and account for any lens distortion. As a result, the software is able to accurately predict intersection positions when the checkerboard is relatively poorly resolved. A quantified study of checkerboard resolution and its effect on overall accuracy is included in the next section.

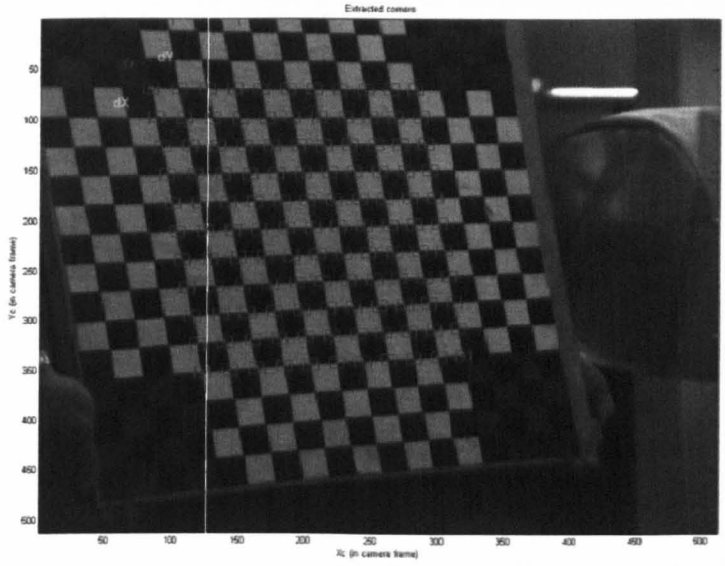

Figure 3.6. A checkerboard image after automatic intersection detection, the positions of the rectangular regions are set by the user clicking on four corners of the checkerboard.

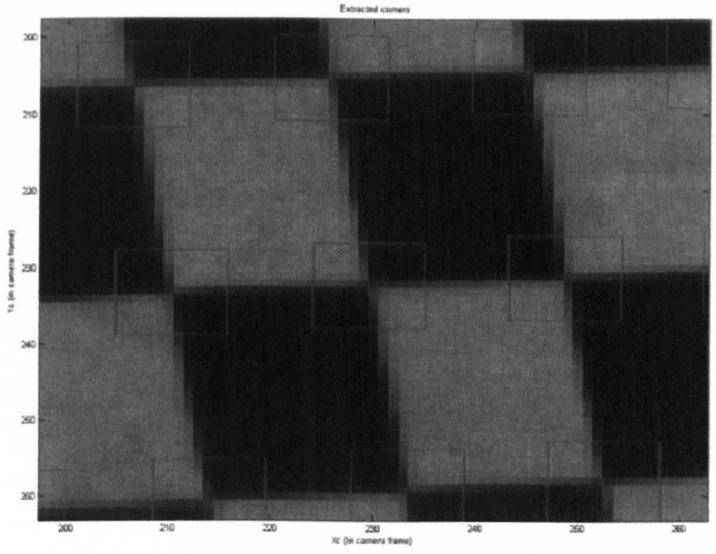

Figure 3.7. The checkerboard shown in figure 3.6 at a higher zoom level, the intersections can be seen as points within each rectangular region.

- Calculating Camera Parameters:

  To produce a usable 3D calibration cameras are calibrated individually to give intrinsic parameters such as focal length, principal point and pixel skewness. With this information, the two cameras are calibrated as a stereo system, giving external parameters which define the cameras with respect to position and scale.
  The intrinsic parameters can be used to re-project the intersection points back onto the calibration image using the position of the checkerboard's top corner and the physical size of each square. An error can be calculated from the pixel discrepancy between the re-projected intersection point and the point detected by the software, as shown in figure 3.8. This error is dependent on the quality of the calibration and the accuracy of the detected intersection points. The calibration can be improved by manipulating the initial camera parameters to generate more realistic initial conditions. E.g. by changing the order of the distortion model, or giving a better initial assumption of pixel skewness. Increasing the size of the search regions shown in figures 3.6 and 3.7 can improve the quality of the interpolation used to detect checkerboard intersections, but can also cause false detection and increase error.
  Altering the parameters of calibration in this way can also be done to calibrate a system which would otherwise fail. This might be when the quality of the images are not sufficient, the intersections have been badly detected, or when no solution converges and the software algorithm is unable to calibrate the system. The checkerboard toolbox allows the user to change the parameters so even a badly recorded set of calibration images can result in a usable calibrated system.
  The pixel distance between the detected and re-projected intersection points can be plotted in [U V] co-ordinates for every checkerboard position and an average error value is given (see figure 3.9). At this stage individual checkerboard positions can be removed from the calibration if their error is still large after attempted improvements. When both cameras have been calibrated, their parameters are combined to form a complete stereo calibration, one such calibration is shown graphically in figure 3.10.

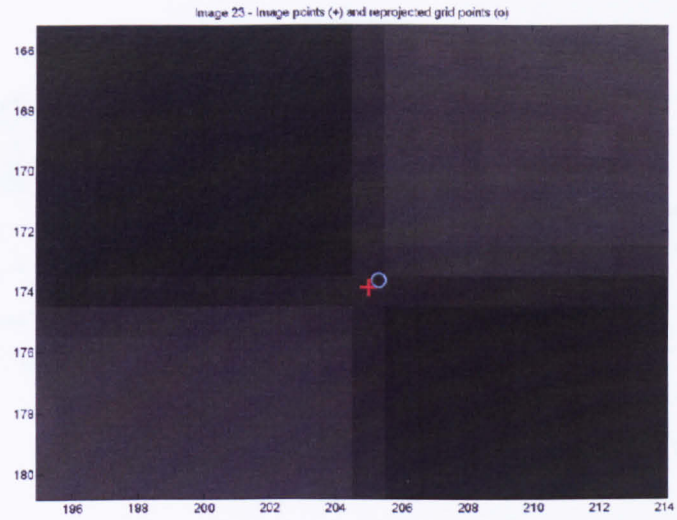

Figure 3.8. Comparison between the intersection detected by the software (+) and the re-projected intersection point (O)

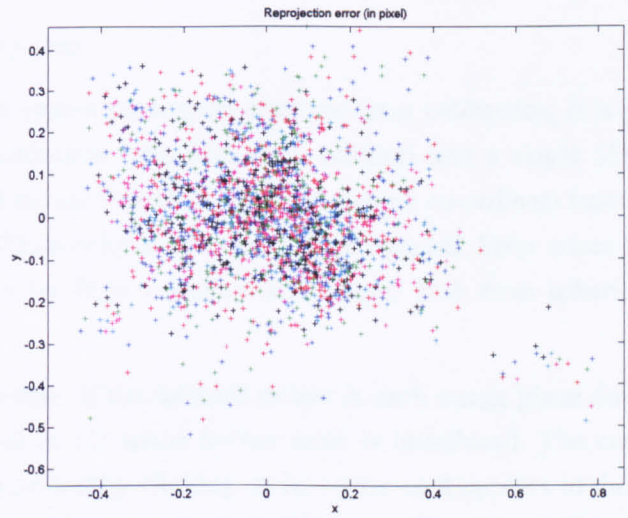

Figure 3.9. A plot of the re-projection error for a typical calibration, the average [U V] error in this case is [0.19 0.14] pixels.

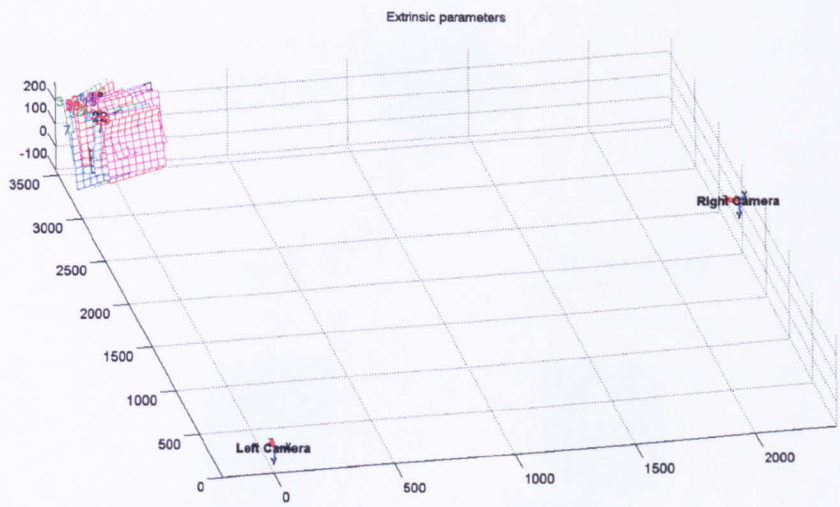

Figure 3.10. A schematic of a completed 3D calibration, showing the position of the left and right camera with relation to the checkerboard positions (Note the origin and axes-set centred around the left camera)

(d) Re-projecting 3D points

With the stereo system parameters obtained from calibration, it is possible to re-project a pair of [U V] co-ordinates (one from each camera) into a single 3D point using Matlab scripts included with the calibration software. A simple co-ordinate transformation and origin translation puts the 3D co-ordinate into the desired axes-set. Error arises from the difficulty in picking the desired point from a pair of 2D images, both from sphericity errors and point resolution.

- *Sphericity error:* If the selected points in each image plane don't correspond to the desired point in 3D space further error is introduced. The centre of a sphere can always be selected by clicking on its centre as it appears in the image plane, this is not the case when non-spherical objects are the object of study. The difficulty in selecting points in the image plane is illustrated in figure 3.11. This error can minimised by using spherical control points or selecting points on a flat surface.

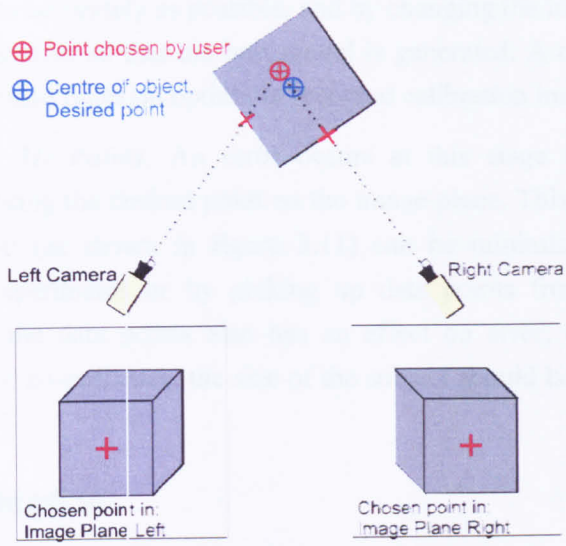

Figure 3.11. Re-projected point error, an illustration of the error resulting from selecting the centre of an object's surface when wanting to track an object's centre. Parallax, and image skewness means this error is always present when tracking the centre of non-spherical 3D objects.

- *Point Resolution and feature recognition:* When identifying and recording the [U V] co-ordinates of data points, the ability to accurately identify each point depends on how well they are resolved. In a camera system of limited pixel size this is invariably dependent on their size in the image plane. Automatic tracking software is less prone to this error than manually tracked points.

3.3.1 Summary and Conclusions

In summary, identifying the sources of error in each stage, steps can be taken to ensure that they are minimised.

- *Camera Set-up:* It is vital that settings are chosen to give well exposed, crisp images that have the objective clearly visible in both cameras at all times. This ensures that the data points are all visible and the system is also set-up optimally for the proceeding experiment.

- *Recording Calibration Images:* Previous experiments have shown that the checkerboard should be recorded at angles between 20-50 degrees and that over 15 calibration images should be recorded. Realistic limitations on measuring checkerboard angle mean that the angle is based purely on human judgement. As a result, at least 20 calibration images should be recorded each time to account for possible void images resulting from bad positioning. The size of the calibration squares must be known in order to accurately define the system, this can be done with a travelling microscope.

- *Generating Camera Parameters:* The error resulting from calibration can be

intersections as accurately as possible, and by changing the initial conditions used to calibrate the system so that the best model is generated. A calibration system with minimal error also relies on optimally recorded calibration images.

- *Re-projecting 3D Points:* An error occurs at this stage from the difficulty in accurately picking the desired point on the image plane. This distortion and error in point selection (as shown in figure 3.11) can be minimised by using spherical markers in experiments or by picking up data points from a flat surface. The resolution of the data points also has an effect on error, especially if manually extracting their co-ordinates, the size of the subject should be maximised within the image plane.

3.4 Error Quantification

3.4.1 Aim

The processes and sources of error in calibrating 3D space and re-projecting points have been identified, this section aims to quantify some of these errors through an experiment investigating the effect calibration resolution has on calibration accuracy.

3.4.2 Methodology

Two cameras were trained on a specific calibration volume, this volume was calibrated at five different levels of camera zoom to alter the size of the checkerboard in the image plane (see figure 3.12). The physical calibration volume is kept constant throughout the experiment as a rough $0.5 \times 0.5 \times 0.5$m cube. Twenty five calibration images were recorded at each zoom level giving five calibrated systems at different checkerboard resolutions.

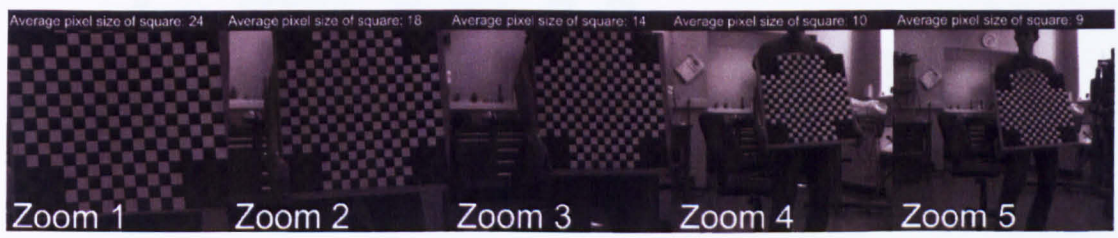

Figure 3.12. Five calibration images at five different levels of zoom taken from the left camera, the decreasing resolution of the checkerboard is reflected in the decreasing square size.

The squares on the checkerboard used in this experiment were measured using a travelling microscope, the horizontal and vertical sides of 10 random squares were measured and an average value taken. Each side was measured as **31.5mm** to within 0.01mm, with negligible variance.

The square sides can also be measured by selecting adjacent checkerboard intersections from an image pair and re-projecting the points into 3D space using the calibration software. The intersections were detected automatically using the calibration software. The calibration

software automatically detects intersection points as part of the calibration. Ten adjacent points were selected randomly from within the software and re-projected back into 3D space. The distance between adjacent points is calculated by measuring the length of the resultant (in pixels) between the two points.

In this way the accuracy of the calibration process and effectiveness of the point detection software can be assessed and the effect of decreasing checkerboard resolution has on this accuracy can be evaluated.

3.4.3 Results

Calibration Error

The pixel error (as illustrated in figure 3.8) of each of the five calibrations is shown in figure 3.13. It can clearly be seen that the error decreases as the resolution of the checkerboard decreases. The resolution of the checkerboard is denoted by *square size*, the average size of a checkerboard square as it appears in the image plane and is shown in figure 3.12, corresponding to the specific zoom level. Error is significantly lower in the vertical V direction of the image plane than along the horizontal U for the first three calibrations for both the left and right cameras, this switches for the final two calibrations.

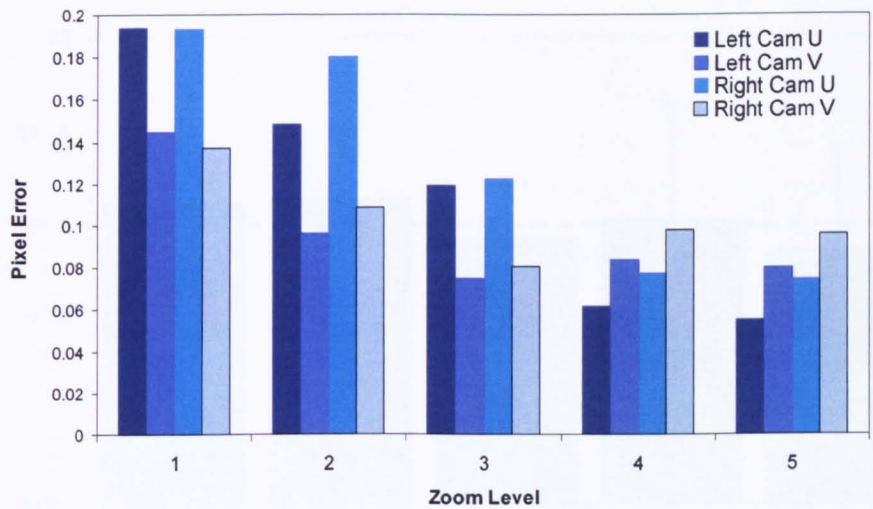

Figure 3.13. The pixel error of each calibration for the left and right cameras in both the U and V direction

In figure 3.14, pixel error is substituted for mm error by using a pixel/mm value based on the average square size in pixels and the measured square size of 31.5mm. The decrease in error is no longer obvious, a large increase in error can be observed in the V direction. Error in the U direction more than halved when measured in pixels. When measured in mm a decrease of 20% is only apparent for the left camera, staying around constant for the right. The maximum percentage error of the measured square size is 0.8% at zoom level 1, going to just over 1% at zoom level five.

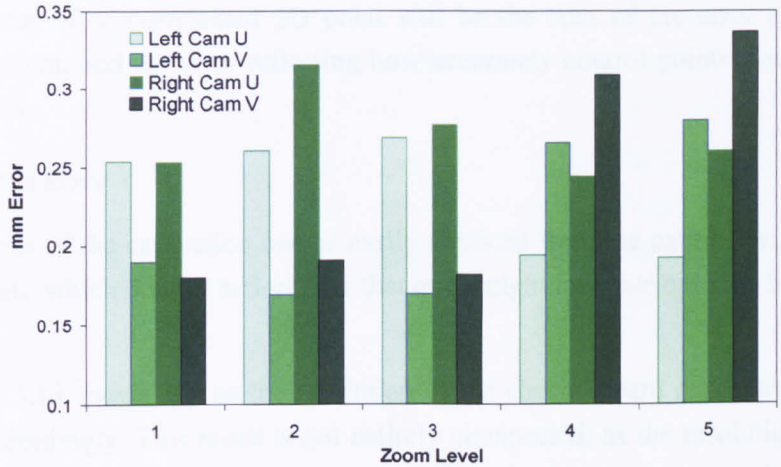

Figure 3.14. The mm error of each calibration for the left and right cameras in both the U and V direction

Figure 3.15 shows the mean and standard deviations of the measured square sizes for each of the five calibrations as calculated by the point detection software. The mean keeps very close to the measured value of 31.5mm although the variance increases as the size of the checkerboard decreases.

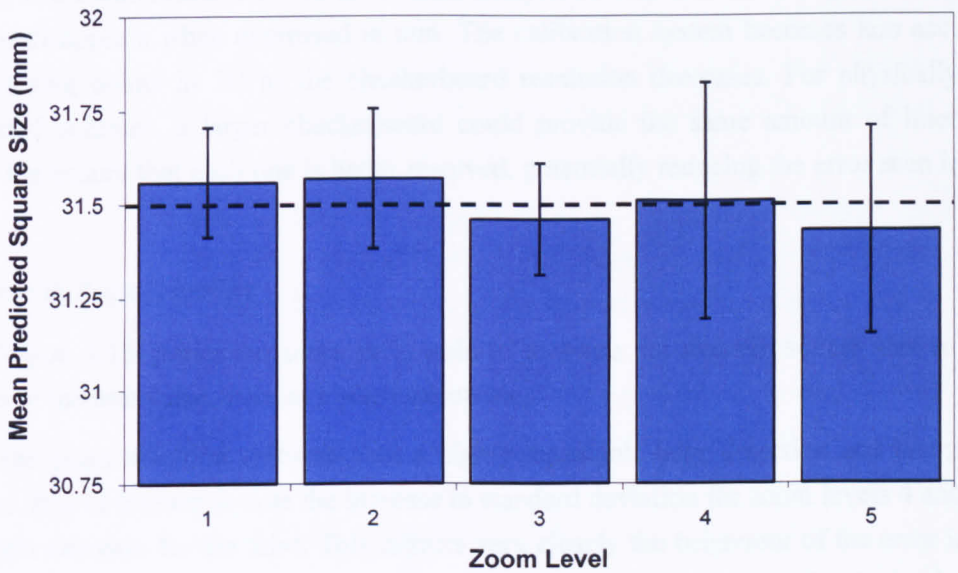

Figure 3.15. The mean square size, measured using automatic point detection, plotted against corresponding zoom level. The standard deviation is shown as vertical error bars at each zoom level. The measured square size of 31.5 mm is shown as a horizontal line.

3.4.4 Discussion and Conclusions

The error of a re-projected 3D point will be the sum of the error arising from the calibrated system, and the error reflecting how accurately control points were selected from the 2D images.

(a) Calibration Error

The error of the calibration can be easily obtained from the calibration software, but is given in pixels, which doesn't reflect how that error might translate onto the final re-projected point.

Figure 3.13 shows that as the resolution of the checkerboard decreases the pixel error decreases accordingly. This result is not entirely unexpected; as the resolution of the system drops the software is still able to consistently detect checkerboard intersections, reflected by the accuracy of square measurement shown in figure 3.15. There will be a resolution at which this breaks down and the intersections are graphically indistinguishable, but the purpose of this investigation was to establish the effect of decreasing resolution, not testing its limits. As the size and resolution of the control volume decreases any errors in the calibration system also consist of fewer pixels.

Figure 3.14 shows that this does not necessarily mean a more accurately calibrated system. If the calibration is converted to mm, analysis reveals that the strong downward trend in error disappears when expressed in mm. The calibration system becomes less accurate at re-projecting points in 3D as the checkerboard resolution decreases. For physically larger calibrated volumes, a larger checkerboard could provide the same amount of intersection points but ensure that each one is better resolved, potentially reducing the error seen in figure 3.14.

(b) Error in Point Selection

Figure 3.15 shows the software is able to measure the average square size to within 0.1mm of the true value, even at lower resolutions.

The point selection software uses a highly repeatable edge detection and interpolation method. It is of interest to note the increase in standard deviation for zoom levels 4 and 5, and the slight decrease for the third. This mirrors very closely the behaviour of the error in the V dimension seen in figure 3.14, suggesting that the increase in variance is due to the decreased accuracy of the calibration system used to generate the results, rather than from the selection of the points themselves. This experiment uses the same checkerboard images to calibrate the volume and to measure the checkerboard squares. It is not possible to separate the error of calibration from the error arising from point selection. Taking the pixel distances directly from the images yields no meaningful results; a value given in pixels has no direct physical bearing without the calibration system, and any variance in the measurement is just as likely to come from skewing of the board due to its orientation as from inherent variability in the

measurement technique. Despite this it would appear that the variability in point selection is unlikely to increase as the resolution decreases. A reasonable conclusion, is therefore that the highly repeatable point detection method is unlikely to increase variability unless the image quality decreases vastly.

The point detection method used by the software is undoubtedly very accurate and repeatable, and is a good example of the many automatic point tracking methods. Like any automatic tracking system using relatively simple image processing, its range of operation is limited. The checkerboard has to be well lit, it cannot be too slanted and has to be in full view of both cameras. The situation becomes more complicated when trying to track individual markers or a ball's trajectory. Noisy images, reflections and visual obstructions can confuse all but the most intelligent tracking methods.

This study, rather than give a definitive figure of the accuracy of this 3D method has shown the considerations which must be taken into account when trying to maximise the accuracy of 3D re-projection, these are:

- *Ensure the calibration accuracy is sufficient.*The size of the calibrated volume as well as the stated pixel error must be taken into account when assessing this.
- *Ensuring the software is able to detect the checkerboard intersections.* This study has shown the software to be highly repeatable in point selection, even when the size of the checkerboard within the image plane is reduced. This doesn't mean that the method is failsafe, every consideration mentioned previously in this chapter still applies; the checkerboard images must be well exposed, sufficiently well oriented and entirely visible in both cameras.
- *Using a control volume of appropriate size.* The size of control volume and checkerboard not only has implications for calibration accuracy, but how accurately points in the image plane can be selected by a user. The smaller the object of study appears in the image plane, the harder it is to resolve and select the desired point of study. It is conservative to state that a manually selected point may have an error of ± 0.5 pixels in the image plane, how this translates as an error in mm is dependent on the scale of the calibrated volume. In general though this is not much larger than 1% for the measured square size of 31.5 mm.

3.5 Chapter Summary

This chapter provided an assessment of the checkerboard calibration method. Identifying possible sources of error and providing methodological guidelines in order to maximise its use in further experiments. Examples of this include the correct camera set-up, an optimised calibration procedure, and a minimisation of re-projection error through the correct use of image analysis algorithms.

A final study looked into the effect of image quality and resolution on system accuracy by using a number of calibrated volumes of varying size within the image plane. Generally, the calibration method becomes more variable as the resolution of the checkerboard within the images decreases, the point selection software is very repeatable when given images of sufficient quality. Generally the control volume and size of checkerboard should be as large within the image plane as possible; not only does this decrease the variability of the calibrated system, but makes subjects much easier to distinguish and will minimise error when manually selecting points. With this knowledge, future experiments can be designed in order to give the most accurate results possible, whether this is repeatable laboratory work, or player shot analysis.

4 Player Shot Analysis – Experiment and Method

4.1 Introduction

The literature review confirmed that the best way to perform a player shot analysis would be to extract all essential shot characteristics using 3D videogrammetry. The shot characteristics are defined as the ball and racket linear and angular velocities and the impact position of the ball on the racket face. To keep the intrusion into the player's environment as low as possible, visual racket markers should be used (as opposed to active radio emitters for example) and only two cameras should be used to record the player's shot and the testing should be performed in the player's natural environment (an indoor or outdoor court). It is therefore necessary to develop a practical methodology which has minimal intrusion, is portable enough to enable recording in different locations and achieves a high level of accuracy.

The development of a practical method able to extract the linear and angular velocities and impact position from a player's shot consists of several sections. The first section outlines a theoretical method which enables the calculation of these values using videogrammetric techniques. The second section develops a practical method which will best put the theoretical technique into practice. The third section follows the development of an analytical methodology which extracts the shot characteristics from the recorded data.

4.2 Aims

This chapter describes the development of a system which will be used to record a tennis player's shot and extract all its vital elements in three dimensions. The system will be:

- Transportable;
- Present a minimal intrusion into the player's environment;
- Is able to capture the linear and angular velocities and impact position of the ball and racket pre and post-impact.

4.3 Extracting ball and racket movements

Like most videogrammetric technique, the extraction of useful data from recorded images relies on discrete markers being used to indicate the position of designated points on the subject being tracked.

When tracking these points in 3D, planes can be used to indicate regions in space and vectors to indicate movement. This work focuses primarily on the racket and ball characteristics immediately prior to, and after the instant of impact. For this reason it is only necessary to track the ball and racket movements over a small time period pre and post impact. If ball and racket movements are tracked over a sufficiently small time period, we can assume that the accelerations are appreciably zero, this is discussed later in the chapter. By

assuming linear velocities, the pre and post impact shot characteristics can be calculated using simple vector mechanics.

4.3.1 Co-ordinate systems

When defining shot characteristics it is sometimes useful to describe them according to either a *global* or *local* reference frame. In this case the global reference frame refers to a constant axes-set oriented within 3D space, this is aligned according to the user's preference. The local reference frame is aligned to the racket face at all times, and hence changes with racket movement. The global axes set is defined as [U,V,W] and the local axes set as [x,y,z].

The ball

The centre of the ball can be tracked as a point in space, rotations can be monitored using discrete markings upon its surface. When tracked over a numbers of instances, the ball positions can be used to define three velocity vectors describing the ball's movement in three directions.

The Racket

Unable to be tracked as a single point, the racket can be tracked by defining its face as a plane in space with an associated axes-set and origin. Three points are necessary to define a plane in space. Markers attached to the racket can act as singular points with which to define this plane, and if the relative positions and orientations of the markers are known, they can also be used to define an associated local axes-set and racket origin.

A plane is defined algebraically as:

$$aU + bV + cW + d = 0 \qquad \textbf{[4.1]}$$

The coefficients *a, b, c* and *d* can be calculated from the 3D position of three points $\mathbf{P_1}$, $\mathbf{P_2}$ and $\mathbf{P_3}$ in 3D space, if their respective co-ordinates are defined in an [x y z] system as:

$$\mathbf{P}_1(U_1,V_1,W_1) \qquad \textbf{[4.2]}$$

$$\mathbf{P}_2(U_2,V_2,W_2) \qquad \textbf{[4.3]}$$

$$\mathbf{P}_3(U_3,V_3,W_3) \qquad \textbf{[4.4]}$$

The coefficients are defined as:

$$a = \begin{vmatrix} 1 & V_1 & W_1 \\ 1 & V_2 & W_2 \\ 1 & V_3 & W_3 \end{vmatrix} \quad b = \begin{vmatrix} U_1 & 1 & W_1 \\ U_2 & 1 & W_2 \\ U_3 & 1 & W_3 \end{vmatrix} \quad c = \begin{vmatrix} U_1 & V_1 & 1 \\ U_2 & V_2 & 1 \\ U_3 & V_3 & 1 \end{vmatrix} \quad d = \begin{vmatrix} U_1 & V_1 & W_1 \\ U_2 & V_2 & W_2 \\ U_3 & V_3 & W_3 \end{vmatrix} \qquad \textbf{[4.5]-[4.8]}$$

The definition of the local co-ordinate axes set is dependent on the position of the individual markers, but an axis perpendicular to the racket face can be calculated from the values of the coefficients from equation 4.1, defined in global co-ordinates and given as the local *z* axis in this case.

$$\hat{\mathbf{z}} = \frac{a\mathbf{U} + b\mathbf{V} + c\mathbf{W}}{a^2 + b^2 + c^2} \quad [4.9]$$

A knowledge of the racket's position and orientation at every instant allows the velocities (both linear and angular) of any point on the racket face to be calculated.

Velocity Calculation

It has been assumed that all accelerations are zero over the period of testing, for this linear assumption to be valid, the testing must be executed over a sufficiently small time period. The time period of recording is dependent on the recording frame rate of the high speed camera, and will be discussed later in the chapter. By performing a linear regression of position against time in each axis, the velocity in each respective direction can be calculated. This method can be used to obtain values of velocity directly prior to, and after, the ball's impact on the racket.

This is a simple calculation for the ball, which is represented as a single point in space. Its velocities can be calculated directly from the ball's change in position over time. The racket is defined as a plane with associated angular velocities, and as such, each point on the racket face has a different linear velocity.

The velocity of a point on the racket face is calculated by tracking its position in 3-D over a small time period. A linear fit in each direction gives the velocity. The position of a point on the racket plane is calculated using the racket's local axes-set and the point's distance from the local origin.

The velocities can be expressed in the global or local axes-set, but as the local-axes set changes with the orientation of the racket, velocities expressed in this way have limited meaning and are only usually applicable for specific calculation regarding impact conditions.

Angular Velocities

For ball spin, Carré **2000** outlines a method to calculate 3D spin from markings on a ball's surface. However, the resolution of the images in this current study is not high enough to re-create this with sufficient accuracy. Single-axis spin can be calculated by counting the time it takes for a single ball revolution.

Racket angular velocity is defined around a point in space. For convenience and to aid comparison, this is usually set as the racket's COM which is easily calculated by measuring the racket's balance point prior to testing.

The angular velocity around an axis at any instant can be calculated by comparing the velocity of the COM with that of a point along an axis perpendicular to that of the spin, as illustrated in figure 4.1.

If v is the difference in velocities, and r the distance between the two points, the angular velocity in that particular direction can be calculated by:

$$\omega = \frac{v}{r} \qquad [4.10]$$

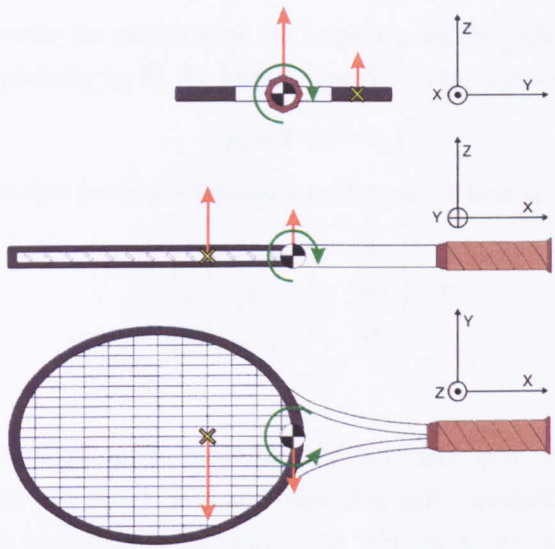

Figure 4.1. Three diagrams showing how angular velocity around a local x, y and z axis is calculated by comparing the COM's velocity with that of a point along an axis perpendicular from the spin axis.

4.3.2 Impact Position

An accurate knowledge of the impact position is a vital factor in the determination of the shot's output conditions. The impact position can be calculated using a bisection method; the ball's velocity vector and initial position give its position within the control volume at any instant. The plane equation at any instant is calculated from the separate positions of the racket markers (as shown in equations 4.1-4.8) which are calculated in the same way as the ball's position.

If the plane equation is as shown in equation 4.1, and the position of the ball is given by (U_b, V_b, W_b), the perpendicular distance, D between the ball's position and the racket plane is given by:

$$D = \frac{|aU_b + bV_b + cW_b + d|}{\sqrt{a^2 + b^2 + c^2}} \qquad [4.11]$$

A simple bisection routine, calculating over ever decreasing time intervals can find the time at which D is appreciably zero, and hence the instant of impact.

From the impact instant come the impact positions, and once the global position of the ball at impact is known, it can be transformed into local co-ordinates through an origin translation and axes transformation.

Three unit vectors are used to describe the local axes-set:

$$\hat{\mathbf{x}} = [U_x, V_x, W_x] \qquad [4.12]$$

$$\hat{\mathbf{y}} = [U_y, V_y, W_y] \quad [4.13]$$

$$\hat{\mathbf{z}} = [U_z, V_z, W_z] \quad [4.14]$$

If $\mathbf{P_i}$ is used to denote the position of the impact point in global co-ordinates, and the racket's origin is given globally by $\mathbf{P_o}$ the impact position in local co-ordinates $\mathbf{p_i}$ is given by:

$$\mathbf{p_i} = \mathbf{T} \cdot (\mathbf{P_i} - \mathbf{P_o}) \quad [4.15]$$

where $\mathbf{T}$ is the global to local co-ordinate transformation matrix given by:

$$\begin{bmatrix} \hat{\mathbf{x}} \\ \hat{\mathbf{y}} \\ \hat{\mathbf{z}} \end{bmatrix} = \begin{bmatrix} U_x & V_x & W_x \\ U_y & V_y & W_y \\ U_z & V_z & W_z \end{bmatrix} = \mathbf{T} \quad [4.16]$$

4.3.3 Playing Angle

Previous work investigating the mechanics of spin and spin generation often mention the incident angle between the racket face and incoming ball. Goodwill and Haake **2002b** and Knudson **1997** have both investigated spin citing the 'playing angle' as a factor affecting spin generation. The playing angle is easy to measure and control in a laboratory setting where the racket is often held stationary. Although more complex, it is also possible to calculate the playing angle for recorded shots in the player shot analysis.

Playing angle values obtained from player shot analysis can be compared with previous investigations into spin and validate questions which arise when developing a predictive model; are the right playing angle values being used in testing? How well does the playing angle correlate with ball spin generation?

The playing angle is calculated using the ball and racket velocities, and the local axes *z* which is perpendicular to the racket face. The instant of impact is calculated during the calculation of the impact position, and the playing angle is calculated at this instant.

The calculation of the playing angle consists of three distinct steps (figure 4.2):

1) The resultant angle between the velocities of the ball and racket's impact point is calculated with respect to the global horizontal U axis using the dot product. If $\mathbf{v_{IP}}$ is the relative velocity of the impact point and ball at the instant of the impact, and $\hat{\mathbf{U}}$ the global U axis, the first angle is:

$$\theta_1 = \cos^{-1}\left(\frac{\mathbf{v_{IP}} \cdot \hat{\mathbf{U}}}{|\mathbf{v_{IP}}|}\right) \quad [4.16a]$$

2) In the laboratory, the racket is often held vertically or horizontally when the ball is fired onto its surface. On a court, the player could be holding the racket in a variety of different orientations with relation to the court. The angle between the racket's normal and U axis (effectively, how the racket is tilted away from the vertical) is calculated to move the playing angle from a global to a local reference frame.

$$\theta_2 = \cos^{-1}\left(\hat{\mathbf{z}} \cdot \hat{\mathbf{U}}\right) \qquad \textbf{[4.16b]}$$

3) The sum of these two angles gives the playing angle, described diagrammatically in figure 4.2.

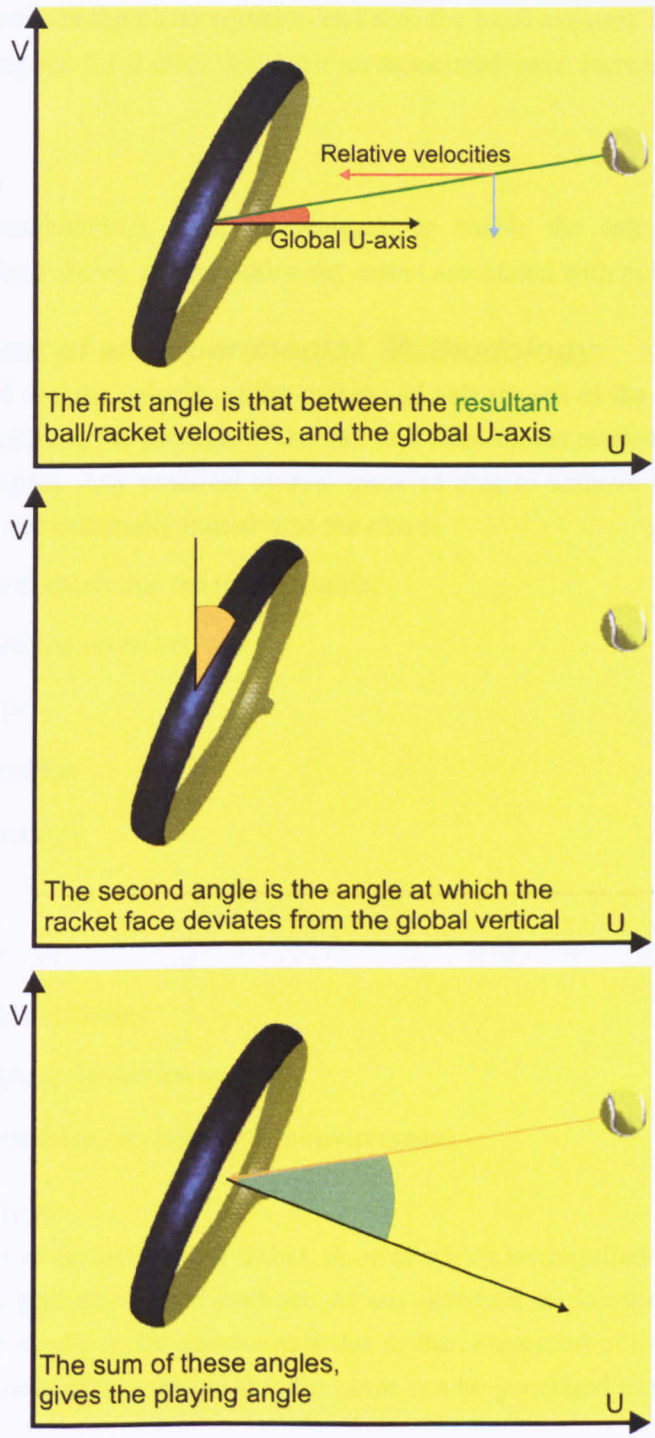

Figure 4.2. A diagrammatic explanation of how the playing angle is calculated

4.3.4 Errors

The errors likely to arise from this analytical method come from the accuracy of the ball and racket marker positions. Any error coming from the ball's position will generate corresponding errors in the velocity and hence trajectory of the ball. Errors in the racket markers produce errors in the plane equation and also the local axes-set. Points re-created on the racket face using the local axes will have an associated error increasing away from the racket origin.

4.3.5 Conclusions

A practical methodology must be designed to enable the calculation of the shot characteristics outlined above, and minimise any errors associated with point reprojection

4.4 Development of an experimental Methodology

The linear and angular velocity of the racket and ball as well as the impact position can be calculated by recording the position of the ball and three racket markers over a small time interval close to impact. Any practical system must be able to achieve this aim whilst still remaining portable and minimally intrusive to the player.

This section will determine the most suitable:

- Marker position on racket
- Marker type
- Camera position
- Camera Settings
- Lighting

In order to achieve:

- High marker visibility
- High marker re-projection accuracy
- Minimal intrusion into the player's environment

4.4.1 Marker Position

Five markers will be used on the racket, three of which are required to define the racket face as a plane, and generate a local axes-set. At any instant a marker may be obstructed by the ball or player or simply made un-trackable due to the orientation of the racket. Thus, two of the markers are redundant to ensure that the plane can be generated in the event of marker obstruction.

If five racket markers are positioned as shown in figure 4.3, two of the markers 1-3 can be used to define an initial x or y axis, with a third enabling definition of the plane and hence

the perpendicular z-axis. The cross product of the z-axis and initial axis gives the final axis necessary to define the full co-ordinate set.

Figure 4.3. A diagram showing the marker positions to enable reliable plane generation. Marker 1 is situated at the top of the racket in line with the central main string. Markers 2 and 3 are directly opposite each other, in-line with the central cross string and markers 4 and 5 can be placed anywhere in the throat region of the racket.

The relative positions of markers 1-3 are needed to define the axes-set. From figure 4.4, the distances a and b are used to calculate the angle θ using simple trigonometry and calculate the position of the origin.

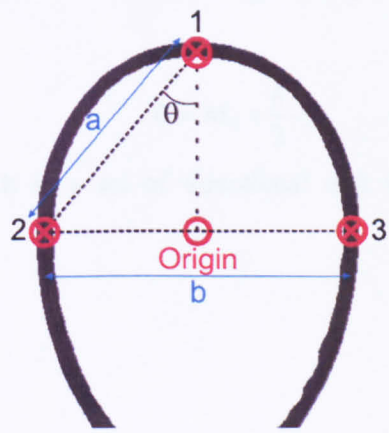

Figure 4.4. The relative positions of markers 1-3 on the racket face. The distances a and b can be used to calculate θ and the position of the origin.

If the marker positions 1-3 are defined as:

$$\mathbf{M}_1 = (U_{M1}, V_{M1}, W_{M1}) \quad \textbf{[4.17]}$$

$$\mathbf{M}_2 = (U_{M2}, V_{M2}, W_{M2}) \quad \textbf{[4.18]}$$

$$\mathbf{M}_3 = (U_{M3}, V_{M3}, W_{M3}) \quad \textbf{[4.19]}$$

A directional unit vector calculated from the positions of markers 2 & 3 is designated as the local y-axis:

$$\hat{\mathbf{y}} = \frac{\mathbf{M}_3 - \mathbf{M}_2}{|\mathbf{M}_3 - \mathbf{M}_2|} \quad [4.20]$$

This is used with the local z-axis (From equation 4.9) to calculate the local x-axis using a cross-product:

$$\hat{\mathbf{x}} = \hat{\mathbf{y}} \times \hat{\mathbf{z}} \quad [4.21]$$

If marker 2 or 3 is obstructed from view, a directional unit vector calculated from the position of markers 1 & 2 (or 1 & 3) can be designated as an *intermediary* local x-axis

$$\hat{\mathbf{x}}' = \frac{\mathbf{M}_2 - \mathbf{M}_1}{|\mathbf{M}_2 - \mathbf{M}_1|} \quad [4.22]$$

An intermediary y-axis is calculated from a cross-product:

$$\hat{\mathbf{y}}' = \hat{\mathbf{z}}' \times \hat{\mathbf{x}}' \quad [4.23]$$

An axis rotation of θ degrees gives a correctly orientated local x-axis:

$$\hat{\mathbf{x}} = \hat{\mathbf{x}}' \cdot \cos\theta + \hat{\mathbf{y}}' \cdot \sin\theta \quad [4.24]$$

The correctly orientated local y-axis is then calculated using another cross-product calculation:

$$\hat{\mathbf{y}} = \hat{\mathbf{z}} \times \hat{\mathbf{x}} \quad [4.25]$$

An origin $\mathbf{O} = (U_O, V_O, W_O)$ is defined as being situated in the stringbed centre, between markers 2 and 3:

$$\mathbf{O} = \mathbf{M}_2 + \frac{b}{2} \cdot \hat{\mathbf{y}} \quad [4.26]$$

These calculations result in a set of directional unit vectors describing an axes-set orientated as in figure 4.5.

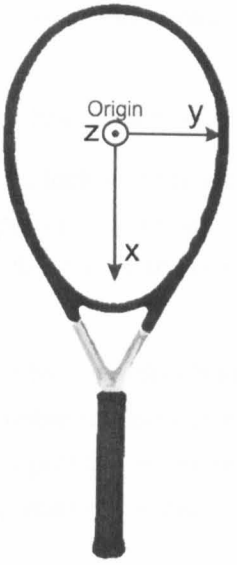

Figure 4.5. A diagram showing the orientation of local racket axes. The origin is located in the stringbed centre, and local z-axis perpendicular to the racket face, out of the paper.

The marker positions outlined in this section can be used to create a racket plane and local axes-set. These will be used, along with the ball's trajectory, to calculate every shot characteristic outlined in the previous section.

4.4.2 Marker Type

With the position of the racket markers chosen, this section assesses which type of marker are most suitable for this methodology. Three types of marker were investigated, and are shown graphically in figure 4.6.

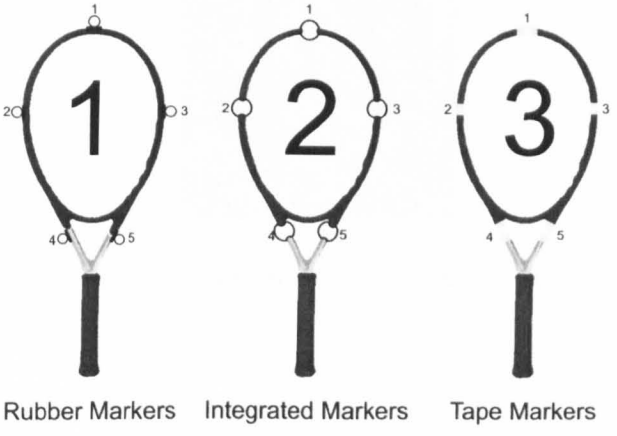

Figure 4.6. The three different types of marker considered for this methodology.

Rubber Markers

Used extensively in biomechanical testing, highly reflective spherical markers are readily available and can be easily attached to the racket using adhesive tape. As they are

spherical, their centres are easily and accurately tracked from any viewpoint by tracing a circle around their circumference.

In spite of accurate tracking, they have a number of drawbacks:

- The markers sit on the frame, their centres are several mm from the surface of the racket. Not only does this present inaccuracy in terms of racket face reproduction, but it also presents a considerable distraction and obstacle to a player using the racket.
- These markers are obstructed by the racket frame at certain angles; figure 4.7 shows an early impact test using rubber markers in which one is obstructed by the racket frame. Although this is not a problem when redundant markers are used, if the ball or player obstructs another marker, it increases the likelihood of rendering the recording unusable.
- These markers have a tendency to detach during high speed swings, regardless of how firmly they are secured to the racket frame. They are in a vulnerable position, if the racket makes contact with the player's body or clothing, as it tends to in a serve, the marker is very likely to become detached.

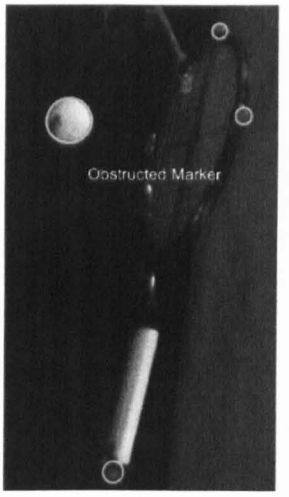

Figure 4.7. A marker obstructed by the racket's frame is highlighted in red, this obstruction increase the likelihood of void tests.

Integrated Markers

As an attempted solution to the obstruction problems of the rubber markers, integrated markers were cut away and attached around the racket frame. Not only does this make the marker visible from nearly every angle, but has a centre situated on the racket frame, minimising the error in face reproduction. These markers were designed to be less prone to the vibration and detachment problems of the rubber markers, but are difficult to manufacture

and apply to a racket. It is likely that in a player testing scenario, racket markers would have to be applied as quickly as possible making them particularly unsuitable in this respect.

The increased size (a result of being applied around the racket frame) and protrusion of these markers presents a distraction and obstruction to anyone using a racket with them applied.

Tape Markers

A band of reflective tape placed around the racket produces a marker of very low mass and effectively zero protrusion. Their lack of sphericity presents a problem with accurate marker tracking. Without a traceable circumference the centre cannot be found as reliably as with the other marker types. Greater subjectivity is involved in tracking the marker's centre and its appearance within the image plane changes according to its skew and position.

The tape is easily and quickly applied to the racket frame, and the time to prepare a racket for testing, and hence the intrusion into the player's environment is minimal.

The lack of protrusion of the markers can cause problems with visibility. Although they wrap entirely around the frame, they do not raise from its surface, causing visibility problems at particularly oblique angles as shown in figure 4.8.

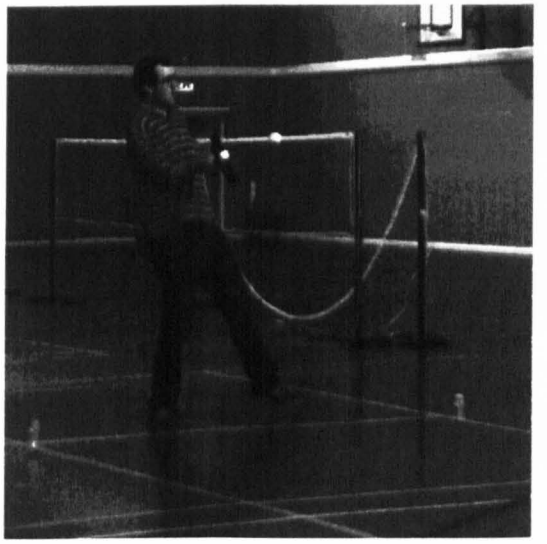

Figure 4.8. A recorded image illustrating the lack of visibility of tape markers at certain racket angles.

The negligible mass, and minimal protrusion of tape markers present a minimal distraction to a player using a racket to which they have been applied, minimising intrusion into the player's environment is a vital element to this methodology.

4.4.3 Conclusions

Despite inaccuracies in tracking, tape markers are best suited for use in this methodology. They wrap around the frame, giving good visibility over a range of angles.

Their low mass and the minimal obstruction to the player makes them ideal for use in recording a player's shot.

The sphericity of the rubber and integrated markers enables accurate tracking of their centres. Even disregarding the problems with obstruction and preparation that each one presents, these marker types are too distracting and obstructive to a player using them on a racket. Their increased accuracy and visibility in certain cases is of no consequence if the player will not, or is unable to use a racket to which they have been applied.

Although un-quantified at present, the errors introduced by using tape markers can be measured and minimised through proper camera placement which ensures minimal skewing and maximum visibility of the markers during the period of their analysis.

4.4.4 Camera Position

The two cameras must be positioned around the court in order to provide the best view of the ball and racket markers. Their position must also present no distractions or obstacle to players on the court. The suitability of four camera positions was tested for use with the tape markers chosen in the previous section. Figure 4.9 shows the arrangement of the cameras tested for use in this method.

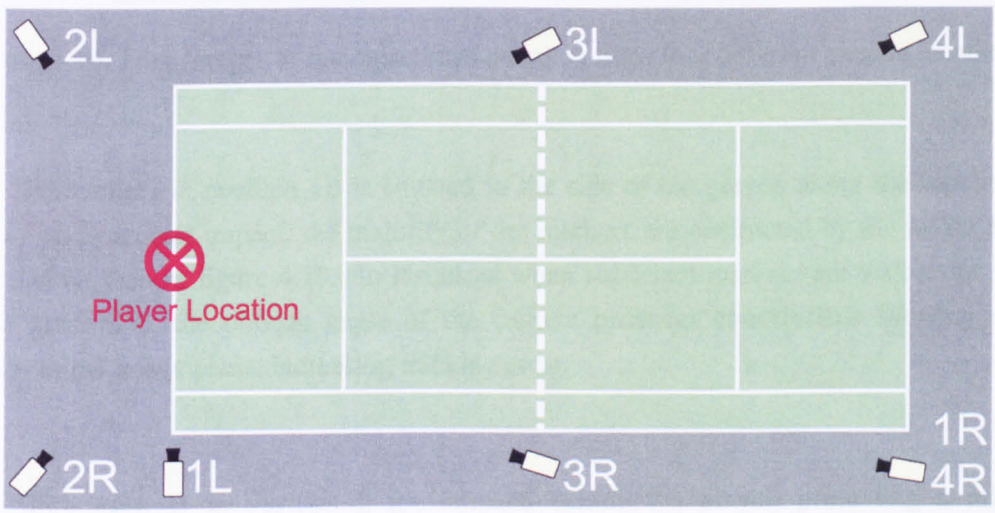

Figure 4.9. The six separate camera locations used in the suitability study. Numbers indicate how the cameras are situated for each of the four camera positions tested.

A player, situated in the position highlighted in figure 4.9, was filmed performing a shot for each of the four camera positions. Four images of the impact instant from selected camera locations are shown in figure 4.10.

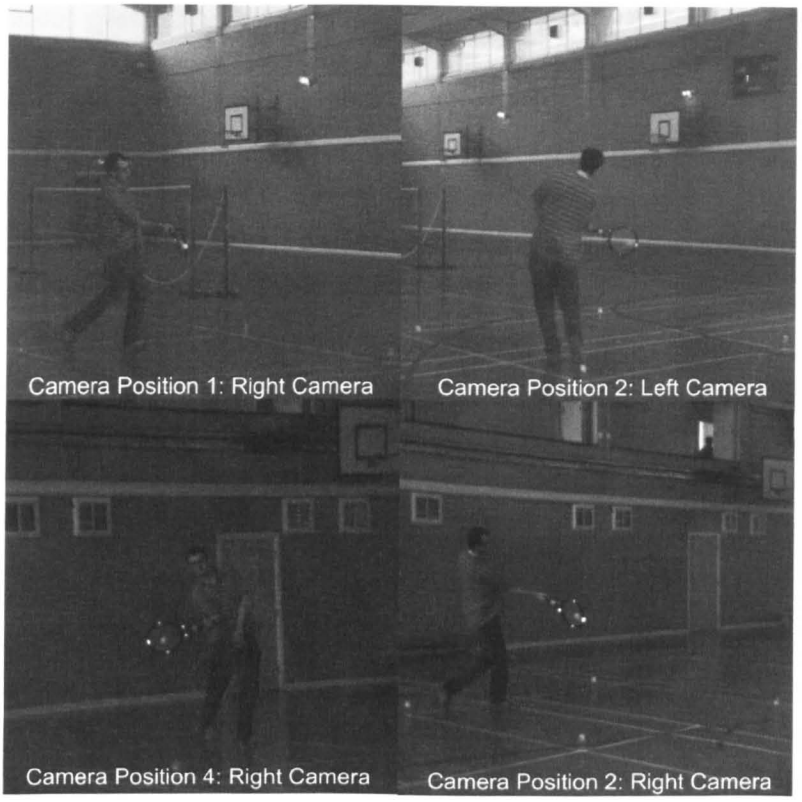

Figure 4.10. Four images of the impact instant taken from four different camera locations.

Side-on

The camera in position 1L is situated to the side of the player, along the baseline. At frames on or around impact, the majority of the markers are obstructed by the racket frame, (this can be seen in figure 4.10.) In instances when sufficient markers are visible for racket plane generation, the oblique angle of the camera produces considerable skewing of the marker in the image plane, increasing tracking error.

Rear

Both cameras in position 2 are situated behind the player, presenting a minimal distraction. Any wires or equipment are entirely absent from the court itself. Figure 4.10 shows that all markers are clearly visible in both cameras, with minimal distortion. In this case the ball is on the other side of the racket and there is no possibility of the ball obstructing a marker. The racket frame and stringbed however, obscures the ball from view, especially around impact. There is also a risk with this camera configuration that the player themselves may obstruct the ball or racket during impact.

Front

Camera positions 3 and 4 are both entirely in front of the player, providing an un-obscured view of the ball at impact and removing the player as a possible obstacle. Camera

position 4 is placed even further away from the player at the end of the court. In the position shown in figure 4.9, the cameras do present a significant obstacle to any player on the other side of the court, and are at a high risk of being hit by the ball in play. It is possible to move the cameras further away from the tennis court but problems then arise concerning image resolution and the limits of the zoom capabilities of the lens equipment. The greater the level of zoom that is used for an image, the smaller the proportion of the lens that is being used and the more light is required to achieve the same quality of image.

Camera position 3, with each camera located at either side of the net, is more obliquely angled with the player and racket markers than in position 4, increasing the distortion of the markers within the image plane. If the cameras are moved further away from the net, into a wider position, the skewness of the markers increases but the cameras are less of a distraction to the player and at less risk of being hit by the ball.

4.4.5 Conclusions

Tape racket markers are best observed when the cameras are placed in front of, or behind the player. Positioning a camera to the side of the player gives images of high skewness, and often results in blocked markers. When the camera is placed behind the player, the player becomes a possible obstacle to ball and marker tracking, and at frames around impact, the racket frame and stringbed obscures the image of the ball.

Cameras positioned in front of the player produce good images of the racket markers, which have low amounts of distortion and are not obscured by the player. The ball is in clear view around impact, but may block a racket marker. Five markers are used in total; the two redundant markers ensure this is not a great problem. Cameras placed at the rear of the court reduce skewness more so but present a considerable distraction to any player on that side of the court and are at serious risk of damage through impact. The risk of damage can be reduced by positioning the camera at either side of the net.

Position 3 offers the best compromise of marker and ball tracking against player distraction and obstruction. The racket and ball are clearly trackable, the cameras are not at particular risk of being hit (when testing capable players) and they will be largely out of view of a player on the court.

4.5 Camera Setting

In order to accurately record shot characteristics, there must be enough data points to analyse and the markers must be composed of a sufficient number of pixels within the image plane and be un-blurred. This relies on appropriate camera settings being used throughout the experiment.

4.5.1 Frame rate

The frame rate determines how many data points can be extracted from the images in a set time period. 10 data points will be used when assigning a linear fit to the data, this gives a

good compromise between confidence in the fit, and the time taken to extract the data points for each shot.

When extracting 10 points from before and after the impact, what frame rate must be used in order to give a small enough time period over which to still assume linearity?

In the study by Elliott and Marsh **1989** a biomechanical analysis of the forehand stroke (which forms the majority of this shot analysis) gives typical biomechanical angles and angular velocities of the shoulder, elbow and wrist over a 0.14 second period. These values can be used to give a typical arc traced by the tip of the racket during this time period. An assessment can then be made of which time period is reasonable to assume linearity, and hence the most appropriate frame rate to use in this testing.

A simplified scenario for a typical forehand shot was re-created using the following assumptions (figures 4.11 and 4.12.)

- The angles between torso, shoulder and elbow are equal to those found in Elliott and Marsh **1989**
- The angle at the elbow stays constant throughout the swing, reflecting the findings in the study made by Elliott.
- The lengths of the upper arm and forearm are taken from a handbook of anthropometric data (DTI **1998**), and cited as the 'upper arm length' and 'back of elbow to grip', the length of the racket is the standard length of most tennis rackets.
- The racket and resultant arm length are exactly in line at the time of impact
- The shoulder and wrist rotate perpendicularly to the resultant length at an angular velocity according to the values found in Elliott's study. These values were at intervals of 0.02 seconds throughout the recorded time and are assumed constant over each period.

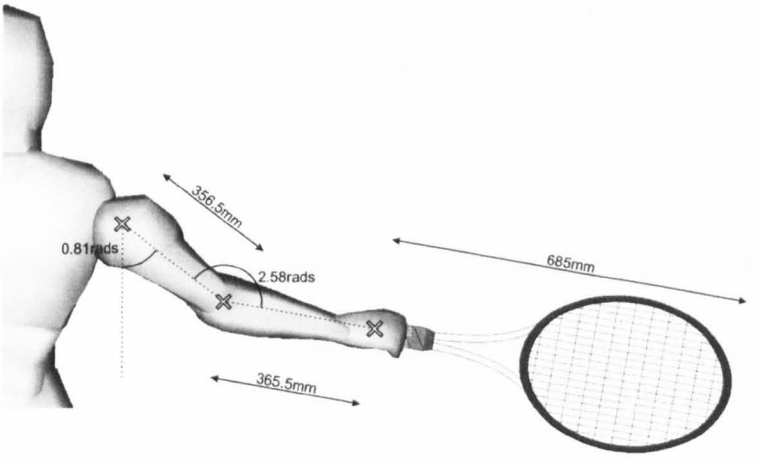

Figure 4.11. A simplified shot situation used to assess the testing frame rate.

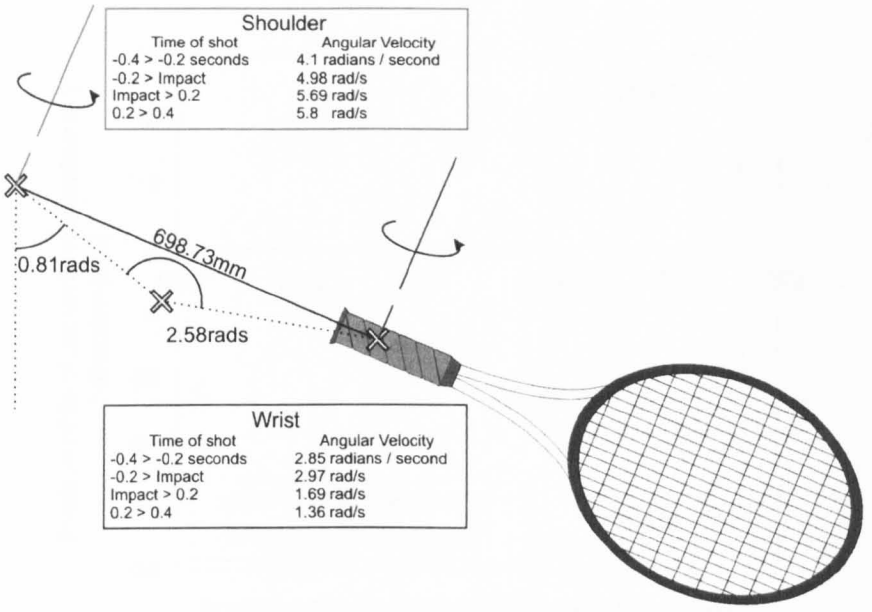

Figure 4.12. The resultant distance of the arm sections (calculated using the cosine rule), the axes of rotation and relative orientation of the racket. Also shown are the angular velocities of the shoulder and wrist measured at different time periods in Elliott's study.

Using these assumptions, the movement of the racket was tracked over three different time periods; 0.1, 0.2 and 0.4 seconds before and after impact. If 20 data points are tracked in total for each impact (10 before, and 10 after impact), the time periods above correspond to frame rates of 1000, 500 and 250 frames per second. The angular displacement of the arm and wrist (as seen in figure 4.13) is calculated over each time period, enabling the movement of the racket tip to be tracked as a series of x, y positions.

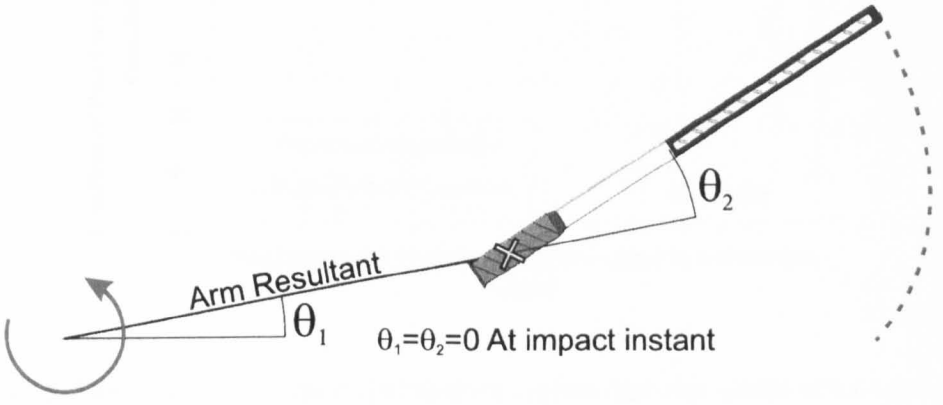

Figure 4.13. An illustration of the angular displacement conventions used when calculating the racket movement of a typical shot.

The quality of a linear fit to these positions reveals which is the most appropriate frame rate to use in this methodology. Figures 4.14 - 4.16 show these positions with a linear regression fit and the corresponding R^2 values.

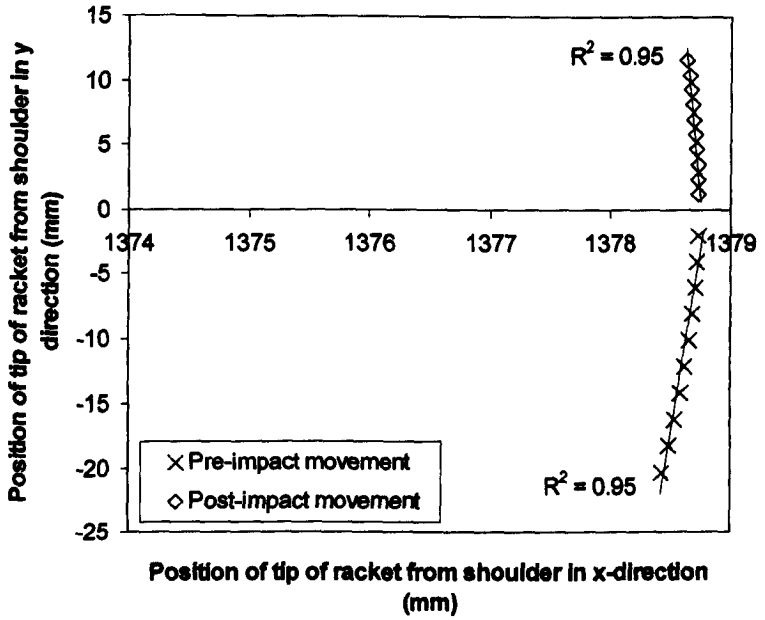

Figure 4.14. The movement of the racket tip for a typical shot over a total of 0.02 seconds

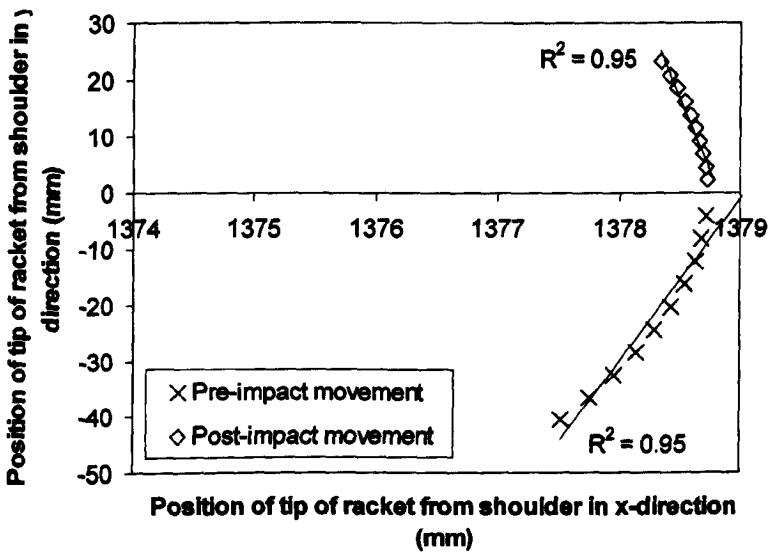

Figure 4.15. The movement of the racket tip for a typical shot over a total of 0.04 seconds.

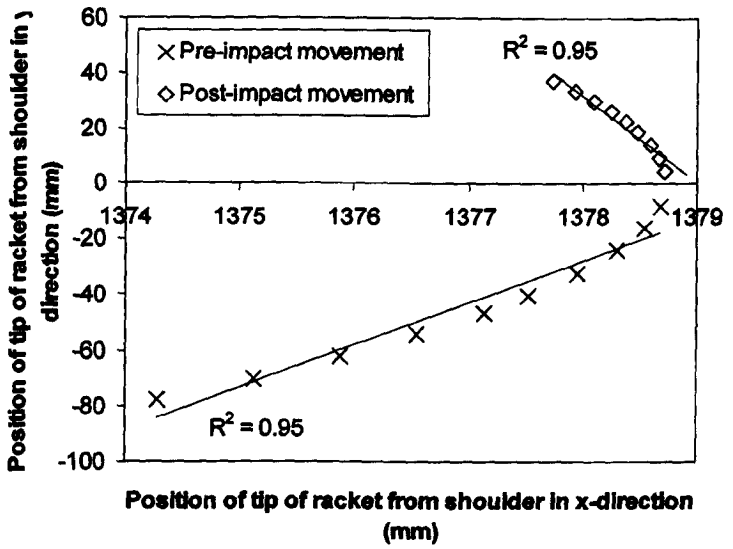

Figure 4.16. The movement of the racket tip for a typical shot over a total of 0.08 seconds.

Each plot has the same scale in the x-axis, and whilst the R^2 values are very similar, the degradation of fit as the time period increases is clear. The angular acceleration observed by Elliott in his study also suggests a decrease in linearity as the time period of recording increases. In order to obtain accurate values of the pre and post impact conditions, it is necessary to track positions as close to the instant of impact as possible. For this reason, the player shot analysis will record the player shots at 1000 frames per second, and hence a time period 0.01 seconds before and 0.01 seconds after impact a total of 0.02 seconds.

4.5.2 Zoom level

The size of the player and racket within the image plane will determine how well resolved, and hence how accurately the ball and racket markers can be tracked. Conversely, the longer the focal length of the lens on the camera, the smaller the control volume in which to test the player and the harder it is to fully capture the player's shot.

A 2 × 2 × 2 metre volume is sufficiently small so that it can be accurately calibrated with a 1 × 1 metre checkerboard. The ball and racket markers can be clearly defined, and a full shot can be recorded with the player in a number of positions. For testing in a competition or open practice there will be no control over where the player is situated on the court. A series of preliminary tests revealed that during practice, the player is situated centrally, just behind the court's baseline for a large proportion of the practice session. For this reason the control volume is placed behind the baseline in the centre, a common location from which players take shots, especially in practice conditions.

4.6 Lighting

Without proper illumination, the ball and racket markers cannot be distinguished sufficiently for accurate tracking. If the control volume is badly lit, the necessity for a longer

shutter speed is much more likely to result in the blurring of images and error introduction in marker tracking. The video recording for this methodology review was performed indoors with supplementary lighting. Retro-reflective tape markers (as shown in figure 4.17.) were used to give the distinctive marker points seen in figure 4.10.

Filming indoors requires supplementary lighting in order to be able to use a sufficiently fast shutter speed. Even then the ball is difficult to define due to the highly directional nature of the lighting used. In order for the markers to be visible the lights have to be placed behind or very close to the camera, illuminating their field of vision. In the camera position chosen for this method, any lighting used presents a serious distraction to a player on the court and it is unlikely a player would consent to its use.

Natural light gives much better image quality than any artificial light available for this testing. Furthermore, it presents no distraction to the player and allows very high shutter speeds to be used in clear weather. The lack of directionality of sunlight means that high contrast reflective markers must be used rather than the lower contrast retro-reflective markers used indoors. A non-directional white reflective tape placed on a black matt tape produces a marker tracked because of its high contrast rather than reflected light, shown in figure 4.17.

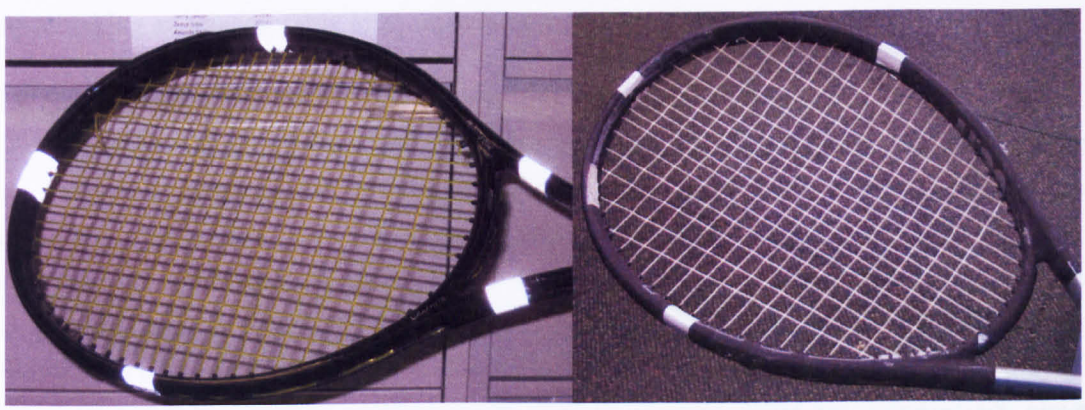

Figure 4.17. The retro-reflective markers used in indoor testing (left) compared to the high-contrast markers used for outdoor testing (right).

4.7 Triggering

Although only 0.02 seconds of video will be used to extract data points from the player's shot, much more footage will have to be recorded in order to guarantee that the essential frames surrounding the impact have been captured. The method of triggering, and the amount of footage to record are vital aspects of this methodology.

In a repeatable laboratory based experiment it is possible to trigger the cameras using a photodiode switch (see chapter 6 for further details) which allows a much shorter period of footage to be captured whilst still ensuring that the vital frames are recorded. When recording players on a court, this highly repeatable method of triggering is not possible. A manual

trigger switch, activated by an observer at the instant the player strikes the ball activates the cameras to record footage before and after this point in time. The human variability involved in triggering the cameras at the impact instant means that more footage must be saved in order to capture the essential frames.

Each impact is recorded as a series of bitmap images and is downloaded from each camera onto a separate laptop via an Ethernet network connection. Several factors affect the length of time necessary to download each impact onto the laptop's hard drive:

- The number of images recorded for each impact;
- The size (resolution) of the images being recorded;
- The format of the images.

When the images are being downloaded from a camera no other recording can take place and it is therefore vital to select the best size of image, format, and number of images for each impact to maximise the efficiency of the triggering method.

Repeated trials of this process have revealed that around 300 frames, or 0.3 seconds of 512 × 512 pixel bitmap images is the ideal for this methodology. Three hundred frames is the optimum trade-off between failing to capture the essential frames around impact, and the impact taking an unacceptably long amount of time to download.

4.8 Summary

A number of assessments and tests have shown that the ideal methodology for player shot analysis involves recording a player on an outdoor court, with five high-contrast, tape markers being placed around their racket as shown in figure 4.3. Two cameras placed at either side of the net record the player within a 2 × 2 × 2 m volume at 1000 frames per second for 0.3 seconds, and are triggered by an observer at the instant the player hits the ball. Twenty milliseconds of footage is required to obtain the data points necessary to calculate the player's shot characteristics. Lighting should not be used in order to avoid any unnecessary player distraction.

4.9 Analytical Methodology

Using the recorded footage of a player's shot, the shot characteristics are calculated in three separate stages:

- Extraction of 2D data points from recorded images;
- Reprojection of 2D data points into a single set of 3D data points;
- Calculation of the final shot characteristics from the extracted 3D data point set.

With the player footage recorded as a series of digital images, each of the above stages is undertaken using a custom-written Matlab™ program and the operation of each is discussed below.

4.9.1 Extraction of 2D Data Points

The 2D data points of three racket markers and the ball's centre must be extracted from the 20 image pairs which are analysed for each shot. Due to the varying marker shape and noisy images obtained when filming a player on an outdoor court, a manual tracking method was used.

A Matlab™ program was written to overcome a number of issues that occur when using the point selection software used in previous work (specifically, the calibration method assessment in chapter 3). In overcoming these problems, the speed of data point extraction is greatly increased and the efficiency of the process is improved accordingly. Following point selection, the program outputs a table of data in Microsoft Excel™ format, separate data sheets are used for the marker points and ball centres. For the purposes of clarity, this program shall be called *Extractor* in future references.

Upon loading the shot images within *Extractor*, the selected images from each camera are displayed adjacently within the same window, as shown in figure 4.18. The left and right images are always synchronised to correspond to the same instant in time, which is especially useful when tracking the racket markers. If a marker is obstructed in one image the appropriate substitute marker can be selected in both images substantially easier than if each image was analysed separately.

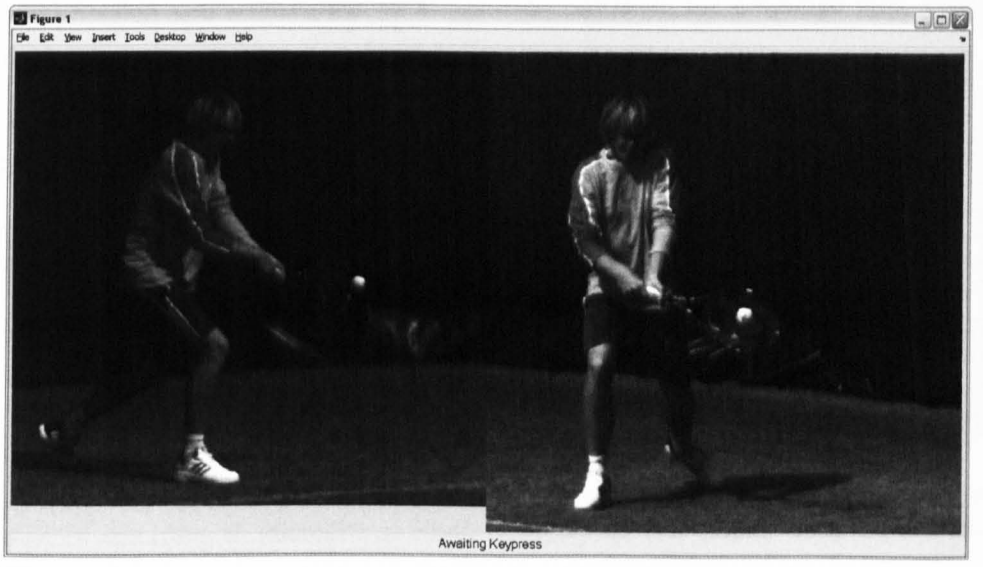

Figure 4.18. The 2D point extraction program. After the images from each camera are loaded into it, they are displayed adjacently as shown here.

4.9.2 Marker selection

The centres of three markers are selected from the displayed images using a cross-hair cursor. Each image can be enlarged to aid in marker selection, and increase the resolution of the output co-ordinates (shown in figure 4.19).

Figure 4.19. A window showing marker selection on the zoomed images. The high contrast markers and ball are clearly visible

The image frames are cycled through using the computer keyboard and markers are selected in 10 image frames both before and after the impact frame.

Each of the five racket markers is assigned a number according to the set-up shown in figure 4.3. The marker's number is allocated using the computer keyboard prior to the marker's selection and corresponds to a separate column in the outputted data sheet. Data from the left and right cameras is split up further into separate columns.

The organisation of the marker co-ordinates according to the marker number, image frame and camera is best illustrated in the example output data sheet shown in figure 4.20.

Marker	M1				M2			
	Left Cam		Right Cam		Left Cam		Right Cam	
File No.	U	V	U	V	U	V	U	V
131	141.458	213.4706	279.2261	248.6571	174.937	216.4958	305.5454	255.7361
132	142.063	211.6555	274.8697	247.0235	175.3403	215.084	301.7336	253.921
133	142.6681	209.437	270.5134	245.2084	175.7437	213.4706	298.4664	252.2874
134	143.8782	207.6218	266.3387	243.0303	176.5504	212.0588	294.8361	250.2908

Figure 4.20. Part of an example output data sheet, showing the organisation of the marker co-ordinates according to number and image frame, split into points from the left and right camera

4.9.3 Ball selection

The ball centres are selected using a circular cursor of variable size (figure 4.21). The circle's radius is varied, using the keyboard according to the size of the ball in the image. Correctly positioning the cursor around the ball's image ensures that the centre is selected in each frame. The ball is selected in the appropriate image frames in the same way as the racket markers. The output sheet in this case consists of a single column of U V co-ordinate data.

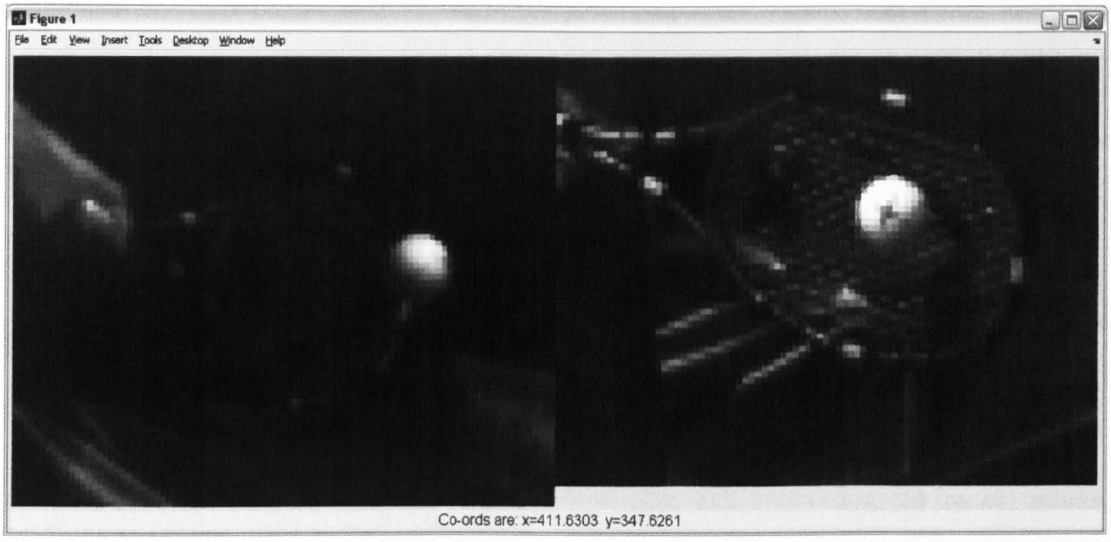

Figure 4.21. A window of ball selection. The circle surrounding the ball in each image frame tracks the position to four decimal places.

With the 2D positions of the ball and three racket markers tracked in 10 image frames before and after the frame of impact, the co-ordinates can be transformed into 3D using the 3D parameters calculated at calibration.

4.9.4 Transformation of 2D Data Points

Using Matlab commands included in the 'checkerboard calibration toolbox' provided by Strobl et al. **2007** a Matlab program was written which automates the translation of the 2D points into 3D. Upon completion of the 2D point tracking, the results are passed to the 3D translator program, which from now on will be referenced as *Translator*.

The commands provided by the calibration toolbox can only translate a single column of data at a time. *Translator* automates this process translating the positional data from the ball and racket markers to greatly improve the speed of point translation.

The steps to translation are as follows:

- Loading of the previously saved 2D data ;
- Loading of the corresponding calibration parameters;
- Calibrating the ball and racket;
- Saving the 3D data sheet output.

Loading Previously Saved 2D Data

The *Extractor* automatically exports the selected 2D data into the *Translator* program, but the option exists to load 2D data from a previous session if necessary.

Loading Corresponding Calibration Parameters

In order to accurately transform the 2D data into 3D, a set of calibration parameters calculated from the time of testing is necessary. A directory is selected which contains the calibration parameters and a Microsoft Excel sheet containing the local axes-set data.

Calibrating the Ball and Racket

Each impact is calibrated automatically by *Translator* which uses the algorithms present in the calibration toolbox to transform the columns of 2D data loaded into *Translator*

Saving the 3D Output

Two data sheets are produced from *Translator*, one containing the racket marker positions in 3D, the other containing ball data. The format is similar to that of the output from the *Extractor* program, but the separate 2D columns from a left and right camera are replaced by a single column of 3D data. An example of this output data sheet is shown in figure 4.22.

3D Point data (mm)

	Marker 1			Marker 2			Point 3		
Frame No.	X	Y	Z	X	Y	Z	X	Y	Z
-175	-1070.64	-1365.2	-764.184	-1009.82	-1171.04	-736.638	-1044.59	-1358.61	-565.136
-174	-1060.99	-1359.8	-772.591	-994.011	-1161.59	-739.745	-1029.13	-1351.98	-562.368
-173	-1031.22	-1351.82	-778.358	-974.233	-1152.35	-741.779	-1010.65	-1347.15	-570.008
-172	-1008.3	-1342.61	-786.454	-959.784	-1144.3	-743.268	-994.593	-1341.27	-574.075

Figure 4.22. A portion of the 3D data sheet given as an output after 2D point translation.

4.9.5 Calculation of the Shot Parameters

The marker and ball positions directly before and after the instant of impact allow the calculation of the shot characteristics outlined earlier in this chapter. A Matlab program has been written to automate this process.

The calculations involved in generating the shot characteristics which are outlined at the beginning of this chapter are implemented within this program, which shall be referred to as *Calculator*. As well as automating the process of calculating the shot parameters, several other features have been added in order to maximise the flexibility of the program and assist with shot analysis.

The features of *Calculator* are summarised below:

- The calculation of linear velocities in 3 dimensions;
- The calculation of angular velocities of racket around its COM;
- The calculation of impact position on racket face, (given graphically and numerically);

- The calculation of a 'racket angle', this is discussed in the next chapter, put simply it is the angle between the racket and ball's movement, taking into account the racket's orientation to the court.

In order to make these calculations, *Calculator* is given the data sheet containing the 3D positions of the ball and racket markers, and a sheet containing information about the racket used in the shot. Racket information includes the distances between markers 1, 2 and 3 (see figure 4.4), the length, width and balance point of the racket and hence the relative positions of the stringbed centre and racket's COM.

After the relevant data has been loaded into *Calculator*, the frame of impact and frame rate of the camera is entered, this tells *Calculator* which parts of the shot are before and after the impact, and how much time passed between each image frame. This is an important step, during testing it may not be possible to capture 10 images both before and after the impact, resulting in the impact frame not being located on the middle row of the data.

The results of the calculations are displayed in a window like the one shown in figure 4.23. A graphical display of a racket shows the relative position of the racket's COM and the impact point, plotted as crosses on the racket face. A point on the racket face can be calculated by clicking on the graphic, or by entering a pair of local co-ordinates. The selected point is plotted as a circle, and its velocity shown in the result window, in this way the racket tip velocity or velocity of the impact point, can be calculated easily.

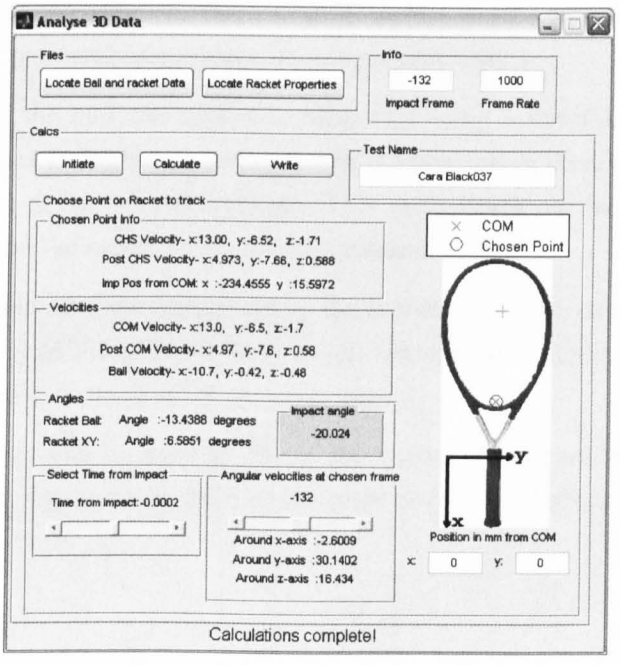

Figure 4.23. The window of the *Calculator* program, showing the results of the shot calculations and displaying the position of the COM, impact point and a user selected point graphically on a racket face.

These results can be saved in the form of a Microsoft Excel sheet for future analysis. If necessary the racket plane and ball position data can be used to calculate other shot characteristics for a more in-depth analysis. The results shown in figure 4.23 do not represent the limit of this methodology, any aspect of 3D vector space can be extracted from this data, so as well as positions, displacements and velocities, the intersection between racket and ball and the associated angles between the racket and ball trajectories. With prior knowledge of the ball and racket's mechanical properties, it is also possible to calculate associated energies and momentum values for the system.

4.10 Chapter Summary

This chapter has gone through the development of a methodology which extracts vital characteristics from a player's shot. This method focuses primarily on the movement of the racket and ball immediately before and after the impact

The racket and ball's linear and angular velocities are calculated from images of a player's shot recorded using two high speed cameras. The player is filmed on an outdoor court with each camera placed at either end of the court's net, each shot is filmed at 1000 frames per second for 0.3 seconds and triggered manually by an observer. The player has five high contrast tape markers added to their racket to enable the calculation of the shot characteristics, the ball has lines added so that its absolute spin rate can be counted manually.

The images obtained from testing are processed using three bespoke Matlab programs written specifically for the tasks of; extracting 2D points from a pair of images, converting these points into 3D space and calculating the shot characteristics.

The velocity of the ball and racket is calculated using a linear regression of position against time. The racket is defined as a plane using the position of three markers on the racket face, two are used to define a local axes set. This method allows the impact position and velocity of any point on the racket's face to be calculated.

The ball's velocity and the movement of the racket as a plane can be used to calculate many different aspects of the player's shot which haven't been explicitly described in this section, this is covered in more detail in the next chapter.

This methodology can be used to obtain the typical shot characteristics of high level tennis players and investigate the ways in which these players perform at this level.

5 Player Shot Analysis, Testing, Results and Conclusions

5.1 Introduction

The previous chapter outlined the development of an experimental methodology which can extract the three dimensional linear and angular velocities of the ball and racket. This method can be used to measure typical shot characteristics from high level players for model validation and general investigation into player shot behaviour.

It was decided to use the Wimbledon Qualifying Tournament as a source of high-level players. The tournament runs in the week prior to the main tournament. The nature of this tournament means that great players of the past and future are all fighting for the same goal. This fact is exemplified in 1977 when an 18 year old John McEnroe reached the semi-finals of the championship after going through the qualifying stage.

It is reasonable to assume that players competing in the qualifying tournament play at a very high level, and are able to reliably produce shots typical of standard competition play.

Using the methodology described in chapter four, the shots of several players competing in the 2006 Wimbledon Qualifying Tournament were recorded, this chapter describes the specifics of the methodology used in this testing, and discusses the results in an in-depth analysis of player shot trends and characteristics.

5.2 Aim

This chapter will assess the typical shot characteristics of high level male and female tennis players as exhibited at the 2006 Wimbledon Qualifying Tournament. As well as presenting general values of velocity, spin and impact position, a more in-depth analysis of player mechanisms such as spin generation and shot efficiency will give a deeper understanding of how a racket model may relate to a real-world situation, and which firmly held tenets of tennis playing technique hold up to deeper scrutiny.

5.3 Specifics of the Qualifying Tournament Methodology

Although the general method follows that as described in the previous chapter, some aspects of the methodology are specific to the location and nature of the testing. This section describes the location and details of the testing procedure, the camera and equipment placement, volume calibration and the marker application and measurement. All of these specifics have been chosen to minimise the intrusion into the player's environment.

5.3.1 Location and Testing Procedure

The testing took place on a practice court with an area to its side in which the computer equipment could be set up. The players were made aware that cameras would be present on the court when they booked the court to practice. Upon arrival at the courtside the players were given details of the testing and asked whether they would like to participate in the shot

analysis. If they agreed, markers were attached to the racket, the racket was measured and the player continued as normal with their allocated practice time. No requests were made to the player regarding their shot-type, stance or even position on the court. The player was simply asked to proceed with their normal practice routine. The player was recorded when they made a shot within the calibrated control volume. This reduced the number of shots recorded in a given time, but did not distract the player by forcing a different practice routine than they may have been used to.

Camera and Equipment Placement

The extra room available at either end of the net allowed the cameras to be placed further away than specified in the previous chapter. The left camera was placed around a metre from the nets edge. The room available to the side of the court allowed the right camera to be placed entirely off the court as shown in figure 5.1. The cameras were focused on the centroid of a 2 × 2 × 2 m volume situated at the baseline, from this orientation all the markers were visible at the point of impact and for 30 or so frames either side, a total of 0.06 s, three times the required 0.02 s for full shot analysis. In good daylight an exposure time of 100 μs can be used, producing clear images with no blurring or distortion. The wires from the left camera were trailed along the foot of the net (three in total) so as not to present an obstacle on the court. The computers and measurement equipment was under a covered area to the right of the court, out of the player's line of sight.

Figure 5.1. The two cameras used in the Qualifying Tournament player shot analysis. Camera 1 is placed at the far left side of the court, camera 2 is placed entirely off the court to the right hand side.

5.3.2 Volume Calibration

The control volume was calibrated using a checkerboard with 60 mm squares, held in around 40 positions. Due to the comparatively small size of the checkerboard compared to the

control volume; more than the usual 20 – 25 checkerboard positions referred to in chapter 3 were required. The local axes set was calibrated using an orthogonal frame placed on the court behind the centre of the baseline. The global x-direction runs parallel to the length of the court, the global z-direction along its width, and the global y-direction lies vertically as in figure 5.2. Placing the frame on the ground aligns the axes set with the court in the horizontal plane. The positions of reflective markers were used to define the axes, as described in chapter 3. Figure 5.2 shows how the global axes set was aligned according the court's baseline. The positioning of the cameras and size of the control volume means that serves were not visible to record or analyse. A recorded image size of 512 × 512 pixels restricted the recorded image volume to the 8 m^3 mentioned above, which ensured the racket markers and ball were of sufficient size within each image. This restriction in height of 2 metres means that during a serve, too many racket markers were off-camera to allow analysis.

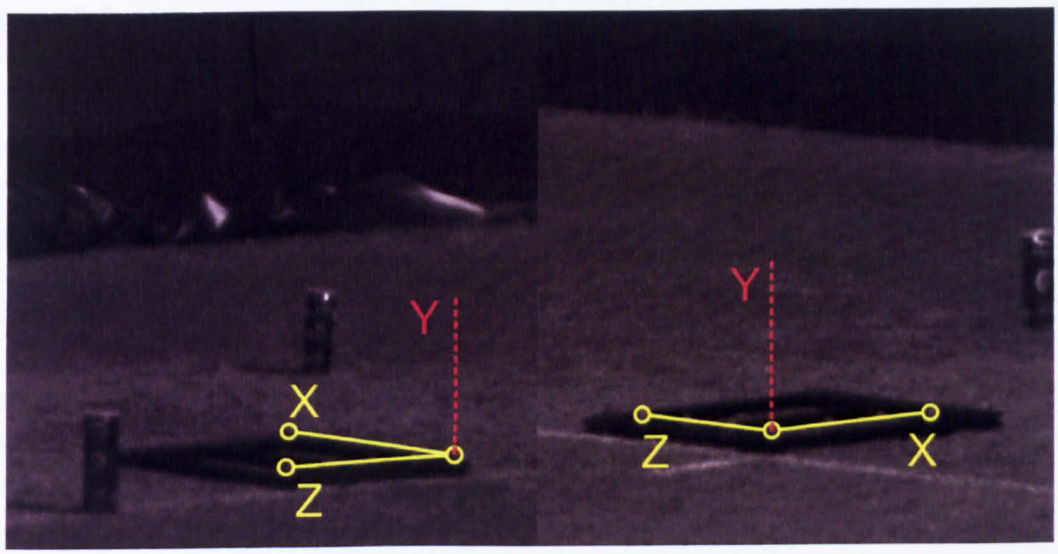

Figure 5.2. A diagram showing the alignment of the global axes according to the baseline. Three reflective markers set at a right angle are used to define them.

5.3.3 Marker Application and Measurement

The markers, applied as stated in the previous chapter, were secured to the racket immediately prior to the player's practice session. The tape markers were prepared in advance so that they could be applied as quickly as possible. Once the markers had been applied, the racket was placed on a grid of square centimetres and photographed from several angles in order to measure the distances between the markers, the racket's length and its width. The squares in the image were used to obtain a pixel/mm calibration ratio which could be used to measure the relative marker positions. Distance markings along the length and width of the grid allowed the racket dimensions to be measured even if the entire racket was not present in the photograph. The mass and balance point of the racket were taken from an online database of racket specifications. (USRSA **2007**). The make and model of the racket was noted during testing. Figure 5.3 shows a typical racket example.

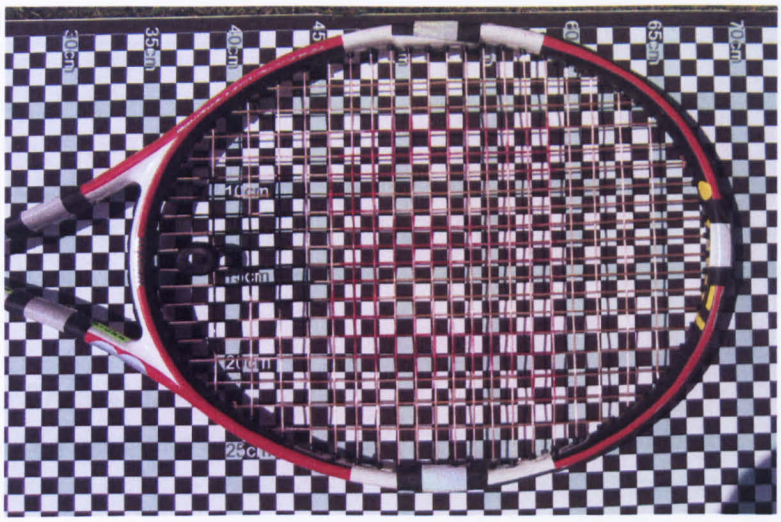

Figure 5.3. A typical racket measurement photograph, showing the marker positions on the racket, as well as the length and width of the racket.

In total, 106 shots from 16 different players were recorded over the three days of the qualifying tournament's duration. They were analysed using the bespoke Matlab software described in the previous chapter. The results obtained from this analysis are discussed in the next section.

5.3.4 Error and reliability

The calibration and manual marker tracking was measured to produce results with an accuracy of around ±2.5mm. This was assessed by tracking the distances between racket markers, which can be measured directly from the racket and compared with the distance between the re-projected co-ordinates. Every other characteristic other than ball spin is derived from this original positional information, and hence accuracy. The ball spin is measured directly from the recorded images and hence varies in accuracy. The frames taken for a full revolution are counted and the spin in revolutions per minute is calculated. A ball with high spin will complete a revolution in fewer frames than one spinning slowly, a misjudgement of a single frame therefore results in a higher error. For example, for images recorded at 1000 frames per second, a ball is judged to have completed a revolution in 20 frames, it has completed a single revolution in 0.02 seconds, or is spinning at 3000 rpm, miscounting this by a single frame results in spin values of 2857 or 3157 rpm, yet if the ball is spinning at half the speed, the error constituted from a single frame is 1463 and 1538 rpm, nearly five times smaller. The unreliability of this result means that the spin values are presented to the nearest hundred. Figure 5.4 shows how the percentage error decreases as ball spin decreases.

Rpm	Frames for 1 revolution	% error with + 1 frame error
3000	20	5
2000	30	3.33
1000	60	1.67

Figure 5.4. A table showing the number of image frames, and the percentage error of the spin measurement taken from a recorded shot. Assuming a + 1 frame error in measurement, it can be seen the percentage error decreases as the recorded spin value decreases.

5.4 Typical Shot Characteristics

This section investigates the range of values obtained through player shot analysis, such as typical velocities, spins and impact points. Direct comparisons between players have been avoided, because players were not asked to perform in any particular way (e.g. high spin or velocity), a direct comparison is rendered meaningless.

5.4.1 Results

This section deals with raw values obtained from the player shot analysis and are plotted as histograms, giving a graphical representation of how the values are spread over the recorded range. The mean and standard deviation will also be given. In many cases, the results are quoted according to a local or global axes set, although these have been described previously they are shown in figure 5.5 as a reminder.

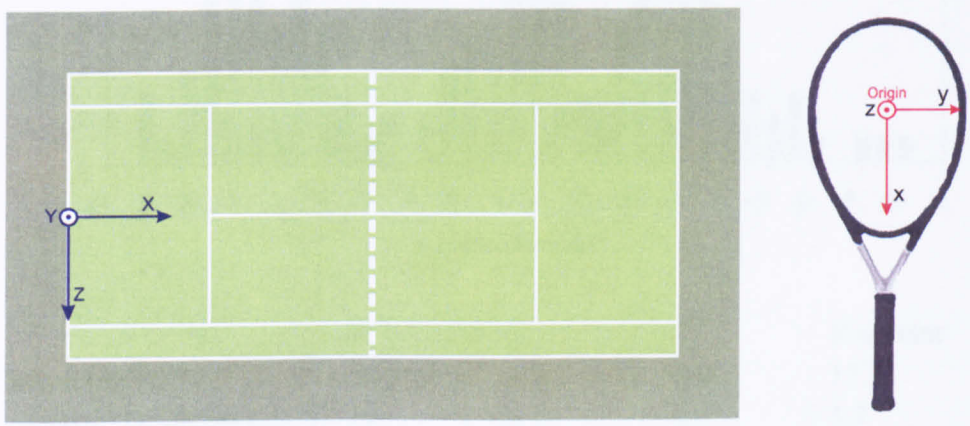

Figure 5.5. A depiction of the global and local axes on a tennis court and tennis racket.

Velocities

The velocities of the ball and racket are measured before the impact, but after impact, only the velocity of the ball is included. An investigation into the momentum balance of the racket and ball before and after impact revealed that the mass of the players arm and shoulder interferes with the movement of the racket after impact has occurred. For a freely suspended racket, the momentum of the ball and racket should be balanced before and after impact according to the principle of conservation of momentum. An investigation showed that for a

hand held racket, the momentum is rarely balanced, the mass of the shoulder and arm alter the behaviour of the racket following impact. It follows that the movement of the racket after impact are not due to the impact alone, rendering them inappropriate for model validation and investigation.

Racket Velocities

The velocities of the racket are given from the centre-of-mass (COM) to give comparative values. Since the location of the impact point is different for each shot.

Figure 5.6 shows the spread of the COM velocities for shots played by male players, expressed in each of the three axes shown in figure 5.2. The mean values and standard deviations are shown also. Figure 5.7 shows the same frequency distribution, but for female players. All the velocity values shown below are for racket velocities prior to impact only.

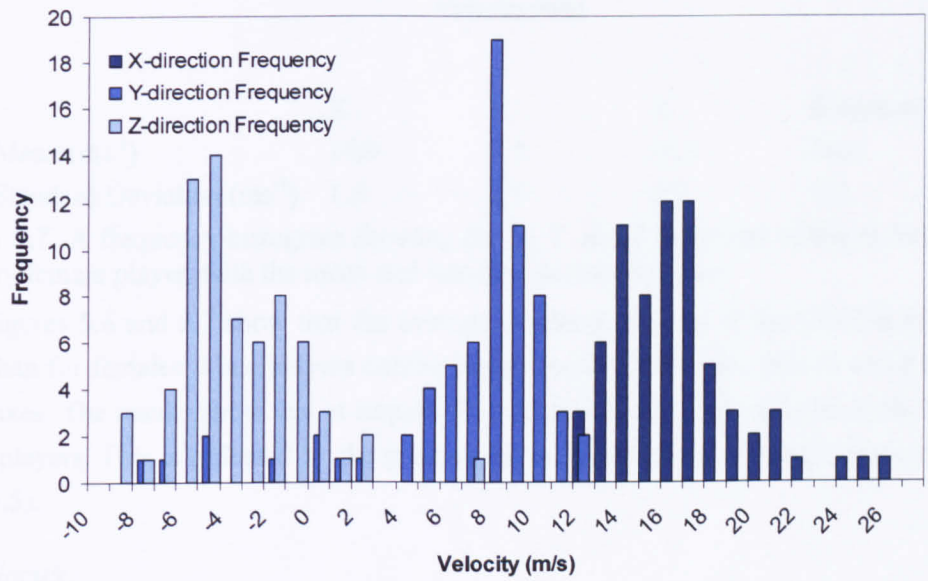

	X	Y	Z	Resultant
Mean (ms^{-1})	16.0	6.2	-4.4	17.7
Standard Deviation (ms^{-1})	3.0	4.2	2.9	5.9

Figure 5.6. A frequency histogram showing the X, Y and Z velocities of the racket's COM for every male player. The mean and standard deviations are listed below the plot.

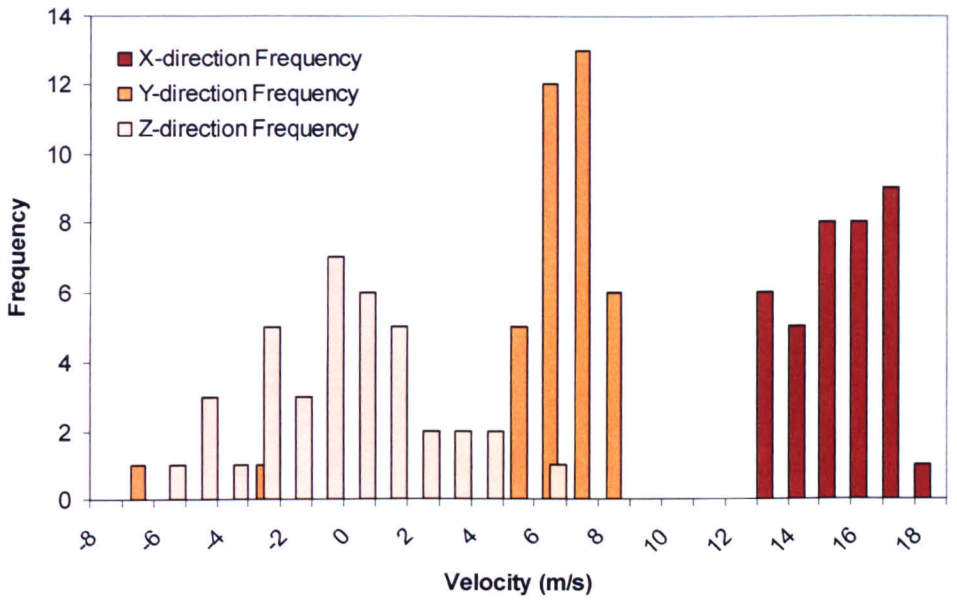

	X	Y	Z	Resultant
Mean (ms^{-1})	14.9	5.5	-1.1	16.0
Standard Deviation (ms^{-1})	1.5	2.9	2.7	4.2

Figure 5.7. A frequency histogram showing the X, Y and Z velocities of the racket's COM for every female player, with the mean and standard deviation values.

Figures 5.6 and 5.7 show that the average resultant velocity of the COM is higher for males than for females. Male players exhibit higher racket COM velocities in all of the three global axes. The results show that at impact, the racket is moving upwards for both male and female players. This is reflected by the positive values in the global Y direction (as shown in figure 5.5).

Ball Velocities

The inbound and rebound or (pre-impact and post-impact) velocities of the ball are measured; the pre-impact velocities for every shot played by a male player are shown in figure 5.8 along with the mean and standard deviations values. The pre-impact ball velocities, means and standard deviations for every female player are shown in figure 5.9. Table 5.9b shows the corresponding X velocities for intervals of vertical 'Y' pre-impact ball velocities for both male and female players.

The post-impact ball velocities for the male players are shown in figure 5.10 and the post-impact ball velocities for the female players are shown in figure 5.11

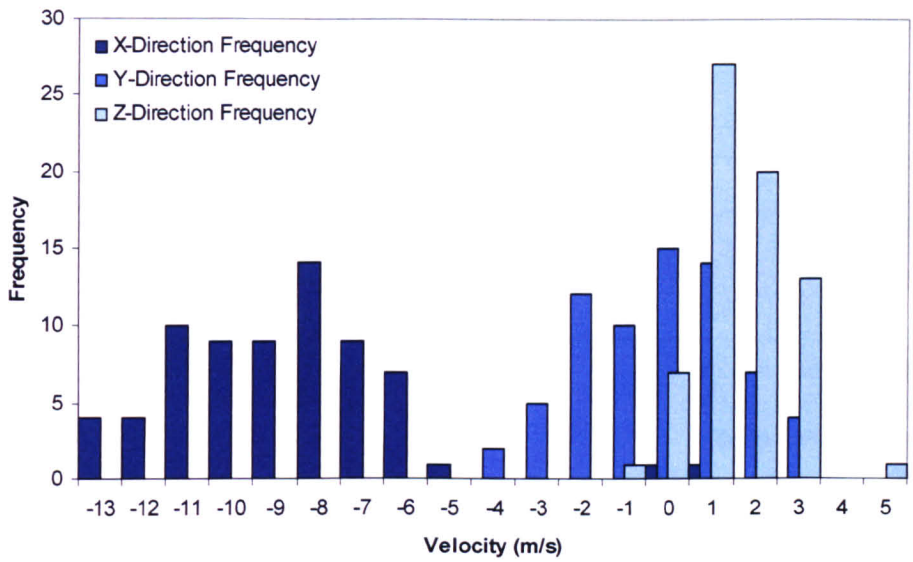

	X	Y	Z	Resultant
Mean (ms^{-1})	-9.3	-0.6	1.1	9.4
Standard Deviation (ms^{-1})	2.7	1.7	1.0	3.4

Figure 5.8. The pre-impact ball velocity frequencies, means and standard deviations for every male player

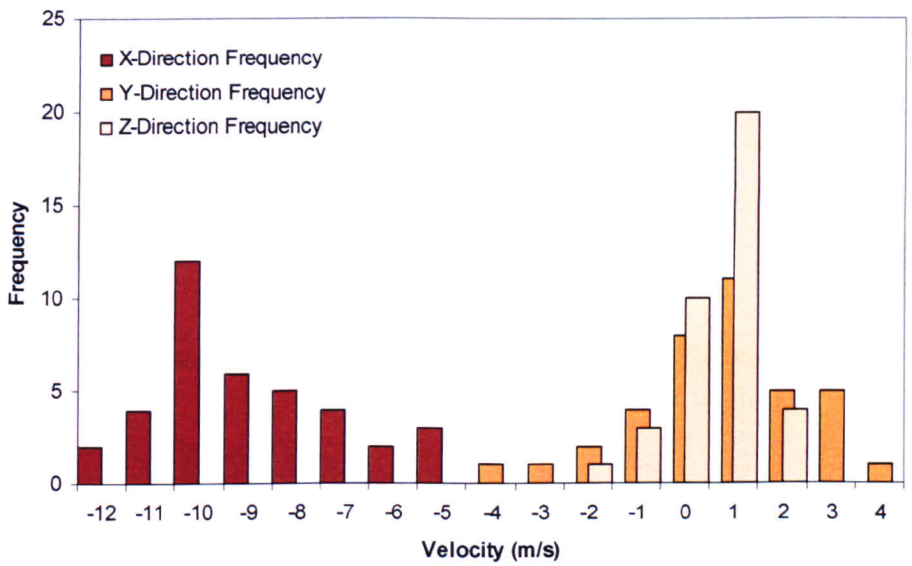

	X	Y	Z	Resultant
Mean (ms^{-1})	-9.3	0.2	0.1	9.3
Standard Deviation (ms^{-1})	1.9	1.7	0.9	2.7

Figure 5.9. The pre-impact ball velocity frequencies, means and standard deviations for every female player

Range of vertical ball velocity (ms^{-1})	Mean 'Forward' ball velocity (ms^{-1})
$2 < x < 5$	8.41
$0 < x < 2$	9.58
$-1 < x < 0$	10.39
$-4 < x < -1$	9.63

Table 5.9b. The range of pre-impact vertical ball velocities for both male and female players, and the corresponding average X velocities for each interval.

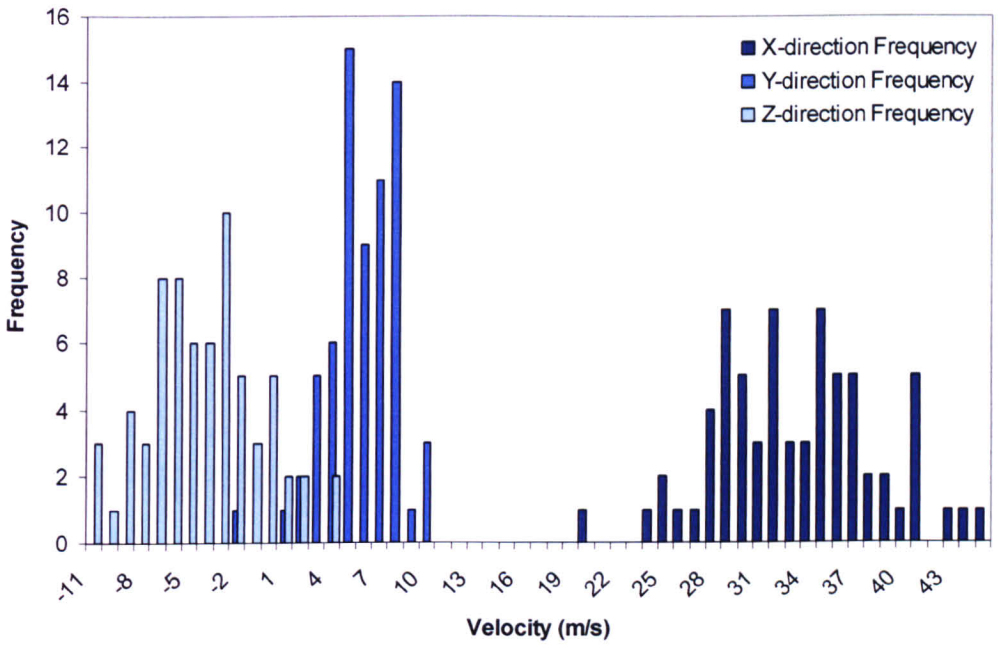

	X	Y	Z	Resultant
Mean (ms^{-1})	32.9	5.4	-4.7	33.6
Standard Deviation (ms^{-1})	5.0	2.2	3.6	6.6

Figure 5.10. Post impact ball velocity frequencies for every male player

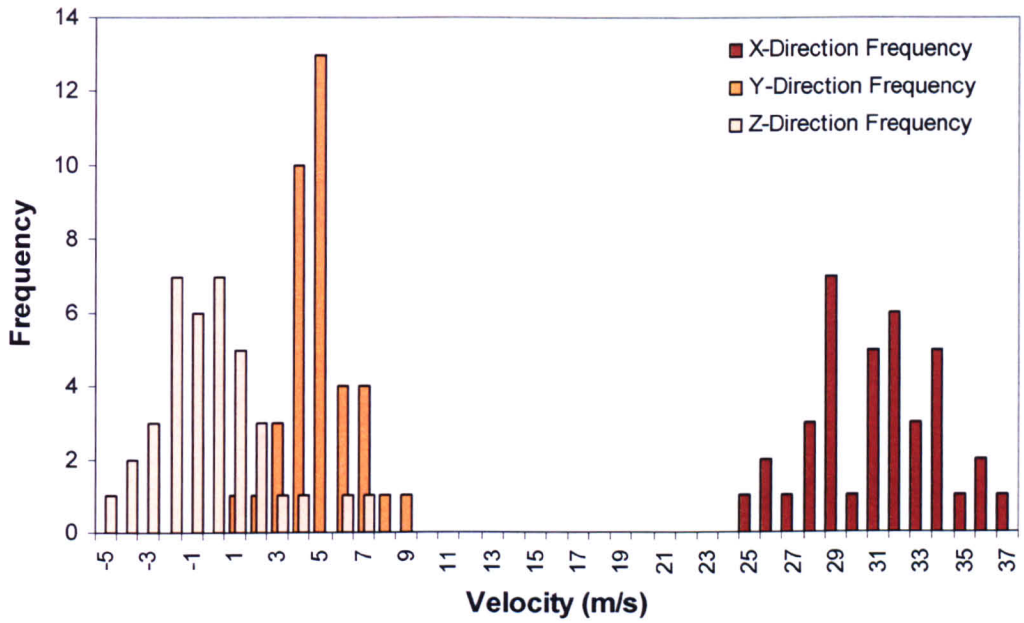

	X	Y	Z	Resultant
Mean (ms^{-1})	30.5	4.5	-0.8	30.9
Standard Deviation (ms^{-1})	3.0	1.5	2.5	4.2

Figure 5.11. Post impact ball velocity frequencies for every female player

Before impact, the ball is moving in a very similar way for both male and female players within the errors. The negative X velocity shows the ball moving away from the net, towards the player. The average Y velocity shows that in both cases, the ball is not moving significantly upward or downward at the instant of impact on average. A positive Y velocity shows that ball is moving upward at impact, whilst a negative, that is moving downwards. The spread of results suggests that players hit the ball when rising, when at the top of its bounce, and after the bounce. Figure 5.9b shows that generally, the player only hits the ball on the rise, when it is approaching them slowly. If the incoming ball velocity increases, the player tends to hit at the top of the bounce, or even after the ball has reached its apex.

After impact, the resultant ball velocity for male players are 8% higher. This shows that despite being given very similar balls before impact, male players are able to hit the balls with a greater final velocity. This is reflected in the higher racket velocities before impact for male players.

Angular Velocities

Racket Angular Velocities

The angular velocity of the racket is measured around the three local axes at the racket COM, the sign convention of the angular velocities are according to the right hand rule,

following the local axes as defined in chapter 4 (figure 4.5). The angular velocity frequencies for male players are shown in figure 5.12, and figure 5.13 displays the values for the female players.

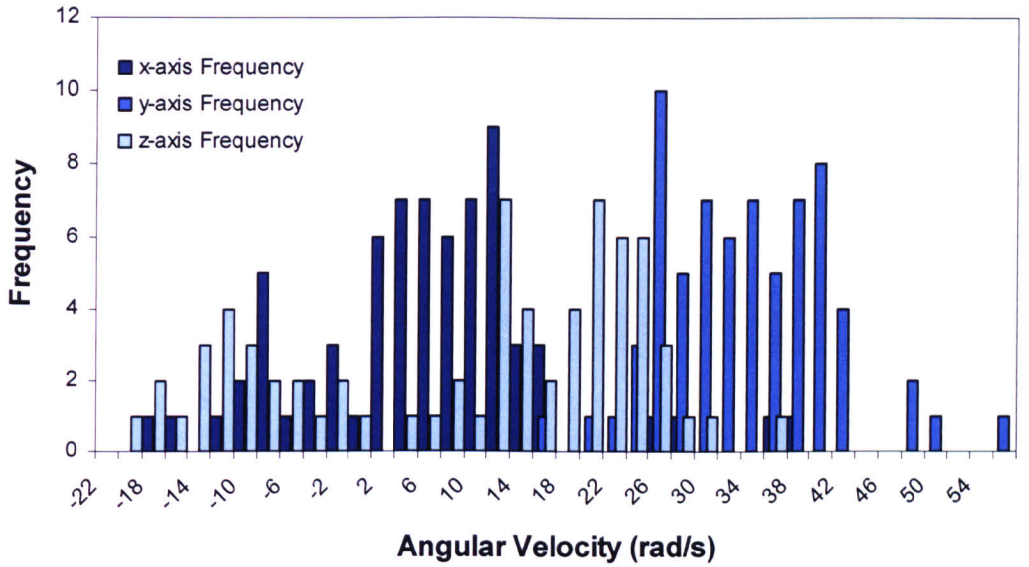

	x	y	z	Resultant
Mean ($rads^{-1}$)	2.8	30.5	6.5	31.3
Standard Deviation ($rads^{-1}$)	10.3	7.4	14.9	19.6

Figure 5.12. Angular velocity frequencies for every male player.

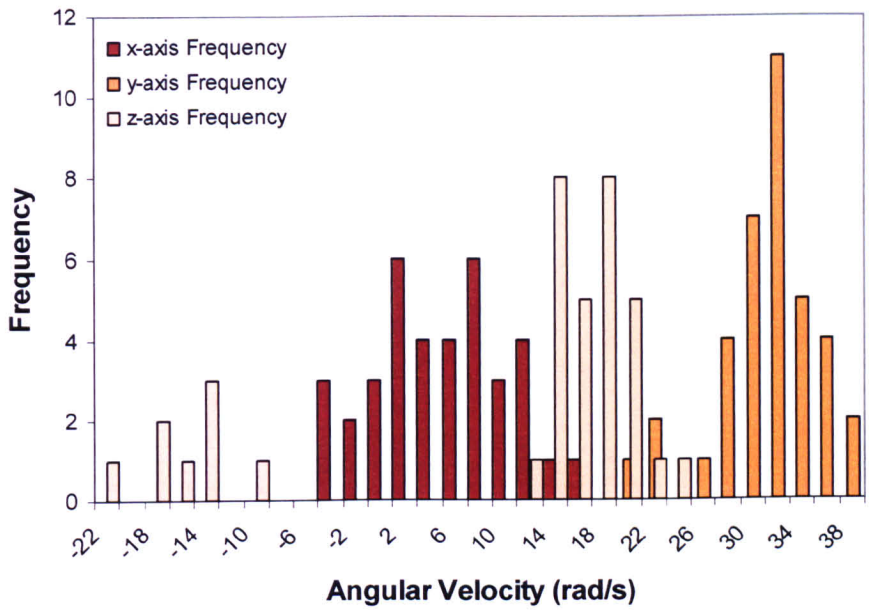

	x	y	z	Resultant
Mean ($rads^{-1}$)	4.3	30.2	8.9	31.8
Standard Deviation ($rads^{-1}$)	5.3	4.1	14.0	15.5

Figure 5.13. Angular velocity frequencies for every female player.

There is very little variation in racket angular velocity between male and female players. The majority of the angular velocity is around the local *y* axis, associated with rotation about the wrist. No negative rotation values were observed about the *y* axis, such an action would decrease the velocity of the impact point and decrease the effectiveness of the shot. Rotation around the local *z* axis corresponds to a 'chopping' action of the racket. Rotation around the local *x* axis is associated with racket twist, a movement which players would try to keep to a minimum at impact.

Ball Spins

The ball spins were counted manually from the images of each shot, positive spin values denote topspin whilst negative spin values denote backspin. Due to the lack of dimensionality of the spin value (only 1D spin was possible from the captured images) the male and female spin values are both displayed in figure 5.14 along with their mean and standard deviation values.

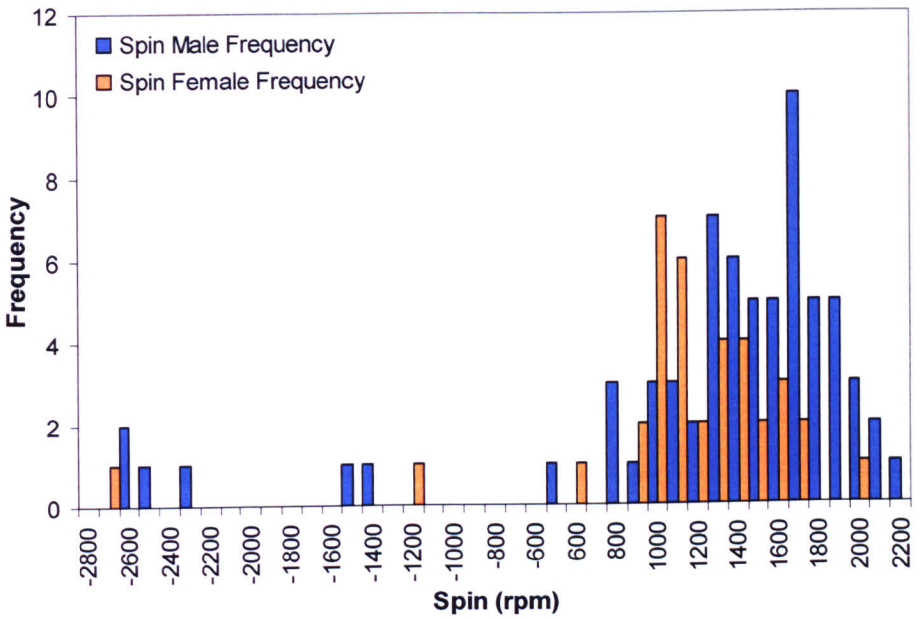

	Male	Female
Mean (rpm)	1125	1036
Standard Deviation (rpm)	1122	812

Figure 5.14. The ball spin frequencies for both the male and female players

Positive ball spin is associated with top-spin toward the net, negative spin associated with back-spin. On average, spin values are very similar for male and female players. The range of values exhibited by male players is higher, and generally they are able to produce higher values. The very few negative spin values seen in these results reflects that most players were forehand, top-spin shots.

Playing Angle

The playing angle frequency distribution of every shot, split into shots played by male and female players, is shown in figure 5.15. A negative playing angle is generally associated with an upward stroke and closed racket face, generally a topspin shot. A negative playing angle generally corresponds to a downward racket stroke and open racket face. This is only generally true because it depends on the relative movement of the racket and ball, but for the shot conditions seen in this player testing, these explanations can be assumed to be the case.

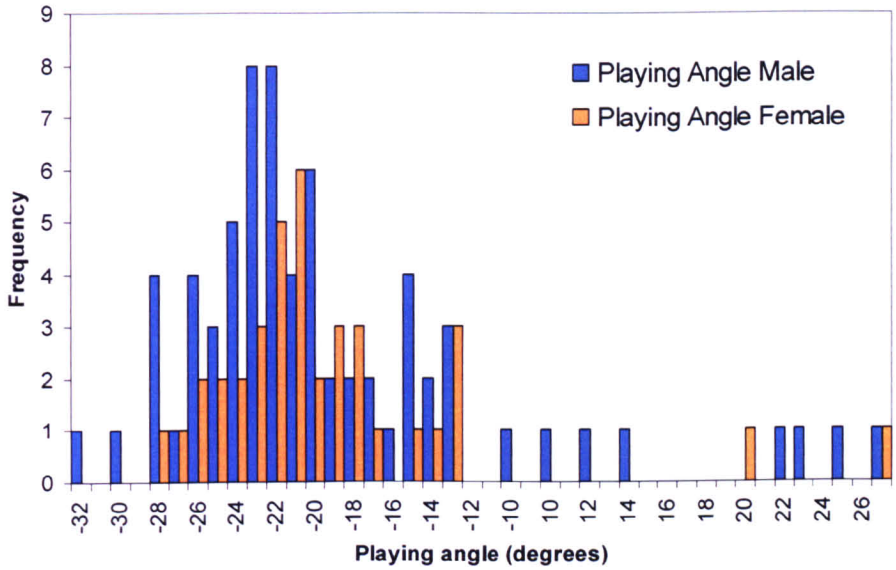

	Male	Female
Mean (degrees)	-17.8	-18.8
Standard Deviation (degrees)	13.2	11.0

Figure 5.15. The playing angle frequencies for both male and female players

Impact Position

The impact position is measured relative to the COM along the local x and local y directions. The positive x-direction goes toward the racket handle, because the location of the COM varies between rackets, every impact location in the x-direction has been translated to distance from the racket butt. A zero value of impact position in the y-direction corresponds to an impact along the racket's central axis, i.e. zero-offset.

The impact position frequencies in the x-direction for the male and female players are shown in figure 5.16. The impact positions frequencies in the y-direction shown in figure 5.17.

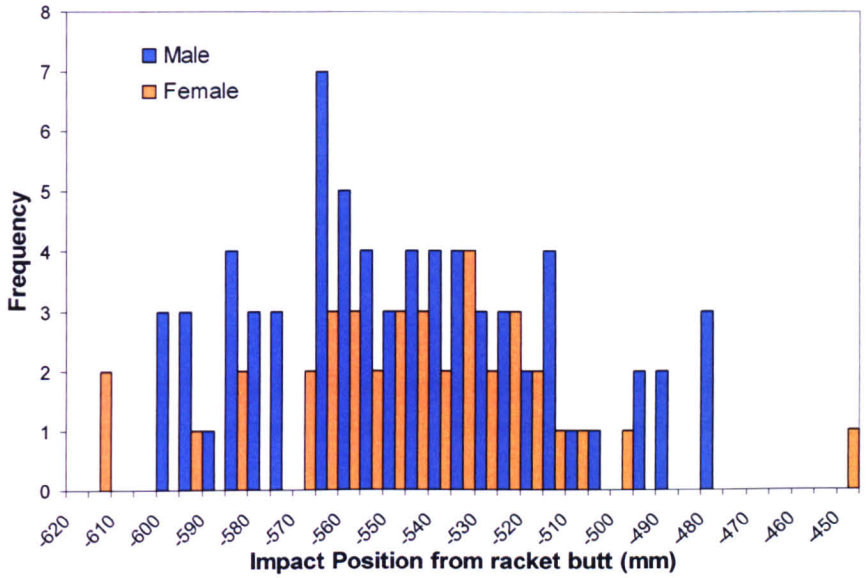

	Male	Female
Mean (mm)	-549.6	-549.2
Standard Deviation (mm)	31.7	30.6

Figure 5.16. The impact position frequencies along the *x*-direction for the male and female players (with respect to the racket butt).

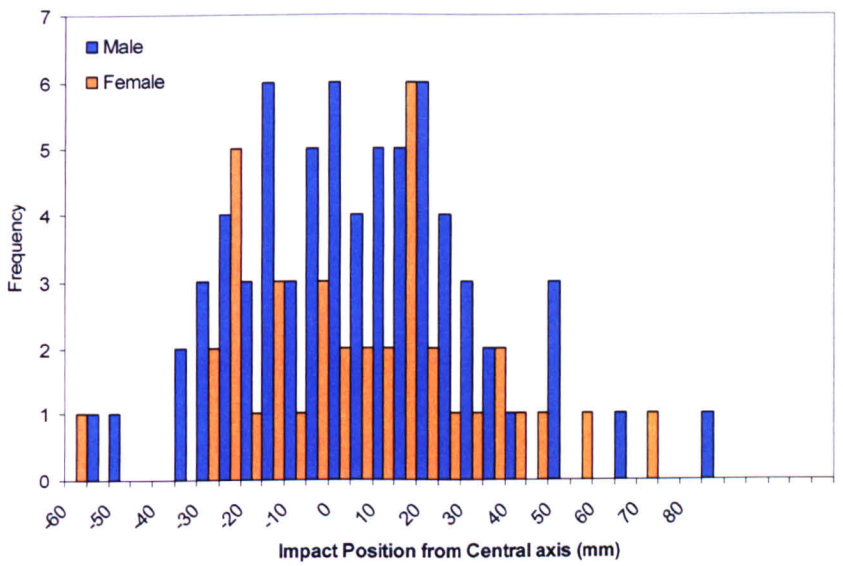

	Male	Female
Mean (mm)	1.7	1.4
Standard Deviation (mm)	26.3	26.5

Figure 5.17. The impact position frequencies along the *y*-direction for the male and female players.

The average impact positions, and standard deviations, are very similar for both male and female players. This suggests that all players are aiming for the same point on the racket, with similar levels of success. The very low average values in the local *y*-direction shows that the desired point of impact lies along the longitudinal axis of the racket. The mass and balance point of the racket varies from player to player. An individual analysis is necessary in order to assess the impact proximity to the so-called 'sweet spots'. Such an analysis is included in the next section in this chapter.

5.4.2 Discussion of results

The results suggest that the ball has a very similar resultant velocity and direction before impact, for both the male and female players. All of these results were obtained in practice conditions; the ball is hit to the player in a very repeatable way, usually by the coach. Generally, both sexes hit the ball toward the top of the arc, this gives the player the necessary time to prepare the shot and get into position. The faster shots (in the global X direction) are generally hit later in their trajectory, it is only in-bound balls that are moving slower than around 9 ms^{-1} that are hit 'on the rise', or soon after the bounce. This is despite traditional coaching wisdom suggesting that hitting the ball on the rise is preferable About.com **2007**.

Given the very similar ball velocities before impact, male players hit the ball with a greater velocity, on average, after impact. The results show that the male and female players hit the ball at a very similar point on the racket and exhibit very similar racket angular velocities.

The higher post-impact ball velocity is therefore due to the higher racket COM velocities generated by the male players. An 11% higher average resultant racket velocity, generates around 9% higher resultant ball velocities.

Post-impact, the ball has a positive vertical velocity. This is as one would expect, and gives the ball the necessary trajectory in order to arc over the net to reach the opposite side of the court.

The higher vertical ball velocity generated by the male players is reflected also by the higher ball spin values. The higher spin generates more down force, allowing the ball to be hit harder and still remain within the boundaries of the court.

As has been mentioned, both male and female players hit the ball, on average, on a very similar point on the stringbed. The longitudinal position was referenced from the racket butt so it could be easily compared between each racket. The mean impact position is located roughly around the racket's stringbed centre, which has been found to be the location on the stringbed which players 'aim' for in previous studies Hatze **1994** and Coe **2000**. The next section investigates whether players are able to hit the ball at different locations on the racket stringbed for different types of shots e.g. toward the racket tip for a wristier shot, or toward the throat for a flatter shot.

The playing angle values obtained from the players were very similar between sexes, but also lower than has been cited in other literature (Knudson **2006**) this could be due to the none-competitive nature of the testing or the type of shots which have been recorded.

The vast majority of the shots were played with top-spin; observation of the footage reveals that the majority of shots were also played on the forehand. This similarity in shot type makes the data useful for comparison, within the range of recorded shots there still exists a variety of spins and velocities. The lack of backhand and volley shots means that further testing is required in order to assess the particularities of these shot types.

Generally, this work has provided a range of values for the baseline top spin forehand which can be used in future laboratory testing. The speeds and spins are generally as expected and the impact positions tally with previous research. This work led to the first published work with accurate 3D values obtained from high level players competing in a qualifying tournament for a grand slam event. The values of racket and ball linear and angular velocity at impact, and the ball's impact position on the racket give further insight into how the top players in the game of tennis execute their shots. This work was performed in collaboration with the international tennis federation as part of their ongoing investigations into player performance and spin generation. The playing angle values obtained in this testing give directly comparable values which can be used in a laboratory based test, not only useful for validation, but as a benchmarking exercise to ensure that the values used in the laboratory are representative of reality.

Further work with players using this methodology would reveal typical values for backhands, lobs, volleys and serves. Working with players at a higher level would increase the validity of these results, and reveal whether their discrepancy with those used in earlier laboratory testing is due to a shortfall in this player testing, or an oversight in the laboratory.

5.5 Trends and Comparisons

This section investigates the effectiveness of the players in an indirect comparison i.e. can one player generate higher ball speeds from lower racket speeds than other players? The players' performance will be assessed using ideal parameters which are discussed in this section, specifically:

- The concept of an 'ideal point' and its relation to the actual impact behaviour of the player;
- The ability of a player to generate spin related to the racket velocity;
- A definition of the player's 'efficiency' and its relation to the ideal impact point;
- A look at how soon after the bounce the player makes contact with the ball;

Before displaying the results of such an investigation, a methodology section describes the various terms which are introduced in this section.

5.5.1 Methodology

The 'ideal' point

This power region or spot is widely documented as being one of the professed three 'sweet spots' Brody **1981**, Kotze et al. **2000**. It is usually stated as being situated at the COM for a ball impacting a stationary racket. This point moves further up the racket for a shot with positive angular velocity around the y axis. The results in the previous section showed that no player ever swung the racket with negative angular velocity around the local y axis (see figures 5.12 and 5.13).

Figure 5.17 shows that every player tries to hit the ball along the longitudinal axis of the racket, this is done because the penalty in power and control away from the racket's central axis is large, due to the effective mass dropping quickly in that direction. The concept of effective mass is discussed below. We can conclude that:

- The ideal impact point will always be between the COM and racket tip;
- The ideal impact point will always be along the centre line of the racket.

The effective mass is the mass the impact location has when represented as a point mass. The further away the impact point is from the COM, the lower the effective mass according to the moment of inertia in that direction. The dead point on a racket has an effective mass equal to that of the ball, resulting in complete momentum exchange, hence the name.

Using simple rigid body mechanics Brody et al. **2002** showed that as the impact point moves away from the COM along the central axis, the effective mass of the point decreases according to:

$$m_e = \frac{IM}{I + Mb^2} \qquad [5.1]$$

where I is the moment of inertia of the racket around a horizontal line through the COM, M is the racket's mass, and b is the distance from the COM to the impact point.

It is also possible to calculate the effective mass of a point in another direction off of the longitudinal racket axis, as shown by Brody et al. **2002**.

$$m_e = \frac{I_2\left(\frac{I_1 M}{I_1 + Ma^2}\right)}{I_2 + \left(\frac{I_1 M}{I_1 + Ma^2}\right)b^2} \qquad [5.2]$$

In this case the suffixes *1* and *2* are used to denote directions along the racket's width and length, a and b represent the distance from the COM to the impact point in each respective direction. Using typical moment of inertia and mass values, a surface plot showing the variation in effective mass away from the COM is shown in figure 5.18.

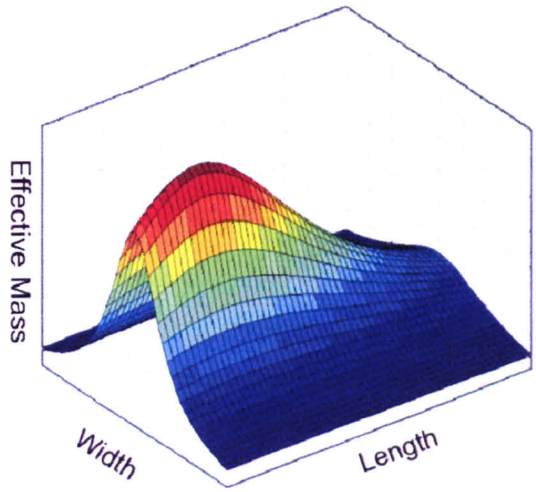

Figure 5.18. A surface plot showing the variation in effective mass away from the racket COM (the highest point on the plot) along a racket's width and length.

Simple mechanics shows that, for an impact on a point with effective mass m_e, the final velocity of the ball v_b' can be calculated using:

$$v_b' = \frac{e \cdot m_e (v_{IP} - v_b) + m_e \cdot v_{IP} + m \cdot v_b}{m + m_e} \qquad \textbf{[5.3]}$$

Here e is the coefficient of restitution, v_{IP} and v_b the velocity of the impact point and ball respectively, and m the mass of the ball. A prime denotes values post-impact.

For a racket moving with both linear and angular velocity, the impact point velocity is;

$$v_{IP} = V + \omega_x \cdot b \qquad \textbf{[5.4]}$$

where V is the linear velocity of the COM and ω_x the angular velocity in the swing direction b is from equation 5.2, and represents the distance of the impact from the COM, in the longitudinal direction.

Combining equations 5.1, 5.2 and 5.3 and differentiating with respect to b gives us:

$$\left(\frac{vmM \cdot b^2 + 2MI\omega_x \cdot b + I(2MV + v(m - M))}{mM \cdot b^2 + I(m + M)} \right) \frac{\partial v'}{\partial b} = 0 \qquad \textbf{[5.5]}$$

This can be solved using the quotient rule, to give a value for b for which v' is a maximum – the ideal impact point. Specifically, b represents the distance from the COM along the longitudinal direction which, upon impact will result in the maximum final ball velocity.

The value of ω_x varies between each shot and the values of M and I vary depending on the racket being used. So not only does the ideal point vary between each player, but also between each shot. The mass and swingweight of each racket is taken from data tables

available at the United Racquet Stringers Association USRSA **2007**, and the velocities were obtained from the recorded data.

With the ideal point defined as an updated power point, its location on the string-bed can be compared with other more established sweet spots, specifically the COP and node point;

COP

Cited often as a sweet spot, the Coefficient of Percussion is the impact point which corresponds to the instantaneous point of rotation being located at the wrist. The location of the COP is constant for each racket (assuming the racket is held at the same point), although the COP has been disputed as a valid sweet spot by Hatze **1998.**

Node Point

A handheld racket vibrates as a freely supported beam with several modes of vibration, each with a higher resonant frequency and successively more node points at which no vibrational displacement occurs. The first mode vibrates with the highest amplitude and as such has two node points, one around the middle of the stringbed, the other toward the handle. An impact at the node point creates no frame vibration and feels very comfortable as a result. It was not possible to test each racket explicitly to find the position of the node point; it was assumed to be positioned at 0.82 of the racket's length. This is the position of the node point in a uniform, freely supported beam and is a good assumption for a tennis racket.

Related to the impact position, another value was calculated which will be called the 'impact success ratio' this is a way of relating the ball impact position to the ideal ball impact position and is defined as:

$$\text{Impact Success Ratio} = \frac{\text{Momentum of ideal point}}{\text{Momentum of actual impact point}} \qquad [5.6]$$

The respective velocities and effective masses of the actual and ideal points were calculated and the ratio between their momentums calculated. An impact success ratio of 1 signifies that an impact is on the ideal point.

Spin Generation

Two different factors are used to measure the ability to generate spin, the playing angle and planar racket velocity. The playing angle, as described in chapter four, relates to the relative orientations of the ball and racket velocity vectors and has often been used in experiments investigating spin generation. The planar racket velocity describes the relative movements of the ball and racket in the racket plane at the instant of impact. Disregarding the velocity of the ball perpendicular to the racket plane is an attempt to relate the spin generation

of a player's shot to simple spin models exhibited by Daish **1972**. Observation of the recorded images shows that many players generate not only top-spin but considerable side spin, because spin is recorded only in 1-D, the planar racket velocity must include the local-x and y directions to show any correlation with spin values. Figure 5.19 shows a diagrammatic explanation of planar racket velocity, it is calculated by transforming the velocity of the impact point at impact from global, into local co-ordinates.

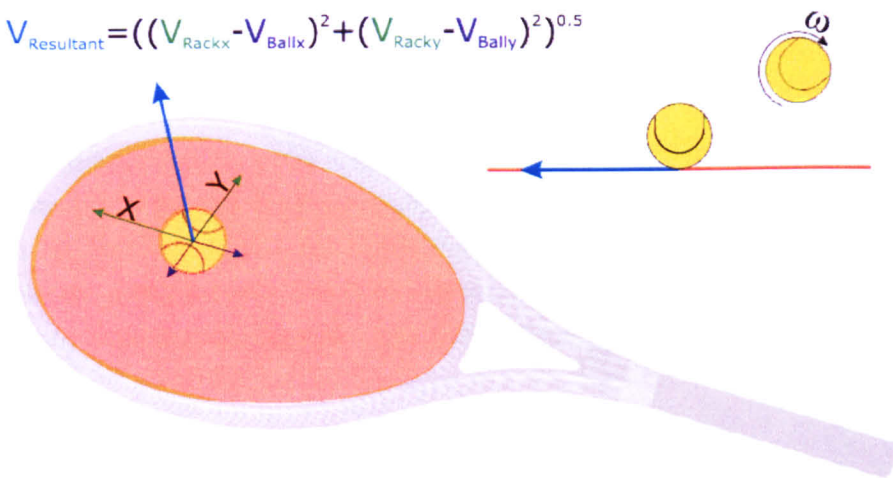

Figure 5.19. An illustration of local axes orientation and the calculation of the planar racket velocity.

Efficiency

A standard measure in engineering and sport, particularly in endurance sports such as cycling and swimming, where it is essential that the maximum amount of effort is transferred into useful output.

Which leads us to the definition of efficiency:

$$\eta = \frac{\text{Useful Energy Out}}{\text{Energy In}} \qquad \textbf{[5.7]}$$

How can the 'useful' energy output of a tennis shot be defined? Assuming that the player is the best judge of shot trajectory and speed, and that the ball falls within the court boundary, a maximisation of the post-impact ball energy would be most 'useful', which expressed in terms of the velocity and spin of the racket and ball (kinetic energies) becomes:

$$\eta = \frac{mv_b'^2 + I_b\omega_b'^2}{MV^2{}_{COM} + I_1\omega_1^2 + I_2\omega_2^2 + I_3\omega_3^2 + mv_b^2 + I_b\omega_b^2} \qquad \textbf{[5.8]}$$

where the inertial properties and angular velocities of the racket are expressed around three axes.

The full inertial properties of the racket are required to calculate a player's efficiency, access to the player's racket details are therefore necessary. It was only possible to obtain the full inertial properties of the rackets used by three players. The twistweight and swingweight were measured as described in Brody et al. **2002** and the spinweight was obtained by using the perpendicular axis theorem, Nave **2005**. The inertia of the ball was calculated as a hollow sphere using the standard values of wall thickness and mass for a Slazenger™ Wimbledon tennis ball. In this way the efficiency of every shot from three players (a total of 32) were analysed.

Impact Timing

The velocity of the ball at the instant of impact gives an indication of how soon after the bounce it was hit. If the ball is hit soon after the bounce, the ball will have positive vertical velocity as the ball is rising. A ball hit at the apex of the ball's trajectory will have zero vertical velocity, a ball hit after this time will have negative vertical velocity. This is easily tracked directly from the velocity data of the ball taken from the player shot data.

5.5.2 Results

Impact point

Figure 5.20 shows the position of the impact point and three sweet spots for 13 of the 16 players tested. Each of the positions shown are averages of the total shots made by each player, only players which made over five recorded shots were included.

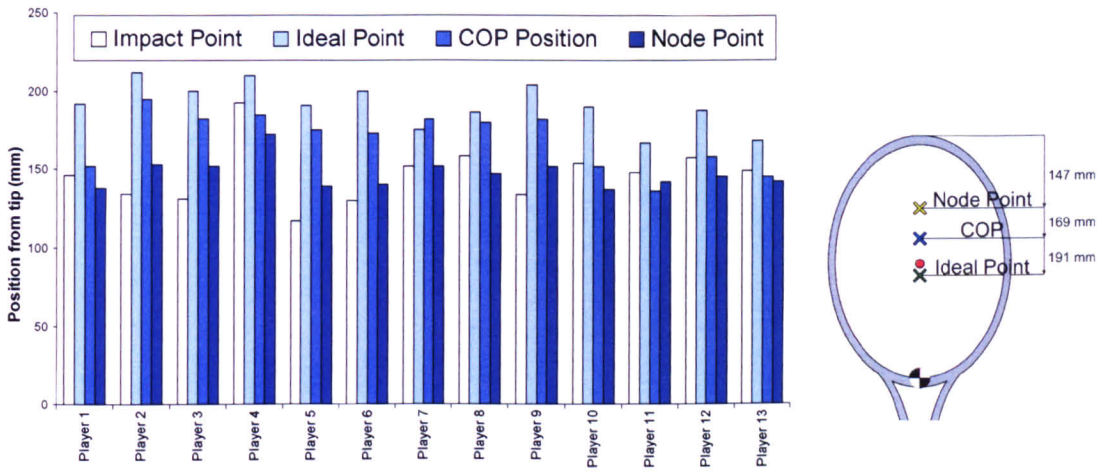

Difference between impact point for all players and the:	Mean (mm)	Standard Deviation (mm)
Ideal Point	44.7	24.1
COP	22.6	27.2
Node Point	0.6	15.5

Figure 5.20. The plotted averages of the impact position, ideal point, COP position and node point for 13 players whom made over five recorded shots. The relative positions of the separate sweet spots are illustrated on the racket head.

Figure 5.20 shows that players hit on the node point of the racket (or at least attempt to). They hit between 20 and 80 mm away from the ideal point of the racket, consistently further toward the stringbed centre than is necessary. Although players hit closer to the centre of percussion, than the ideal point they are still on average 22.6 mm away, suggesting that is not a point that all players consider sweet, and are able to hit as consistently as the racket's node point.

Spin Generation

Figure 5.21 shows the outbound spin of a players' shot according the playing angle. Figure 5.22 shows the outbound spin according to the planar racket velocity. The result of every player's shot is plotted in each case. The player never moves the racket purely in the local x or y direction, the local movement of the racket in every tested shot is shown in figure 5.23, split into the local x and y directions. Generally, depending on how the player is standing, the local y direction corresponds to the global vertical, the global X corresponds to the global horizontal. For clarity, only the top-spin shots are shown.

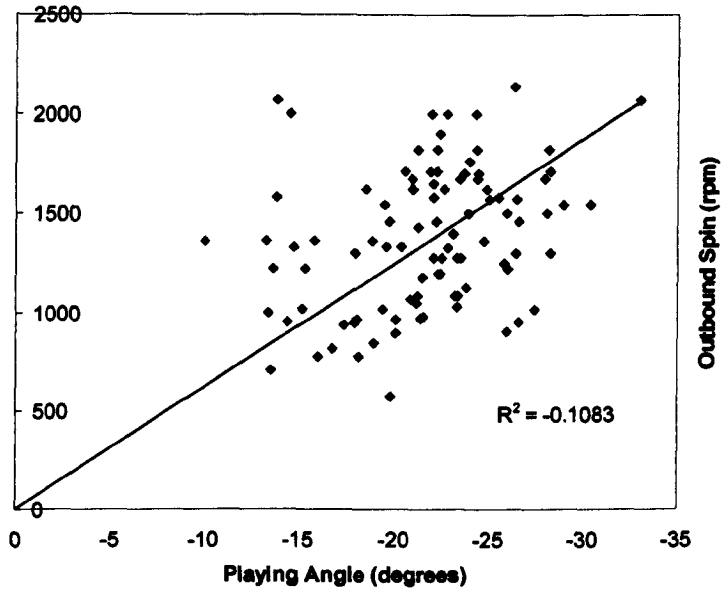

Figure 5.21. A plot of the outbound spin vs playing angle for every player tested

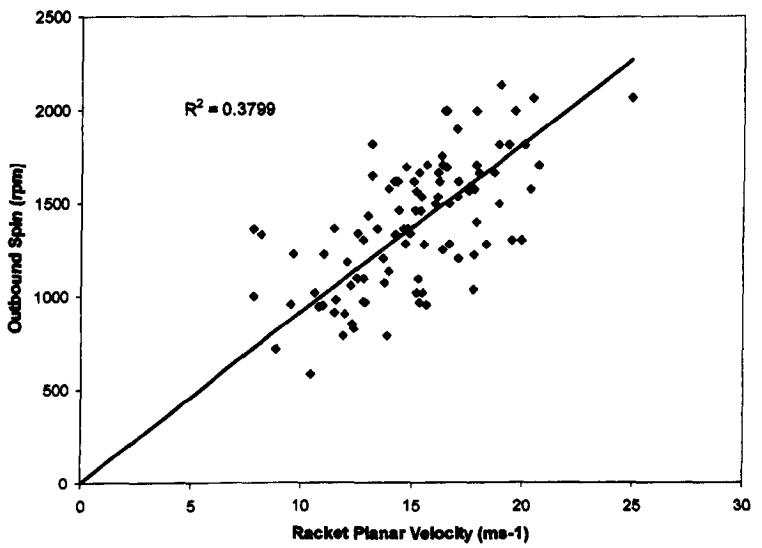

Figure 5.22. A plot of the outbound spin vs planar racket velocity for every player tested.

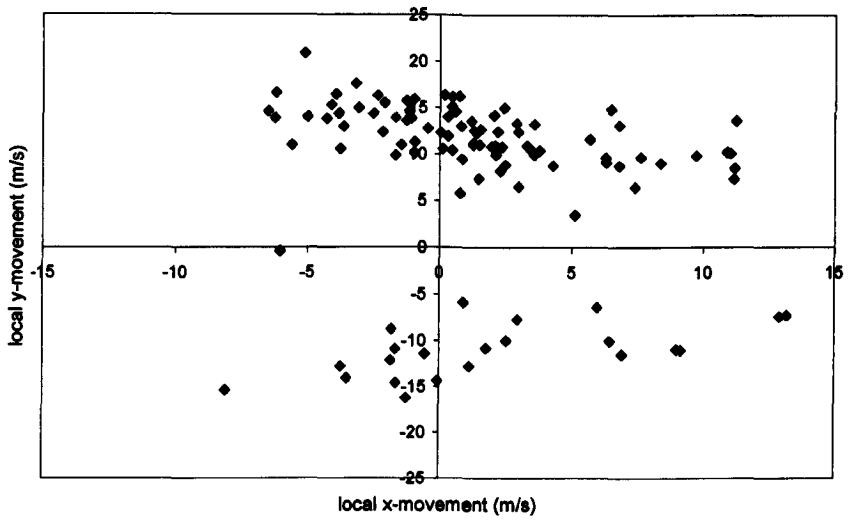

Figure 5.23. The local racket movement of every shot recorded at the instant of impact

Player Efficiency

Figure 5.24 shows the impact success ratio of three players related to the efficiency of the shot, only three players were plotted due to the amount of racket information required to calculate the shot's efficiency. Four separate regions of the plot are highlighted:

1) A region of impacts close to the ideal point, two of the impacts have an impact success ratio of lower than one.
2) An impact that, despite the proximity to the ideal point, is particularly inefficient
3) The opposite of region 2, despite being slightly further away from the ideal point. It is a much more efficient shot.
4) Two points very far from the ideal point and with correspondingly low efficiencies.

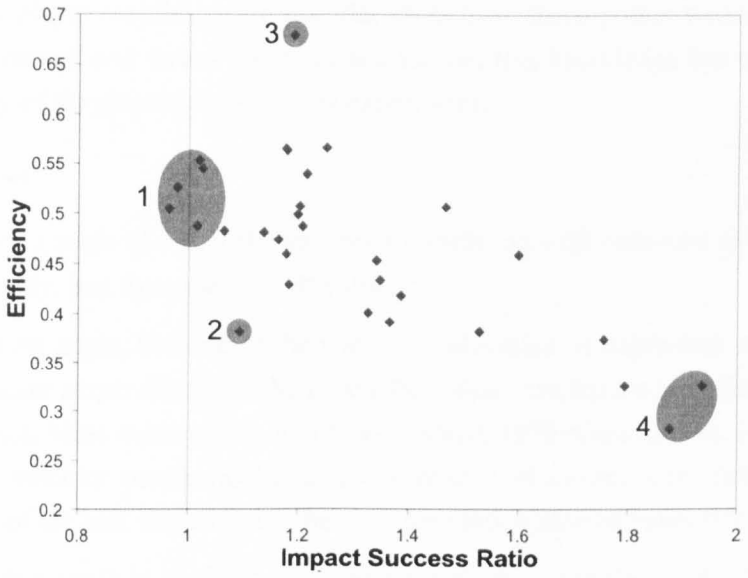

Figure 5.24. The Impact success ratio of the shots of three players related to the efficiency of the shot, the vertical line representing the 'ideal' impact success ratio at the value of 1. Four regions are highlighted on the plot.

5.5.3 Discussion of the results

Impact point

The position of the ideal point along the racket depends on the type of shot played, the amount of 'wrist' action present in the shot determines how far from the COM the ideal point lays. Figure 5.20 shows that the players consistently hit further toward the tip than is necessary, in many cases very close to their racket's node point, also seen by Hatze **1994**. Generally a player could generate more ball velocity by hitting further toward the throat. No player compensates for shot type by hitting further toward the tip on wristy shots, or further toward the throat on flat shots. Because the node point gives the best response at the hand in terms of feel, players learn to repeatedly hit this point.

Whilst the ideal point may result in a higher shot speed, in many cases it may feel unpleasant to hit because of the increased vibration. The ideal point also changes location for every shot, unlike the node point. The results suggest that the decreased vibration resulting from a shot at the node point is more desirable than the reduced shock at the wrist which may result from an impact at the racket's COP.

Many players occasionally hit the ball, even in stationary practice conditions, considerably off the centre line of the racket. The penalty in power and control for off-set shots is so great that it is always more desirable to hit the ball at any point along the central line of the racket than off-set.

Whilst a player may be aware that flat shots have more power when hit in the throat region of the racket, and wristy shots toward the tip, this knowledge has not been put into practice by any of the players tested in this experiment.

Spin Generation

The playing angle of a shot shows a poor correlation with outbound spin generated, this is obvious visually, and from the poor R^2 value.

The playing angle, because of the way it is calculated, is dependent on the velocity of the ball and racket perpendicular to the racket face; these can have a big effect on the playing angle of the shot. Most existing ball spin models Daish **1972**, Cross **2002a**, Haake et al. **2005** state that the velocity perpendicular to the contact surface has very little effect on the outbound spin of the ball, this explains the poor correlation seen in figure 5.21.

The playing angle is useful to describe the trajectory conditions of a ball contacting a stationary surface such as those seen in laboratory spin tests, where the ball velocity is carefully controlled. For the complicated impact conditions seen in player testing, where the ball and racket are both moving, the playing angle is not a sufficient indicator of outbound ball spin.

A clear correlation can be seen between an increase in planar velocity and an increase in spin magnitude (figure 5.22). By disregarding the velocity perpendicular to the racket, this follows the simple model of spin proposed by Daish **1972**.

Only outbound spin was plotted in both figures 5.21 and 5.22, it was found that the correlation became much poorer when the spin change between pre-impact and post-impact spin was plotted. This suggests that the ball grips the stringbed throughout the contact, or that the spin energy of the ball prior to impact is not sufficient to have a significant effect on the ball's spin afterwards within the resolution of the spin values recorded in this study.

The highest ball spin recorded was 2140 rpm, despite the error associated with the spin value, it is still much lower than the highest spins which have been reported in previous studies Pallis **2000**. These lower ball spins may be due to the lower standard of player used, or because recording took place during practice rather than competition conditions. Work by Goodwill et al. **2007** showed that spin levels generally exceed 3000 rpm during competition conditions.

It is interesting to note that the planar velocities in this testing reached up to 20 $m \cdot s^{-1}$, the upper range of the incident racket velocity (that associated with ball speed) is around 30 $m \cdot s^{-1}$. The generation of spin requires a lot of energy, most of which will remain in the racket post impact. If players were to generate spins of $\geq$ 3000 rpm on the groundstroke the planar velocity would exceed 30 $m \cdot s^{-1}$; a large increase. This discrepancy could be due to an ability to generate very high racket velocities that has not been observed in this testing. Or, an ability to generate spins that does not obey the correlation observed in figure 5.22. The spread of

values in figure 5.22 certainly suggests there is another element to spin generation that has not been identified in this testing.

Tracking the local movement of the racket reveals a number of things; the majority of players move the racket mainly in the local y direction which is associated with the generation of top-spin, and tallies with the top spin forehand which constitutes the majority of recorded shots. The negative y values seen represent the few backhand shots recorded, a positive x value corresponds to the shot being made after the apex of the swing (the racket is moving toward the player) and negative x values correspond to shots being made before the apex of the swing (the racket is moving away from the player). This is shown graphically in figure 5.26. A few shots can be seen with disproportionately high values in the positive x-direction. It is interesting to note that these shots belong solely to one player; large amounts of side spin were clearly visible in his recorded shots. Generally, the racket movement in the local y direction is over 3 times higher than that in the x-direction. This is valuable information when trying to design a validating experiment, knowing which racket movements are most relevant, and which ones should be replicated.

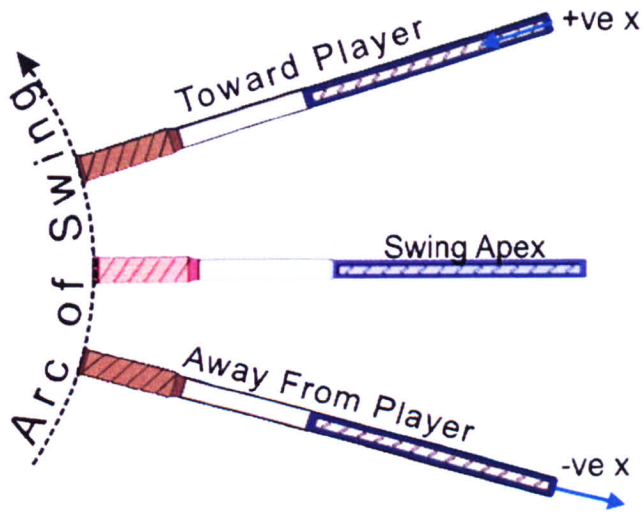

Figure 5.26. A diagram showing how the sign of the local x velocity can be used to ascertain whether a player makes impact before or after the apex of their swing

The spin values seen here and their correlation with planar racket velocity gives an insight into the mechanics of spin generation and possible approaches when devising a predictive model and validating experiment.

Impact Success Ratio and Efficiency

Figure 5.24 illustrates how the efficiency of a shot decreases as one moves away from the ideal point (*impact success ratio = 1*). Four regions were highlighted in figure 5.24 to illustrate the range of values obtained.

Region 1 shows points close to the ideal point, all points have similar efficiencies. Generally the efficiencies are similar because of the similarity in the recorded shots. Regions 2 and 3 show anomalies in the efficiency/success ratio correlation.

Region 2's particularly low efficiency is due to the large amount of energy remaining in the racket after impact. High spin shots require a high planar racket velocity, most of this kinetic energy remains in racket after impact. Region 2 shows a shot with a particularly high spin. Region 3 is particularly efficient, suggesting a very low spin shot, where the planar velocity is low, and most of the energy is transferred into the ball.

For an impact effectiveness higher than 1, the impact point's momentum is too low to make an effective shot, whilst for an impact effectiveness lower than one, too much momentum remains in the racket after impact and the energy of the shot is not maximised. The player's insistence on hitting the ball further toward the throat than necessary (to coincide with the node point) means that very few values of impact effectiveness under one were recorded. Regions 4 shows impacts where the momentum of the impact point was particularly low compared to the ideal point. The shot is correspondingly inefficient. Region 4 shows impacts far onto the offset of the racket, and how ineffective they are compared to impacts closer to the ideal point.

As can be seen a range of different efficiencies are possible with the same value of impact effectiveness, whilst it is not necessary to aim for maximum efficiency, it is quite clearly desirable to try and achieve an impact as close to the ideal point as possible.

5.6 Chapter Summary

The player shot analysis has provided information regarding:

- typical racket and ball linear and angular velocities
- playing angles
- impact positions

for high level players in competition practice conditions. The values seen in section 5.4 are in the vast majority of cases, for baseline forehand top-spin shots.

A player tends to aim to hit the ball at the node point of a racket irrespective of the type of shot they are playing, probably due to the lack of vibration at impact.

Spin in the ground strokes has a peak value of 2000 rpm. To achieve this spin rate, the players have to move their racket face at over 20 ms^{-1}. More testing at a higher level is necessary to investigate the higher spin levels observed during competition conditions.

Calculations of shot efficiency and 'impact effectiveness' further reinforce the concept of an 'ideal point' as being the best place to hit the ball with regards to velocity, although an 'efficient' shot in this sense has little meaning in terms of the best shot type to use.

An investigation into the impact instant suggests that players do aim to hit the ball on the rise but are only likely to achieve this for slower moving balls; the faster the ball approaches the player the further on it is in its trajectory before impact is made.

This work would benefit from using players at a higher level. By asking them to perform in a certain way or filming them in competition conditions one could assume that the recorded shots would be the best the player could produce. This analysis forms a complete method and a promising start to what could be a comprehensive body of work measuring tennis ball/racket dynamics in game play.

Tables 5.27 and 5.28 are two summary tables showing the mean and standard deviation values for the male and female player's shot characteristics respectively. The velocity values tally with rough values that have been obtained in previous studies, although spin and playing angles are lower than had previously been recorded. This may be due to the level of the players tested, or that the data was recorded during practice conditions.

These values can be used to design a laboratory experiment to develop a predictive model, and because of their completeness, can also be used in the model's validation.

As well as obtaining typical shot characteristics, this testing was used to investigate player shot behaviour, the ideal impact point on the racket face, mechanics of spin generation, player efficiency and shot timings.

Whilst not strictly applicable to a predictive model, the investigation demonstrates the strength and versatility of the methodology that was developed in chapter four. The player shot analysis gives a rich insight into the way a player behaves when making a tennis shot and stands as a robust piece of research on its own.

With the information that has been obtained in this testing, a laboratory based impact test can be designed which will provide the controlled results required to validate a predictive impact model with six degrees of freedom in three dimensions.

Male Players

Velocities (ms^{-1})			*X*-direction	*Y*-Direction	*Z*-Direction
Racket					
	Pre-impact	Mean	15.96	6.21	-4.43
		Standard Dev	2.99	4.22	2.87
Ball					
	Pre-impact	Mean	-9.30	-0.64	1.13
		Standard Dev	2.70	1.71	1.04
	Post-impact	Mean	32.86	5.37	-4.72
		Standard Dev	5.04	2.20	3.56

Angular Velocities			Around *x*-axis	Around *y*-axis	Around *z*-axis
Racket					
	Pre-impact (rad/s)	Mean	2.75	30.53	6.46
		Standard Dev	10.30	7.39	14.90
Ball spin (1D)					
	Post-impact (rpm)	Mean	1125		
		Standard Dev	1122		
	Playing Angle (degrees)	Mean	-17.8		
		Standard Dev	13.19		

Impact Position			*x*-direction	*y*-direction	
	mm from tip	Mean	-549.55	1.67	
		Standard Dev	31.66	26.32	

Table 5.27. A table showing a summary of shot characteristic means and standard deviations for all male players tested in the player shot analysis

Female Players

Velocities (ms^{-1})			*X*-direction	*Y*-Direction	*Z*-Direction
Racket					
	Pre-impact	Mean	14.93	5.51	-1.10
		Standard Dev	1.49	2.86	2.71
Ball					
	Pre-impact	Mean	-9.34	0.20	0.08
		Standard Dev	1.89	1.68	0.91
	Post-impact	Mean	30.54	4.47	-0.81
		Standard Dev	3.01	1.54	2.53

Angular Velocities			Around *x*-axis	Around *x*-axis	Around *y*-axis
Racket					
	Pre-impact (rad/s)	Mean	4.33	30.24	8.88
		Standard Dev	5.28	4.06	14.02
Ball spin (1D)					
	Post-impact (rpm)	Mean	1036		
		Standard Dev	812		
	Playing Angle (degrees)	Mean	-18.76		
		Standard Dev	11		

Impact Position			*x*-direction	*y*-direction	
	mm from tip	Mean	-549.22	1.43	
		Standard Dev	30.60	26.52	

Table 5.28. A table showing a summary of shot characteristic means and standard deviations for all female players tested in the player shot analysis